30869

NAME OF AUTHOR/*NOM DE L'AUTEUR* _Walter - John Wilkinson_

TITLE OF THESIS/*TITRE DE LA THÈSE* _A Range Tested Antenna_
for Use with a Dual-Polarized
Riometer

UNIVERSITY/*UNIVERSITÉ* _Alberta_

DEGREE FOR WHICH THESIS WAS PRESENTED/
GRADE POUR LEQUEL CETTE THÈSE FUT PRÉSENTÉE _Master of Science in Electrical Engineering_

YEAR THIS DEGREE CONFERRED/*ANNÉE D'OBTENTION DE CE DEGRÉ* _1976_

NAME OF SUPERVISOR/*NOM DU DIRECTEUR DE THÈSE* _Dr. David Routledge_

DATED/*DATÉ* _Sept. 7_   SIGNED/*SIGNÉ* _W. J. Wilk_

PERMANENT ADDRESS/*RÉSIDENCE FIXÉ* _182 T. wain Drive_
Winnipeg 22, Manitoba
_R3K 0R2_

THE UNIVERSITY OF ALBERTA

A RANGE TESTED ANTENNA FOR USE WITH A

DUAL-POLARIZED RIOMETER

by

(C) WALTER JOHN WILKINSON

A THESIS

SUBMITTED TO THE FACULTY OF GRADUATE STUDIES AND RESEARCH

IN PARTIAL FULFILLMENT OF THE REQUIREMENTS FOR THE DEGREE

OF MASTER OF SCIENCE

IN

ELECTRICAL ENGINEERING

DEPARTMENT OF ELECTRICAL ENGINEERING

EDMONTON, ALBERTA

FALL, 1976

THE UNIVERSITY OF ALBERTA

FACULTY OF GRADUATE STUDIES AND RESEARCH

The undersigned certify that they have read, and

recommend to the Faculty of Graduate Studies and Research,

for acceptance, a thesis entitled "A Range Tested Antenna

for use with a Dual-Polarized Riometer" submitted by Walter

John Wilkinson in partial fulfilment of the requirements

for the degree of Master of Science in Electrical Engineering.

D. Routledge
....
Supervisor

....
Supervisor

....

....

Date Aug 23 1976

DEDICATION

To My Mother and Father

ABSTRACT

Accurate ionospheric absorption measurements to within 1% are
required for beam calibration purposes of a large aperture synthesis
low frequency (12.4 MHz) radio telescope proposed by the University of
Alberta. It is suggested that the best method of obtaining such
accurate absorption measurements is by the use of a dual-polarized
riometer. Because of the high accuracy required, care must be taken
in the choice of the antenna used with the dual-polarized riometer and
to this end a microwave antenna test range was designed and built to
test the important characteristics of antennas likely to meet the
requirements. The design and construction of this antenna test range
is presented and an evaluation of its performance is given. Finally,
after the deficiencies of the antenna test range have been taken into
account, a design is proposed for the most suitable antenna for use
with the dual-polarized riometer based on the range measurements.

The author wishes to express his deep appreciation to his supervisors, Dr. David Routledge and Dr. Fred Vaneldik, for their moral, financial, and technical help (in that order) in the completion of the work leading to this thesis and in the preparation of the thesis itself.

Thanks must also be extended to Mr. Konrad Doerrbecker and the men under his supervision in the Electrical Engineering Machine Shop. The quality of their work was exceeded only by their patience and courtesy. A special thanks is given to Mr. Steve Gomez for his help in the solution of many constructional problems associated with the wooden structure of the range.

An expression of gratitude is extended to Mr. Alejandro Mackay for the help he kindly volunteered to the author with respect to microstrip design, in general, and the microstrip power oscillator, in particular.

The author wishes to thank the National Research Council and the Department of Electrical Engineering for their financial support.

TABLE OF CONTENTS

LIST OF FIGURES

xvi

LIST OF SYMBOLS

SYMBOL

λ = wavelength

ν = electron collision frequency

N = electron density

$f_{o_{F2}}$ = ordinary wave critical frequency of the F2 layer

Q.D.C. = quiet day curve

HPBW = half-power beam width

B = noise bandwidth except in Ch. 2 where it represents the magnitude of the earth's magnetic field vector

B_L = longitudinal component of earth's magnetic field vector $\overline{B}$

B_T = tangential component of earth's magnetic field vector $\overline{B}$

θ = zenith angle except in Ch. 2 where it represents the angle between the direction of propagation and the magnetic field

q = $-e = -1.6 \times 10^{-19}$ coulombs = electronic charge

$\overline{E}$ = electric field vector

$\overline{v}$ = electron velocity vector

$\overline{J}$ = current density vector

m = 9.1×10^{-31} kg = electron mass

ε_o = 8.854×10^{-12} F/m = permittivity of free space

μ_o = $4\pi \times 10^{-7}$ H/m = permeability of free space

$\overline{H}$ = magnetic field intensity vector

X = ω_p^2 / ω^2

Y_L = ω_L / ω

Y_T = ω_T / ω

U = $1 - jZ$

Z = ν / ω

ω = $2\pi f$ = angular frequency

SYMBOL

ω_p $= 2\pi f_p = \sqrt{\dfrac{Ne^2}{\epsilon_o m}}$ = angular plasma frequency

ω_B $= 2\pi f_B = \dfrac{eB}{m}$ = angular gyro frequency

ω_L $= 2\pi f_L = \dfrac{eB_L}{m}$

ω_T $= 2\pi f_T = \dfrac{eB_T}{m}$

n $= \mu - \dfrac{jkc}{\omega} = -\dfrac{j\gamma_w c}{\omega}$ = complex refractive index

μ = refractive index (real part of n)

c = speed of light in free space

k = 1.38×10^{-23} joule/°K = Boltzmann's constant except in Ch. 2 where it is the absorption coefficient

γ_w = wave propagation constant

Δ = phase angle

LCP = left circularly polarized

RCP = right circularly polarized

ν_m = collision frequency corresponding to the most probable electron velocity

T_A = antenna noise equivalent temperature

G = power gain

P_{in} = input noise power

P_{out} = output noise power

F = noise figure

T_o = 290°K due to IEEE definition of noise figure

ϵ_c = power transmission coefficient of cable

ϵ_{ion} = power transmission coefficient of ionosphere

T_{ion} = physical temperature of ionosphere

T_{sky} = equivalent temperature of cosmic noise (sky) background

SYMBOL

I.F.	=	intermediate frequency
I.C.	=	integrated circuit
L.O.	=	local oscillator
CMOS	=	complementary metal oxide semiconductor
TTL	=	transistor, transistor logic
A/D	=	analog to digital converter
D/A	=	digital to analog converter
A	=	absorption
f_{eo}	=	effective operating frequency of ordinary wave
f_{ex}	=	effective operating frequency of extraordinary wave
P_o	=	ordinary wave received power
P_x	=	extraordinary wave received power
A_o	=	absorption experienced by ordinary wave
A_x	=	absorption experienced by extraordinary wave
LEP	=	left elliptically polarized
REP	=	right elliptically polarized
T_{ns}	=	equivalent temperature of noise source power
RMS	=	root mean square
AR	=	axial ratio
α	=	angle of wrap
δ	=	angular arm width
θ_o	=	cone angle
H	=	untruncated cone height
h	=	truncated cone height
D	=	conical spiral base diameter
d	=	truncated conical spiral top diameter

SYMBOL

b $=$ $\dfrac{\sin\theta_0}{\tan\alpha}$

ϕ $=$ azimuth angle

β $=$ phase propagation constant

$M(\epsilon,\tau)$ $=$ polarization state on the Poincaré sphere

2ϵ $=$ Poincaré latitude

2τ $=$ Poincaré longitude

ℓ_e $=$ dipole effective length

T_T $=$ total equivalent temperature of system

T_S $=$ equivalent temperature of received signal power

T_{NS} $=$ equivalent temperature of artificial noise power in environment

P_{RX} $=$ power received

P_{TX} $=$ power transmitted

$Z_{o_{avg}}$ $=$ average characteristic impedance

DVM $=$ digital volt meter

λ_g $=$ guide wavelength

z_o $=$ characteristic impedance

λ_o $=$ free space wavelength

ϵ_R $=$ dielectric constant

RFC $=$ radio frequency choke

CHAPTER 1

INTRODUCTION AND HISTORY

1.1 Introduction

The Electrical Engineering Department of the University of Alberta proposes to build a large aperture synthesis radio telescope in the region known as Seven Mile Flat in southwestern Alberta. The prime function of the telescope, which will operate at a frequency of 12.4 Mhz ($\lambda \sim 24m$), will be the detailed mapping of the complex structure of the galactic continuum radiation. It will also be involved in a preliminary flux density interferometer program for beam calibration purposes. Unfortunately, measurements conducted at such a low frequency as 12.4 MHz must be corrected for absorption which has occurred in the earth's ionosphere. As can be seen from Figure 1.1, this ionized region above the Earth is by no means uniform and its properties are continually changing with time. One instrument which attempts to determine the absorption in the ionosphere at the time that measurements are being carried out is known as a Relative Ionospheric Opacity METER or riometer. Because of the accuracy desired in the measurements performed by the large telescope, it is desired that the absorption measurements carried out by the riometer be accurate to within 1%. This thesis is concerned with what is believed to be the best method of attaining this accuracy, if indeed it can be attained at all. Because of the variability of the properties of the ionosphere with both time and space, this is not a foregone conclusion.

The remainder of this chapter gives a brief historical development of the theory behind radio wave propagation in the ionosphere and an introduction to the various ionospheric investigative techniques.

1
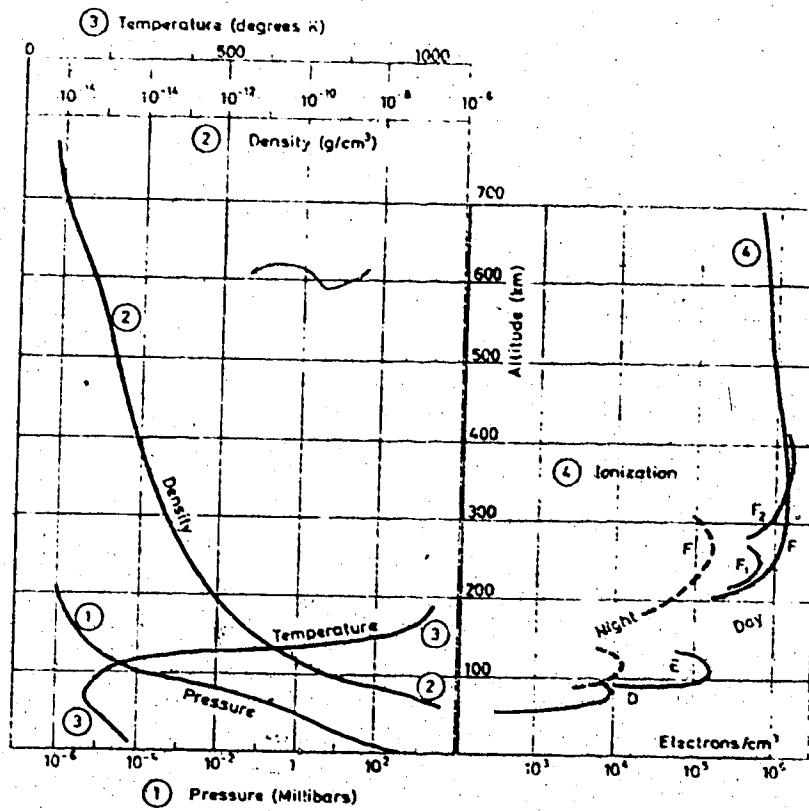
(a) [41]
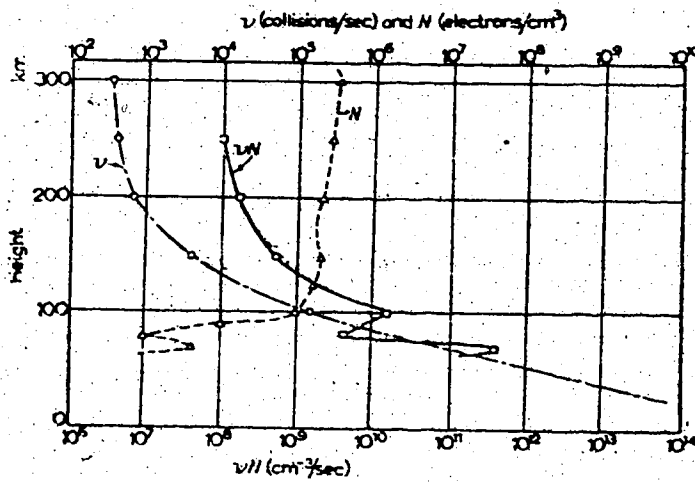
(b) [26]

Fig. 1.1 Properties of the ionosphere.

It concludes with an outline of the technique proposed for the measurement of ionospheric absorption, its advantages and special equipment requirements.

1.2 The Development of the Magneto-Ionic Theory

In order to account for Marconi's seemingly impossible feat of transmitting radio signals over a significant portion of the curved earth, O. Heaviside and A.E. Kennelly in 1902, independently hypothesized the existence of an upper conducting surface surrounding the earth, which gradually came to be referred to as the Kennelly-Heaviside layer.

In 1912, W.H. Eccles made the first attempt at mathematically formulating the theory of Kennelly and Heaviside and deriving expressions for the velocity and absorption of waves passing through a medium containing free charges. Unfortunately, his two basic assumptions, that the effective charges were of atomic mass and that the medium acted as a perfect conductor, led to the conclusion that the collision frequency had to be larger than the angular frequency of the wave; an unlikely result in view of the massive charges involved.

This problem was eliminated by Larmor in 1924, when he not only considered electrons as the effective charges, but also allowed the collision frequency to be small enough so that the medium could be considered a dielectric instead of a conductor.

By 1932, Appleton [1] and Hartree [2], had formulated detailed expressions for refractive index, absorption coefficient, and polarizations of waves propagating in an ionized region permeated by a magnetic field, where electrons were subjected to collisions with heavier particles. These equations, known as the Appleton-Hartree magneto-ionic equations ,

remained essentially unchanged until 1960 when Sen and Wyller [3]
modified them to include the dependence of collision frequency on
electron energy. It is primarily these equations which constitute the
magneto-ionic theory as it is known today and through their use that
ionospheric effects on radio-wave propagation are explained.

1.3 Methods of Ionospheric Investigations

Several options are open to the ionospheric investigator as to
his method of gathering information, but broadly speaking, these methods
break down into two groups: high altitude measurements,and ground based
measurements. It should be pointed out, however, that of the various
probing techniques available at present, only the riometry techniques,
which will be discussed in sections 1.3.4 and 1.3.5, would seriously be
considered by the radio astronomer. The ionospheric absorption presented
to cosmic radio noise at any given time, which is the primary factor to
be determined from a radio astronomical point of view, would be highly
impractical, if not impossible, to accurately extract from the measured
data of the other techniques. They are presented here for completeness
and as secondary sources of information on the ionosphere.

1.3.1 High Altitude Investigations

High altitude studies are carried out through the use of satellite,
rocket and balloon-borne measuring equipment. The great advantage of
this method is that it provides direct information on ionizing radiation
flux, constituent particle densities and energies as well as indirect
information on the heights of absorption, absorbing layer thickness and
layer inhomogeneities. Their great disadvantage is that they are

generally very expensive and/or have a very limited productive life-time. They are most frequently used in the study of polar cap and auroral absorption as well as the monitoring of ionospheric properties during such unusual events as solar eclipses and solar flare-ups. The simultaneous monitoring of the ionosphere by high altitude and ground based equipment has proved fruitful in the calibration of the ground based measurements [4].

1.3.2 The Monitoring of Communication Circuits

The various ground based techniques are graphically illustrated in Figure 1.2. Certainly the oldest technique is the monitoring of a communication channel between two ground stations.

The first direct experimental evidence of an ionized region above
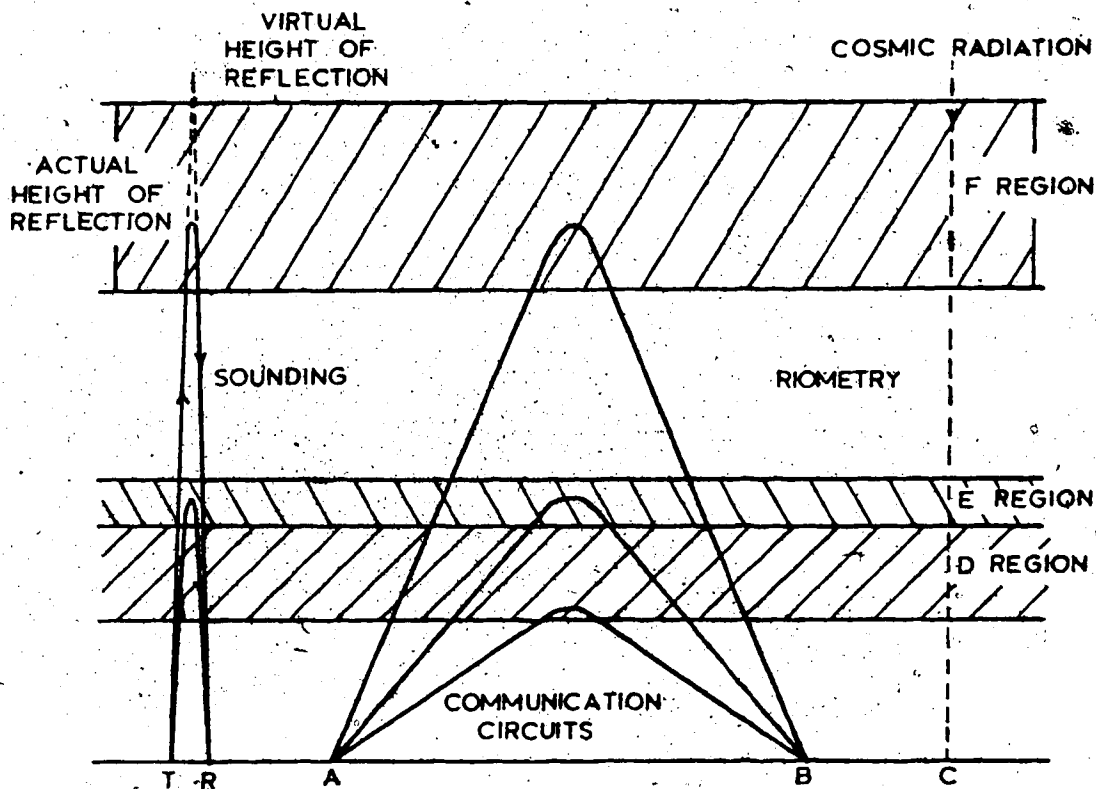
Fig. 1.2 Ground based ionospheric investigative techniques.

the earth came in 1925 when Appleton and Barnett [5] measured the
arrival angle of waves from a distant transmitter. They showed that this
angle of reception was such that a "sky-wave" had to be present and that
the height of the reflecting surface was somewhere between 100 km and
200 km. At this time the magneto-ionic theory was still in its infancy
and a favorite pastime of scientists was the monitoring of communication
circuits in the hope of discovering more about the absorption and fading
phenomena they observed. This eventually led to the determination of
frequencies and times which would ensure favorable propagation and hence
helped in the determination of maximum usable frequency (MUF) charts for
various propagation distances (see Figures 1.3 (a) and (b)).

Today communication circuits are still being monitored; however,
their value now lies in the detection of long term absorption trends,
such as those due to seasonal changes or the sunspot cycle [6]. These
long term absorption trends are of interest to radio astronomers,
especially those working in the lower HF band where ionospheric absorp-
tion is most severe.

1.3.3 Sounding

One year after Appleton and Barnett's discovery, Breit and Tuve [7]
devised the pulse-sounding technique for ionospheric investigation. They
reasoned that if a sufficiently short pulse were sent vertically into the
ionosphere, the time taken for it to travel to the reflecting region and
back might be measured using an oscilloscope with a time base synchronized
to the pulse-repetition frequency. By assuming the pulse to be propagated
at the speed of light, the height of reflection could be determined.
Although their assumption that the pulse travels throughout its path at
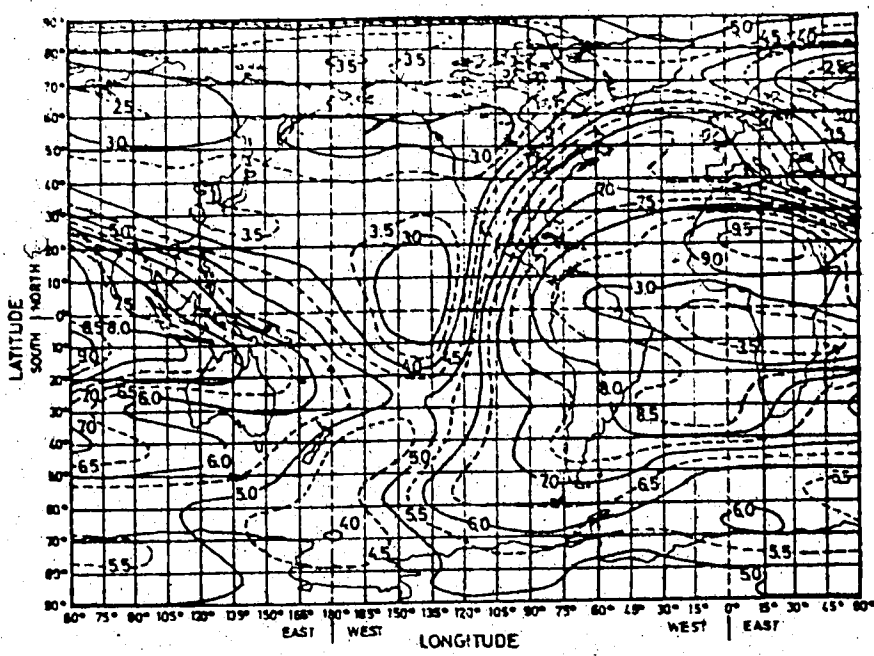
(a) Contour map F_2 critical frequency 1400 GMT December 1963 [50].
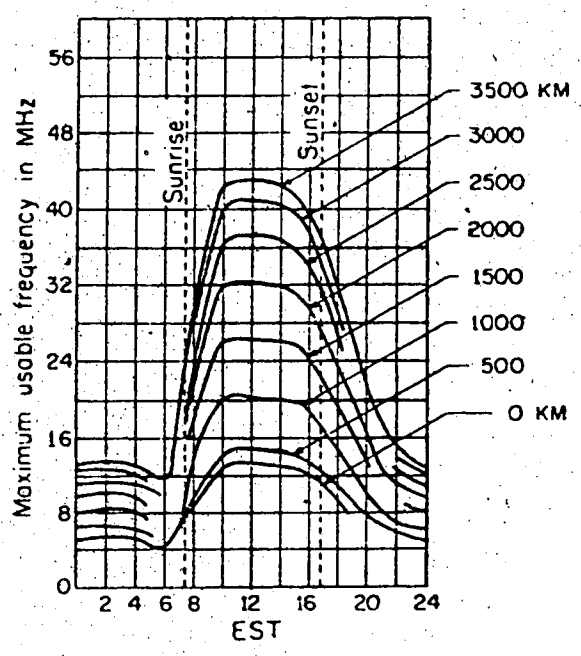
(b) Typical set of MUF curves for a winter month [25].

Fig. 1.3

the speed of light was incorrect (the pulse, composed of a spectrum of frequencies, has a group velocity which decreases in the ionized medium), their simple technique eventually returned a substantial amount of data, especially with respect to layer critical frequencies and virtual heights of reflection.

The technique suffers from the disadvantage of the double path length which requires that the sounding equipment employ the use of a high power transmitter and sensitive receiver. Its usefullness from a radio-astronomical point of view is limited, however, simply because it is incapable of determining quantitatively the degree to which radiation passing downward through the ionosphere is absorbed. The value of soundings, instead, lies in the support role which they play in the correct assessment of data gathered from riometer observations. This will be more evident from the discussion of section 4.2.2.

1.3.4 Standard Riometry

The introduction of the "cosmic noise" method of ionospheric investigations by Shain [8], in 1951, was of primary importance to the knowledge of ionospheric effects on wave propagation at frequencies greater than the ionospheric critical frequencies and was of particular value to radio astronomers.

The method employs the basic assumption that the cosmic noise background radiation observed by a vertically directed receiving antenna beam for any given sidereal time (time relative to the distant stars) is constant, and hence any fluctuation in this level of radiation at the same sidereal time is due to the intervening ionosphere. In theory, the principle is simple; however, its implementation requires the use of very

stable receivers. The real breakthrough came during the International Geophysical Year 1957-58, when Little and Leinbach [9], [10] developed the riometer. The advantage of the riometer was that it continuously compared the antenna noise power with that of a local noise source and equalized the difference; hence, it acted essentially as a sensitive nullmeter where gain fluctuations were relatively unimportant. Then, by monitoring the current of the noise source, the power of the received radiation could be recorded.

Before the riometer could be of any use to radio astronomers, however, a quiet day curve (Q.D.C.), i.e. the cosmic noise level received in the absence of the ionosphere and measured over one sidereal day, had to be determined. Unfortunately, this necessitated the continual monitoring of cosmic noise radiation for a period of approximately one year. The reason for this is, assuming that for a given frequency the condition of negligible absorption does occur, its most probable time of occurrence is found to be just before sunrise [11], [12], [13] regardless of season. Hence, the entire galactic background which may pass directly above the observing station, must have been monitored at some time of the year during this period of expected negligible absorption. Herein lies the problem, since the length of time required for all relevant portions of the sky to be monitored during the best observing period, depends on the rate of rotation and revolution of the earth. In other words, the length of time required to determine the Q.D.C. is largely beyond the control of the observer and is approximately one year. During this time the reference noise source's current-versus-power characteristic , cable attenuation, antenna gain, etc., must all remain extremely stable.

Another possible drawback is that the nighttime absorption may not

in fact be negligible. Several papers (e.g. Mitra and Shain [14]; Lusignan [11]; Schwentek and Gruschwitz [12])have reported high average nighttime absorption values and it seems likely that uncertainties in absorption measurements due to this problem of residual absorption will be worse if measurements are made in a year of high solar activity. As is noted by Heisler and Hower, excellent agreement between experimental and calculated absorption data is achieved for January 1964, a solar minimum year, but using the data of Lusignan a residual absorption of 1.2 dB is found for March 1959, a solar maximum year.

Through a simple extension of the riometry technique, it is possible to eliminate the uncertainty in the measurements due to residual absorption,if indeed it exists, and at the same time reduce the lengthy period required for data acquisition.

1.3.5 The Dual-Polarized Method of Riometry

The effect of the earth's magnetic field on radio wave propagation in the ionosphere is to split the wave into two parts of opposite polarization. One of these waves propagates as if no magnetic field were present and hence is called the ordinary wave (or ray); the other, known as the extraordinary wave, can be affected quite severely.

The electrons which are set in motion due to these propagating waves are continually colliding with heavier particles. The net result of these collisions is to extract energy from the wave, which manifests itself to receivers on the ground as ionospheric absorption. This absorption, however, does not equally affect the two waves, but instead, the extraordinary wave suffers more absorption than the ordinary wave. As has been shown in a paper by Little, Lerfald and Parthasarathy [15],

this effect can be used to determine the Q.D.C. if the observing frequency
is in the 5-15 MHz range. Here the lower frequency limit is set by the
average critical frequency of the ionosphere above the observing station
and the upper, by too low an absorption, making the difference in power
levels between the two rays difficult to detect. Because, as is shown
in Figure 1.4, average absorption depends on latitude, the useful frequency
range will in turn depend on the location of the observing station.
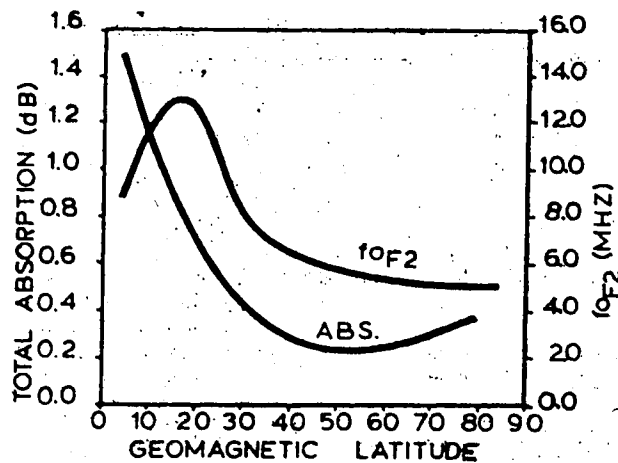
Fig. 1.4 Average zenithal absorption at 32 MHz and F_2 critical
frequency as a function of geomagnetic latitude [53].

In 1956 and again in 1961-62 workers at College, Alaska (geomag.
lat. 65°N) used this method as an alternative to the standard riometry
technique at 5, 10 and 20 MHz and they were able to determine the Q.D.C.
not only more quickly but also more accurately. They found that at
their latitude, the 10 MHz data was particularly amenable to this
technique. However, scientists at the Dominion Radio Astrophysical
Observatory near Pentiction, B.C. (geomag. lat. 55°N) at 22 MHz were

unable to detect any level difference (private correspondence). Since the

average absorption values between geomagnetic latitude 40°N and 70°N are

not significantly different, it would be expected that a riometer

frequency of approximately 10 MHz would also be suited to the method of

Little, Lerfald and Parthasarathy in this latitude range. Due to the

location of the proposed University of Alberta riometer at Seven Mile

Flat (geomag. lat. 60°N) and operation at a frequency of 12.4 MHz, it

would appear that conditions are well suited to the application of

the riometry technique mentioned above, i.e. the dual-polarized method.

As will be explained in more detail in Chapter 4, this method of

riometry, which requires the measurement of the extraordinary ray and

ordinary ray powers, offers the rather substantial advantage of

extracting from the acquired data, absolute power measurements of the

quiet day cosmic noise levels. Hence, observations need not be restricted

to periods of minimum absorption amounting to only 4 or 5 hours per day

but may be made over the full 24 hours, natural and man-made interference

being the only limiting factors.

1.3.5.1 Antenna Requirements

The measuring equipment required for the implementation of the dual

polarized method of riometry is essentially the same as that for standard

riometry. The only major change is in the antenna system.

As was mentioned in the section above, the effect of the earth's

magnetic field is to split an incoming randomly polarized wave into two

components of opposite polarization. In the middle and high latitudes of

the earth these components exhibit nearly circular polarization. Hence,

the method of measurement differs from the standard riometry technique

in that its antenna system must respond to waves of left and right

circular polarization rather than linear polarization.

Several types of circularly polarized antennas were considered,

including crossed dipoles, helices and conical-logarithmic spirals.

As will be explained in greater detail in Chapter 4, for best results from

the dual-polarized method, the antenna system of the riometer was

required to be responsive to circular polarization over most of its beam,

have a circularly symmetric beam with half-power beam width (HPBW) of

approximately 60° and be devoid of side lobes. In addition, ease of

construction of the antenna was of concern, though secondary in importance.

Crossed dipoles were desirable because of the simplicity of their

structure. Their off-axis response to circular polarization was not

considered satisfactory, however, and they were rejected largely for this

reason.

Helices easily met the beam width requirement with a single element

but they appeared to suffer from side lobes. Although little information

was available on their off-axis response to circular polarization, what

there was tended to indicate that it was poor as well. For these

reasons, helices were not considered acceptable.

Fortunately, rather extensive study had been done by Dyson [16],

[17], [18] on the conical-logarithmic spiral, so that a good estimation

of antenna properties could be obtained. It was found that this type

met all the primary antenna requirements admirably well. In addition,

the inherent frequency independent nature of the conical-logarithmic

spiral made it especially attractive because of the added dimension it

afforded to the riometer's usefullness. Riometer observations at

several frequencies make it possible to derive electron density profiles

with height; information which is of considerable scientific importance.

The only major drawback of this antenna was its height which for the characteristics desired was on the order of 30 meters at 12.4 MHz. This was considered excessive and ways of reducing it were investigated. Dyson had shown that because there is a relatively narrow active region on a conical spiral (see Figure 1.5), it can be truncated without significantly degrading the properties of the original untruncated spiral. Moreover, Dietrich and Long [19] suggested that wide cone angle conical spirals exhibit much the same properties as the small cone angle spirals $(2\theta_o \leq 45°$; see Figure 1.5) tested by Dyson, and they afford considerable size reduction.

It was, therefore, the opinion of the author that because of the suitability of the conical-logarithmic spiral antenna to the riometer application, it was worth-while to attempt to reduce its height to a more acceptable level. Because not enough was known on the theory of operation of this antenna, the alteration of its parameters beyond those for which empirical data existed, necessitated the determination of the characteristics of the altered conical spiral by experiment. It is apparent that experimenting with antennas which have dimensions on the order of tens of meters would be, to say the least, difficult. Using a high frequency scale model, however, it would be possible to make parameter changes quickly and easily and the results that these changes had on the important radiating characteristics of the antenna, in this case the antenna's axial ratio and power pattern, could be more easily measured. (The axial ratio expresses the relative response of an antenna to left and right circularly polarized waves and is discussed in more detail in section 6.2.) To this end a compact microwave antenna test range, which

operated at a frequency near 1 GHz, was designed, and constructed atop the Electrical Engineering Building at the University of Alberta.
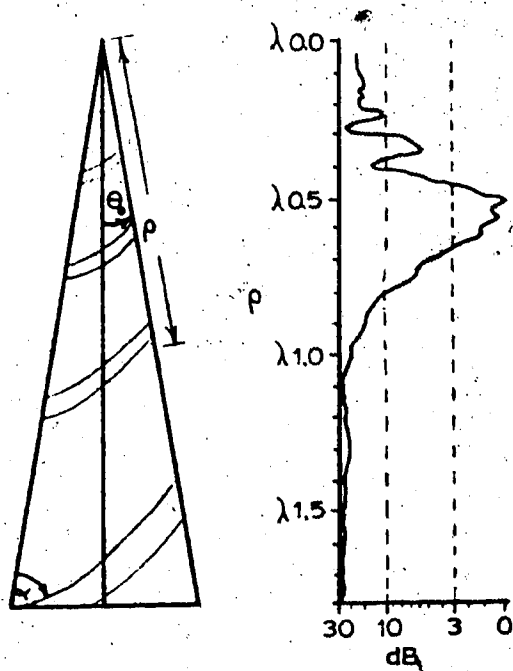
Fig. 1.5 Relative near-field amplitude on a conical spiral with $2\theta_o=20°$, $a=80°$ [18].

At this stage it should be pointed out that, because the pattern and HPBW of both the truncated conical spirals and wide cone angle conical spirals were fairly well defined by Dyson and Dietrich and Long, and since it was expected that the pattern of the riometer antenna would be measured after construction of the full-scale antenna, the axial ratio as a function of zenith angle was the prime factor to be determined.

1.3.5.2 Scientific Importance of the Riometer Measurements

Apart from its prime function of accurately determining the ionospheric absorption, the dual-polarized riometer is capable of supplying additional information of scientific importance.

As mentioned earlier, with conical spiral antenna elements multifrequency absorption data can be gathered which, as will be outlined in section 2.6.1, can be used for the derivation of electron density profiles with height for the time of observation. In fact the single frequency absorption data will also give some indication of the electron densities in the absorbing layers and the heights at which absorption takes place.

The derived sky temperatures for the unattenuated cosmic noise will be important for comparison with the data of Andrew [20].

Eclipses of the sun provide rare opportunities for study of ionospheric properties with respect, in particular, to electron recombination rates [21]. The total solar eclipse of February 26, 1979, to be visible from the northwest United States and Canada may provide just such an opportunity.

The magnetospheric radiation of Jupiter is still largely uninvestigated and polarization studies of this radiation at 12.4 MHz would be of considerable scientific value. The polarization of the Jovian radiation appears to be, at least at the lower frequencies, primarily circularly polarized. Whether the riometer, with its small collecting area of approximately $46m^2$, will be able to detect Jupiter will depend largely on the planet itself. Jupiter is by no means a constant radiating source but instead, displays periods of high activity [22]. At 12 MHz not enough is known about the power levels radiated by this planet but at 20 MHz the average flux density of the Jovian radiation is 10^{-21} Wm^{-2} Hz^{-1} [23]. Douglas suggests that it appears likely that this flux density increases as frequency decreases, at least down to 10 MHz. Thus, for a system bandwidth of 10 KHz radiation from Jupiter should be at least

2% of the galactic sky background.

It is, therefore, apparent that the dual-polarized method of riometry, apart from the advantage of being able to determine the Q.D.C. more accurately and more quickly than alternate methods, is advantageous for several reasons. The dual-polarized riometer should be an extremely useful instrument.

CHAPTER 2

MAGNETO-IONIC THEORY

2.1 Introduction

Details of the magneto-ionic theory are available in the appropriate literature [1], [3], [24], [25]. Only the main assumptions and important steps used in the derivation of its basic equations are presented here.

2.2 The Classical Appleton-Hartree Equations

The medium in which propagation is assumed to exist will first be defined. The ionosphere will be modelled as a region of equal positive and negative charges, uniformly distributed and hence, exhibiting no net space charge. A steady magnetic field $\bar{B}$ permeates this region and without loss of generality, will be considered to lie in the y, z plane (see Figure 2.1). The wave propagates in the z direction and at an angle of θ relative to the imposed magnetic field.
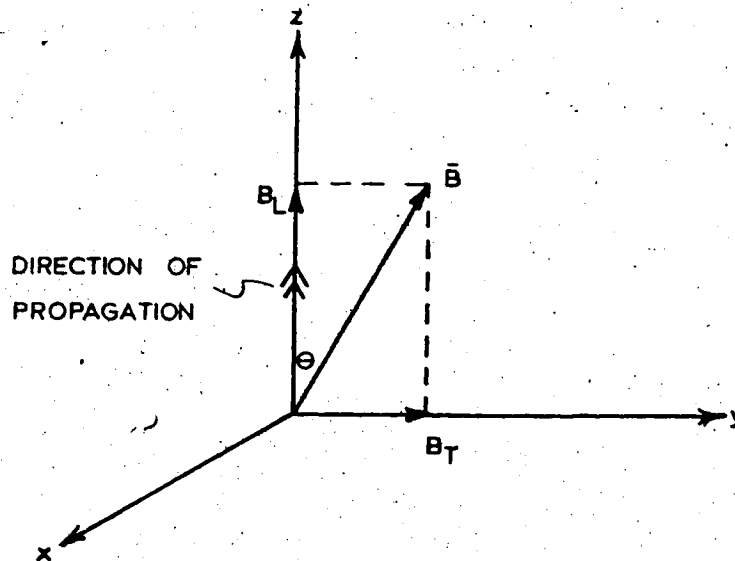
Fig. 2.1 Direction of wave propagation and magnetic field relative to coordinate system.

It is assumed that the fields vary harmonically, i.e. with exp($j\omega t$), and thus the motion of the charged particles is harmonic, although owing to their much larger mass the positive ions are considered relatively immobile and thus unimportant in the propagation of the wave. Due to this relative immobility, the electrons experience collisions with the positive ions as well as with the neutral air molecules so that a combined collision frequency, $\nu = \nu_i + \nu_n$, exists.

In phasor form then, the equation of motion for the electrons becomes:

$$q\overline{E} + q(\overline{v} \times \overline{B}) = j\omega m\overline{v} + m\nu\overline{v}$$

where $q = -e = -1.6 \times 10^{-19}$ coulomb. In rectangular coordinates and after some rearranging, the three components of the above equation become:

$$-e\, E_x = j\omega m \left(1 - j\frac{\nu}{\omega}\right) v_x + e(v_y B_L - v_z B_T) \quad \text{(a)} \qquad \text{(2.1)}$$

$$-e\, E_y = j\omega m \left(1 - j\frac{\nu}{\omega}\right) v_y - e\, v_x B_L \qquad \text{(b)}$$

$$-e\, E_z = j\omega m \left(1 - j\frac{\nu}{\omega}\right) v_z + e\, v_x B_T \,. \qquad \text{(c)}$$

If the medium has an electron density N, and if it is assumed that a movement of electrons constitutes a conduction current, then,

$$\overline{J} = -N\, e\, \overline{v} \qquad \text{(2.2)}$$

and using rationalized MKS units, Maxwell's equations for the medium become,

$$\nabla \times \overline{H} = j\omega\epsilon_o \overline{E} + \overline{J} \qquad (2.3)$$

$$\nabla \times \overline{E} = -j\omega\mu_o \overline{H} \qquad (2.4)$$

$$\nabla \cdot \overline{H} = 0$$

$$\nabla \cdot \overline{E} = -\frac{Ne}{\epsilon_o}$$

Now substituting eq. (2.2) into eq. (2.1) and solving for $\overline{E}$ in terms of $\overline{J}$,

$$\overline{E} = \frac{1}{j\omega\epsilon_o X} \begin{bmatrix} -U & jY_L & -jY_T \\ -jY_L & -U & 0 \\ jY_T & 0 & -U \end{bmatrix} \overline{J} \qquad (2.5)$$

where the following simplifying definitions have been used:

$$X = \frac{\omega_p^2}{\omega^2} \; , \quad Y_L = \frac{\omega_L}{\omega} \; , \quad Y_T = \frac{\omega_T}{\omega}$$

$$U = 1 - jZ \; , \quad Z = \frac{\nu}{\omega}$$

$$\omega_p = \sqrt{\frac{Ne^2}{\epsilon_o m}} = \text{angular plasma frequency}$$

$$\omega_B = \frac{eB}{m} = \text{angular gyro frequency}$$

$$\omega_L = \frac{eB_L}{m} , \quad \omega_T = \frac{eB_T}{m} .$$

Equation (2.5) is, therefore, a constitutive equation for the anisotropic medium and can be more simply expressed as

$$\overline{E} = \overline{\sigma}^{-1} \cdot \overline{J}$$

where $\overline{\sigma}$, the dielectric conductivity, is a tensor quantity.

Using Maxwell's equations (2.3) and (2.4) and assuming that the field quantities vary with position only as $\exp(-\gamma_w z)$, where γ_w is the wave propagation constant, then another relationship can be obtained between $\overline{J}$ and $\overline{E}$ such that

$$\overline{J} = -j\omega\varepsilon_o \begin{bmatrix} 1+\gamma_w^2 c^2/\omega^2 & 0 & 0 \\ 0 & 1+\gamma_w^2 c^2/\omega^2 & 0 \\ 0 & 0 & 1 \end{bmatrix} \overline{E} . \quad (2.6)$$

If now the complex refractive index is defined by

$$n = -\frac{j\gamma_w c}{\omega} = \mu - \frac{jkc}{\omega} . \quad (2.7)$$

where n = complex refractive index of the medium

μ = refractive index (real part of n)

k = absorption coefficient

c = speed of light in free space,

then when eq. (2.7) is substituted into eq. (2.6) and the result into eq. (2.5), it can be shown that

$$\overline{0} = \begin{bmatrix} U(n^2-1)+X & -jY_L(n^2-1) & -jY_T \\ jY_L(n^2-1) & U(n^2-1)+X & 0 \\ -jY_T(n^2-1) & 0 & -U+X \end{bmatrix} \overline{E} \qquad (2.8)$$

The condition for a solution to exist is that the determinant of the coefficient matrix in eq. (2.8) must vanish. The result is a quadratic in n^2 which, when solved, yields the equations

$$n^2 = 1 - \frac{X}{1 - jZ + jY_L R} \qquad (2.9)$$

$$R = \frac{E_x}{E_y} = \frac{1}{Y_L}\left\{ \frac{Y_T^2}{2(1-X-jZ)} \mp \left(\frac{Y_T^4}{4(1-X-jZ)^2} + Y_L^2 \right)^{1/2} \right\} \qquad (2.10)$$

where the upper sign in equation (2.10) refers to the ordinary ray and the lower sign to the extraordinary ray.

2.3 The Quasi-Longitudinal Approximation

In the middle and high latitudes of the Northern Hemisphere the earth's magnetic field at the relatively low height of about 100 km, which represents an effective upper limit to the absorbing region, is closely aligned to the direction of radiation that would be received by a vertically directed riometer antenna beam (see Figure 2.2). If θ, the angle between the magnetic field of the earth and the direction of propagation, is small, the condition
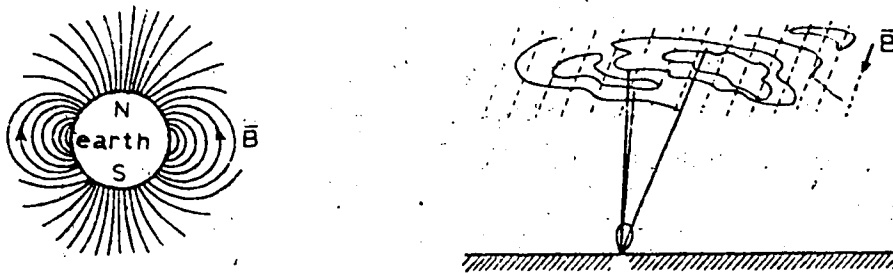
Fig. 2.2 The earth's magnetic field and its direction relative to the
the radiation received by a vertically directed antenna beam.

$$\frac{Y_T^2}{2|Y_L|} \ll |1-X-jZ| \qquad (2.11)$$

may exist. Putting the above equation in a more meaningful form results
in

$$\frac{\omega_B}{\omega} f(\theta) \ll |1-\omega_p^2/\omega^2 - j\nu/\omega| \qquad (2.12)$$

where

$$f(\theta) = \sin^2\theta/2\cos\theta .$$

The gyro frequency, f_B, over most of North America [26] is approx-
imately 1.5 MHz and the largest critical frequency to be encountered
should be that of the daytime F_2 layer, about 8 MHz. Then for an
operating frequency of 12.4 MHz, and assuming a collision frequency that
is insignificant with respect to ω, for worst case conditions (2.12)
becomes

$$f(\theta) \ll 4.8 \qquad \qquad (2.13)$$

For an order of magnitude difference between the left and right hand
sides of eq. (2.13), the graph of $f(\theta)$ versus θ in Figure 2.3 indicates
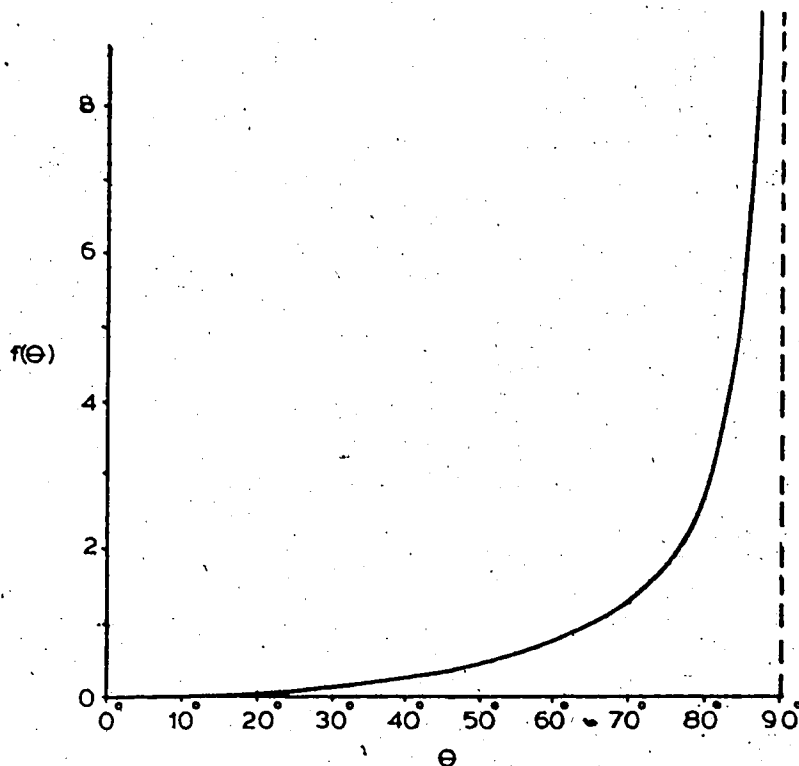
Fig. 2.3 Graphical illustration of function $f(\theta)$.

that the wave must propagate within 50° of the magnetic field. For a
riometer that will be located at 60°N geomagnetic latitude (dip> 70°,[68])
and which will receive radiation from a vertically directed antenna beam
this seems likely. Then assuming that an order of magnitude difference
between the two sides of eq. (2.11) is sufficient justification for
invoking this inequality and using it in eqs. (2.9) and (2.10),
the equations which result are known, as the Appleton-Hartree equations
for "quasi-longitudinal propagation." The inequality of eq. (2.11) is
thus referred to as the quasi-longitudinal approximation.

2.3.1 Wave Polarization

Using the quasi-longitudinal approximation in eq. (2.10)

$$R = \frac{E_x}{E_y} \sim 1 \ \exp \ (\mp j\pi/2) \tag{2.14}$$

for a wave passing downwards through the ionosphere in the Northern
Hemisphere. Recalling that the field quantities vary as $\exp(j\omega t - \gamma_w z)$
then if at $z=0$ the x and y components of the electric field vector in
the wave front can be represented as

$$E_x = E_1 \sin(\omega t)$$

$$E_y = E_2 \sin(\omega t + \Delta)$$

equation (2.14) shows that $E_1 \sim E_2$ and $\Delta = \pm 90°$. Hence, if the upper
sign is used (ordinary ray) the electric field vector (see Figure 2.4)
is seen to be rotating in the clockwise direction as the wave approaches.

$\Delta = -90°$ (E mode) $\Delta = +90°$ (O mode)
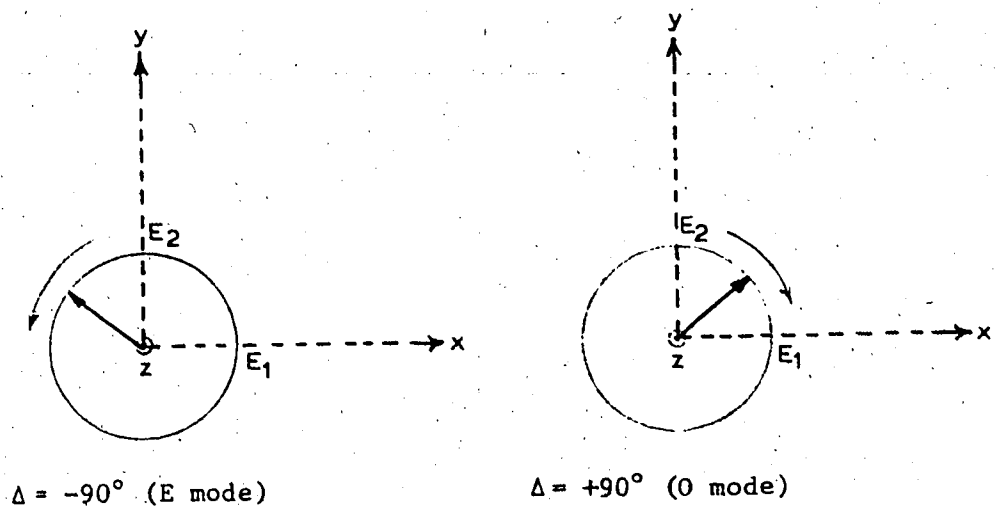
Fig. 2.4 Illustration of polarization of fields, wave approaching.

Using the IRE definition (1942), this wave is said to be left circularly polarized (LCP). Similarly if the lower sign is used (extraordinary ray) the electric field vector rotates in the counter clockwise direction, wave approaching, and is said to be right circularly polarized (RCP).

2.3.2 Wave Propagation Constant and the Absorption Coefficient

Since $n = \mu - jkc/\omega$ and recalling that the propagation constant γ_w, was related to n by $\gamma_w = j\omega n/c$, then

$$\exp(j\omega t - \gamma_w z) = \exp[j\omega(t - \mu z/c)]e^{-kz}$$

and the field quantities will be attenuated as the wave moves along its path.

Using the quasi-longitudinal approximation in equation (2.10), and also the fact that the square of the complex refractive index can be written as $n^2 = \mu^2 - (kc/\omega)^2 - j2\mu kc/\omega$ then, after equating real and imaginary terms

$$\frac{2\mu kc}{\omega} = \frac{X\ Z}{(1 \pm Y_L)^2 + Z^2}$$

After some rearranging and substituting in the appropriate values for X, Z and Y_L defined earlier

$$k = \frac{e^2}{2m\varepsilon_o c} \frac{1}{\mu} \frac{N\ \nu}{\nu^2 + (\omega \pm \omega_L)^2}$$

which, when the constant first term on the right hand side of the equal sign is numerically evaluated, becomes

$$k = \frac{5.31 \times 10^{-6}}{\mu} \frac{N\ \nu}{\nu^2 + (\omega \pm \omega_L)^2} \quad \text{nep/m} \qquad (2.15)$$

2.4 Deviative Absorption

Referring once again to Figure 1.1, it is seen that at a height of 100 km the electron density is approaching its maximum value; however, the electron collision frequency is less than 2% of any operating frequency within the H.F. band. If the ratio $Z = \nu/\omega$ is assumed to be approximately zero, examination of equations (2.9) and (2.10) reveals that the complex refractive index is entirely real and may be expressed

as

$$n\Big|_{\nu=0} = \mu = \left[1 - \cfrac{f_p^2/f^2}{1 - \cfrac{f_T^2/f^2}{2(1-f_p^2/f^2)} \pm \left[\cfrac{f_T^4/f^4}{4(1-f_p^2/f^2)} + \cfrac{f_L^2}{f^2} \right]^{1/2}} \right]^{1/2} \qquad (2.16)$$

Above 100 km the ionosphere for most high frequencies appears as a region of slowly varying index of refraction. Hence, in general, the wave will follow a slightly curved path in the ionosphere. There are times, however, when the electron density will be large enough and vary quickly enough that the ray will be severely bent or even reflected. These conditions will occur when the frequency of the propagating wave is at or near a critical frequency of the ionosphere.

For vertical incidence and when the operating frequency f is greater than the gyro frequency the critical frequencies can be found from eq. (2.16) by setting μ=o. When this is done it can be shown that

$$f_{p1}^2 = f(f-f_B) \qquad \text{(extraordinary ray)}$$

$$f_{p2}^2 = f^2 \qquad \text{(ordinary ray)}$$

and

$$f_{pi} = \frac{1}{2\pi} \sqrt{\frac{N_i e^2}{\varepsilon_o m}} = \text{plasma frequency for level i}.$$

Typically, the highest critical frequencies are those of the day time F_2 layer since this region contains the highest electron densities. For the ionosphere above Seven Mile Flat, the ordinary ray critical

frequency of the F_2 layer, $f_{o_{F2}}$, will be about 8 MHz.

Although the above critical frequencies were derived from an equation which assumed the collision frequency was equal to zero in the region of consideration, i.e. above 100 km, they would be equally applicable if, as is the actual case, the ratio $Z = \nu/\omega$ was very small with respect to 1-X, yet still finite. Near critical frequencies, the refractive index, μ, is still approximately zero and because the group velocity of the wave is related to μ by $V_G = \mu c$, the wave spends more time in the medium. Because of this and the fact that a finite collision frequency does exist, near a critical frequency the wave becomes more susceptible to the effects of collisions, and absorption will occur. Because energy is extracted from the wave during the time that it is being retarded or deviated within the medium, this form of absorption is referred to as deviative absorption.

The significance of the above development is that if cosmic waves do not reach the ground for whatever reason, reflection or absorption, the cosmic radiation received by a ground based riometer will be less than that received if the ionosphere were absent. If the galactic sky background is to be accurately measured, the operating frequency of the riometer must be sufficiently above the highest critical frequency of the ionospheric layers (approximately 3 times $f_{o_{F2}}$)at the time of observation. The elimination of data acquired when critical frequencies are too high can be accomplished with the aid of ionosonde records taken simultaneously with riometer observations. If an ionospheric sounder is not available riometer observations should be restricted to nighttime periods when critical frequencies are sufficiently low.

2.5 Non-Deviative Absorption

These are two types of absorption which can occur in the ionosphere, the deviative type, described in the previous section, which is most severe near critical frequencies and the non-deviative type, described below, which varies approximately as $1/f^2$ with frequency (see Figure 2.5).
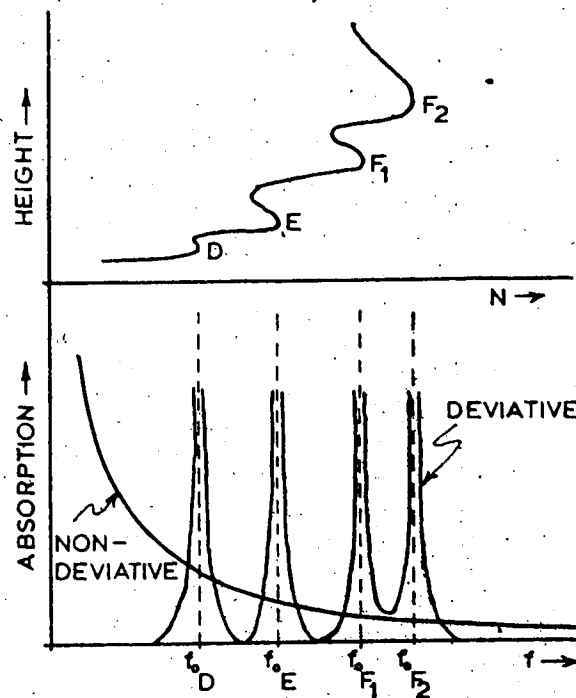
Fig. 2.5 Absorption effects in the ionosphere

In regions where the electron density is small, $\mu \sim 1$ and the region where absorption takes place is said to be "non-deviating" because it does not deviate or retard the wave. From equation (2.15) the absorption coefficient can now be written as

$$k = \frac{5.31 \times 10^{-6} \, N \, \nu}{\nu^2 + (\omega \pm \omega_L)^2}$$

Because k depends on the electron density and collision frequency

which are both functions of height, the absorption coefficient will also
depend on height i.e. $k=k(h)$. Then the total absorption that the wave
experiences along its path, defined as the ratio of the amplitude (E_o)
of a wave which travels a distance $\Delta h = h_2-h_1$ in the absence of
absorption, to the amplitude (E) after travelling in the presence of
absorption, is given by

$$A = \frac{E_o}{E} = e^{\int k(h)dh}$$

or

$$A_{dB} = 20 \log e^{\int k(h)dh} = 4.6 \times 10^{-5} \int_{h_1}^{h_2} \frac{N(h)\nu(h)dh}{\nu(h)^2 + (\omega \pm \omega_L)^2}.$$

In regions where $\nu(h)$ is on the order of, or greater than the
operating frequency (altitudes less than 60 km for operating frequencies
in the HF band), the total path absorption varies as $N(h)/\nu(h)$. However,
at these altitudes $N(h)$ is extremely small ($<10^3$ electrons/cm^3) and
decreases very rapidly with decreasing height while at the same time
$\nu(h)$ is increasing very rapidly. It would therefore be expected that
negligible absorption would take place below about 60 km. By the same
token, at altitudes > 100 km the collision frequency is small and
decreases very rapidly with height while $N(h)$ also decreases but much
slower; therefore it would again be expected that except near critical
frequencies (deviative absorption) little absorption would occur. The
result of the preceding is that the region where most non-deviative
absorption occurs is fairly well defined as lying somewhere between 60
and 100 km.

If for a given operating frequency f, the primary region of
absorption occurs where $\nu(h) >> 2\pi (f \pm f_L)$, absorption becomes in-

dependent of the effective operating frequency of the wave and it would

be expected that the measured power levels of the extraordinary and

ordinary modes would be the same. When $\nu(h)$ is on the order of

$2\pi(f \pm f_L)$ the absorption should vary as f^{-1} and if the absorbing

region conditions are such that $\nu(h) \ll 2\pi(f \pm f_L)$ the absorption

should vary as f^{-2}. In practice, all three may occur as the wave

traverses the lower ionosphere and therefore the absorption's frequency

dependence is often expressed as

$$A_{dB}(f) = C \; f^{-\eta} \qquad\qquad C = \text{constant.} \qquad\qquad (2.17)$$

As will be seen in Chapter 4, this absorption versus frequency relation-

ship, which applies to both the extraordinary wave and the ordinary

wave, forms the base on which the dual-polarized method of riometry is

built.

2.6 The Sen-Wyller Equations for Non-Deviative Absorption

While the development of equation (2.9) is convenient for its

simplicity, it is not strictly true because it fails to take into account

the dependence of collision frequency on electron energy. Sen and

Wyller investigated this problem in their 1960 paper and their formula

for the refractive index for the case of longitudinal propagation

(i.e. $\theta = 0$) is

$$n^2 = \{1 - \frac{\omega_p^2(\omega \mp \omega_B)}{\omega \, \nu_m^2} C_{3/2}(\frac{\omega \mp \omega_B}{\nu_m})\} - j\{\frac{5\omega_p^2}{2\omega\nu_m} C_{5/2}(\frac{\omega \mp \omega_B}{\nu_m})\} \quad (2.18)$$

where, as usual, the upper sign corresponds to the ordinary ray and the

lower sign corresponds to the extraordinary ray, and

$$C_p(x) = \frac{1}{p!} \int_0^\infty \frac{\xi^p e^{-\xi}}{\xi^2 + x^2} d\xi$$

$$\xi = \frac{mV^2}{2kT}$$

V = electron velocity

ν_m = collision frequency corresponding to the most probable

electron velocity.

As is pointed out in their paper, rigorous use of the Sen-Wyller

formula can be avoided with negligible error introduced, if $\nu < .1\omega$

over the effective absorbing region. From Figure 1.1 and recalling

that the effective absorbing region lies between 60 and 100 km, for

an operating frequency of 12.4 MHz this condition seems valid over

most of the absorbing region. The Appleton-Hartree formula for

longitudinal propagation could then be used in place of equation (2.18)

if ν is replaced by $\frac{5}{2} \nu_m$. It should be pointed out, however, that

justification for using the dual-polarized technique for ionospheric

absorption measurements does not depend on the validity of the Appleton-

Hartree or Sen-Wyller formulas. As long as an absorption versus

frequency relationship of the form indicated by equation (2.17) can be

obtained, the dual-polarized riometry technique is applicable.

When the quasi-longitudinal approximation is invoked more error

is introduced; however, Benson [27] has shown that for an operating

frequency greater than 10 MHz and an angle of propagation θ less than

$40°$ the error introduced is less than 1%.

The formulas derived by the Appleton-Hartree development will, therefore, not be significantly in error for an operating frequency of 12.4 MHz if ν is replaced by $\frac{5}{2} \nu_m$. Assuming some electron density distribution with height, these formulas can then be used to calculate the absorption that the extraordinary ray and ordinary ray should encounter as they traverse the lower ionosphere. For frequencies such that the condition $\nu < .1\omega$ is not valid or if greater accuracy is required, equation (2.18) should be employed, rigorous use of which requires a computer.

2.6.1 Derivation of Electron Density Profiles

As was mentioned above, the absorption which should be encountered by a wave traversing the lower ionosphere can be calculated from the theory, if the electron density distribution with height is known. This in practice is a difficult relationship to obtain. However, by expressing the electron density profile with height $N(h)$ as a finite power series of the form

$$N(h) = a_1 h + a_2 h^2 + \ldots + a_n h^n ,$$

the coefficients may be determined from multifrequency riometer measurements made at n different frequencies by solving the appropriate Appelton-Hartree or Sen-Wyller absorption equations [28], [29], [30]. The absorption profile for a given frequency is then obtained by substituting the derived electron density profile back into the absorption equation.

CHAPTER 3

THEORETICAL AND PRACTICAL ASPECTS

OF RIOMETER EQUIPMENT

This chapter begins with an explanation of some of the terms and concepts frequently used in the discussion of noise measuring systems. It then proceeds to use these terms and concepts in the discussion of the basic riometer receiving systems. Finally, an introduction to the riometer equipment is presented with past problems and some possible future improvements outlined.

3.1 Noise Power and Equivalent Temperature

3.1.1 Antenna Temperature

If as indicated in Figure 3.1 a black body enclosure exists such that the space within it is electrically shielded from the outside and at uniform temperature T, and if the inside of its walls are lined with a perfect absorber, then the radiation emitted by the walls will be such that a lossless antenna will "see" (through its directional pattern) a temperature of T. It can then be shown [22] that a power $P = kTB$, where k is Boltzmann's constant and B is the noise bandwidth of the receiving system, could be extracted from it.

If the temperature was not uniform within the volume of the
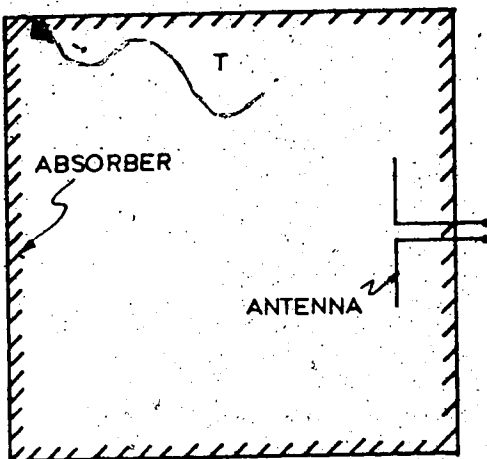
Fig. 3.1 Antenna in black body enclosure at uniform temperature T.

black body enclosure but varied over its extent as $T(\theta,\phi)$, then the temperature of the volume as seen by an antenna with normalized power pattern $P_n(\theta,\phi)$ and beam solid angle Ω_A would be

$$T_A = \frac{1}{\Omega_A} \iint T(\theta,\phi) \, P_n(\theta,\phi) \, \sin\theta \, d\theta \, d\phi \ .$$

3.1.2 Noise Power from a Linear Two-Port

For a linear two-port as shown in Figure 3.2 of power gain G and equivalent temperature T referred to the input, if a power P_{in} is fed into its input terminals the output power available is

Fig. 3.2 A linear two-port.
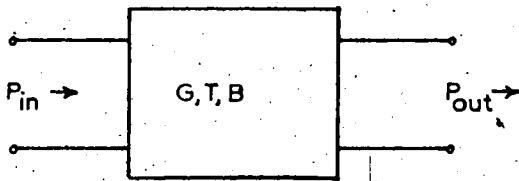
$$P_{out} = G \, P_{in} + G \, k \, T \, B \ . \quad (3.1)$$

If n matched linear two ports, each of gain G_i and equivalent temperature T_i, are cascaded (see Figure 3.3) and if the noise bandwidth B of the system is set by the last stage, then the output power available from the
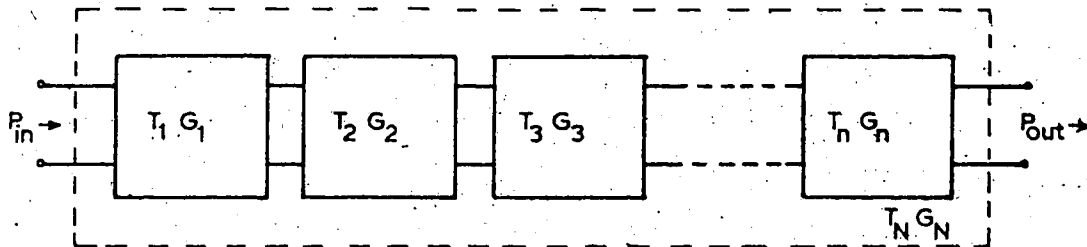
Fig. 3.3 n cascaded linear two-ports.

network is given by the expression

$$P_{out} = G_N P_{in} + G_N k T_N B$$

where

$$G_N = G_1 \cdot G_2 \cdot G_3 \cdots G_n$$

and

$$T_N = T_1 + \frac{T_2}{G_1} + \frac{T_3}{G_1 G_2} + \cdots \frac{T_n}{G_1 G_2 \cdots G_{n-1}} \tag{3.2}$$

Thus the entire network can be treated as a single linear two-port with
gain G_N and equivalent temperature T_N.

An examination of equation (3.2) shows that if the gain G_1 of the
first stage is very large, the noise contributions due to the stages
which follow will be negligible and the noise equivalent temperature
of the network will be essentially that of the first stage. This is a
very useful property in the design of low noise receivers.

3.1.2.1 Noise Equivalent Temperature of an Active Linear Two-Port

For a linear two-port of noise figure F and gain G, it can be
shown that the output power for input power P_{in} is given by

$$P_{out} = G P_{in} + G k(F-1) T_o B \tag{3.3}$$

where $T_o = 290°K$ due to the IEEE definition of noise figure. Comparing
equations (3.1) and (3.3) shows that the noise equivalent temperature
of the active device is $T = (F-1)T_o$.

3.1.2.2 Noise Equivalent Temperature of a Passive Attenuator

For an attenuator at physical temperature T_{phys} and power transmission coefficient ϵ, the power available at its output port for an input power of P_{in} is

$$P_{out} = \epsilon\, P_{in} + k(1-\epsilon)\, T_{phys}\, B. \qquad (3.4)$$

If ϵ can be thought of as the gain of the attenuator, i.e. a gain less than 1, then examination of equations (3.1) and (3.4) shows that the noise equivalent temperature of the attenuator is $T = (1/\epsilon - 1)\, T_{phys}$.

3.2 The Measurement of Cosmic Noise Power

3.2.1 The Power Available at the Receiver Input Terminals

Referring to Figure 3.4, where it has been assumed that the iono-sphere and cosmic noise (sky) background are uniform over the beam width of the receiving antenna, it can be seen that the ionosphere, which is shown as possessing a power transmission co-efficient ϵ_{ion} and being at physical temperature T_{ion}, acts essentially as an attenuator to the incident cosmic noise power.

Therefore from the discussion presented in section 3.1, the power
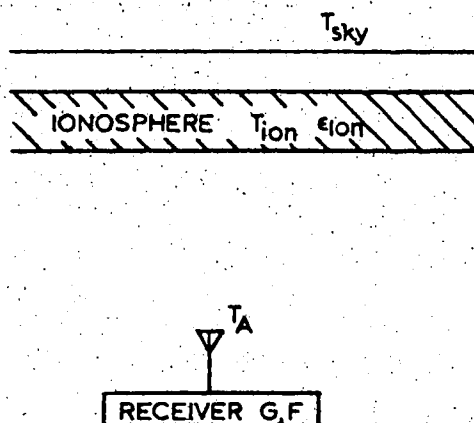
Fig. 3.4 An illustration of a uniform sky background and ionosphere presented to the riometer antenna.

available at the terminals of the antenna is

$$P_A = kT_A B = \epsilon_{ion} kT_{sky} B + k(1 - \epsilon_{ion}) T_{ion} B .$$

If now the antenna is matched to the receiver through a cable and switch of combined transmission coefficient ϵ_c and each of physical temperature T_c, then the power available at the input of the receiver is

$$P_1 = \epsilon_c P_A + k(1-\epsilon_c) T_c B. \tag{3.5}$$

3.2.2 Receiver Systems

The stages referred to in this section as the receiver will in actual fact be those stages of the receiving equipment preceding the detection of power.

3.2.2.1 A Simple Receiving System

From eq. (3.5) and for a matched receiving system as shown in Figure 3.5 with receiver gain G and noise figure F, the power present at the receiver's output terminals will be

Fig. 3.5 A simple self-calibrating receiving system.

$$P_r = G P_1 + Gk(F-1)T_o B + G I \tag{3.6}$$

where I is the interference introduced at the receiver's input. After having satisfied oneself that all parameters are stable, or correcting for those

which are not, any residual variation in P_r is attributed to fluctuations in parameters characterizing the ionosphere and in particular ε_{ion}. It is apparent, however, that this system even with frequent calibrations is extremely sensitive to changes in the gain of the receiver, especially, since typically, the gain of the receiver can be on the order of 100 dB. An improved system developed by Machin, Ryle and Vonberg [31] in which gain fluctuations have little effect, will now be discussed.

3.2.2.2 The Machin, Ryle, Vonberg Receiving System

In the receiving system shown in Figure 3.6 the receiver is switched
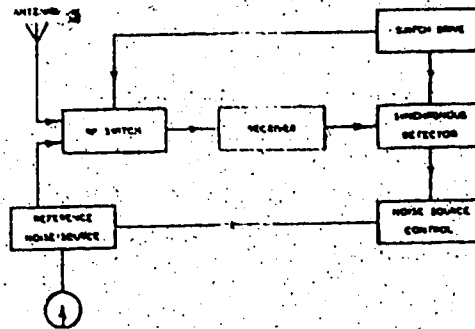
Fig. 3.6 The receiving system as a sensitive null-meter.

at a rapid rate (rapid enough so that the receiver gain does not change significantly over one cycle) between the antenna and a local noise source. Any difference in the power levels appears at the output of the receiver as a component at the switch frequency. By amplifying and detecting this component, the current of the local noise source can be

affected in such a manner as to equalize the powers. If the current through the noise source is proportional to its output power over the usable range, then it is also proportional to the antenna's noise power and hence is the parameter to be recorded. Since the system is basically a null detector, gain variations affect both components equally, and thus are unimportant. This system represents the commonest form of riometer receiving equipment used today.

3.3 Equipment

A schematic of the proposed dual-polarized riometer is shown in Figure 3.7. Except for the antenna system which will be discussed in Chapter 5 the basic equipment blocks will now be examined.

3.3.1 The Receiver

The receiver will be considered to consist of the input band-pass filter, preamplifier and the first and second local oscillators, mixers and intermediate frequency (I.F.) amplifiers.

In order to keep interference at a minimum, the input band-pass filter should have a band width as small as can be attainable without great expense for the center frequency of 12.4 MHz. It is preferable that it be passive so that it does not contribute to a receiver of greater complexity than is required, which can only result in a higher probability of equipment failure and increased power drain.

The gain of the preamplifier should be at least 60 dB in order to eliminate noise contributions due to the mixer and I.F. stages which follow it. Since the noise temperature of the receiver will be set by the input band-pass filter and the preamplifier, a filter of loss less
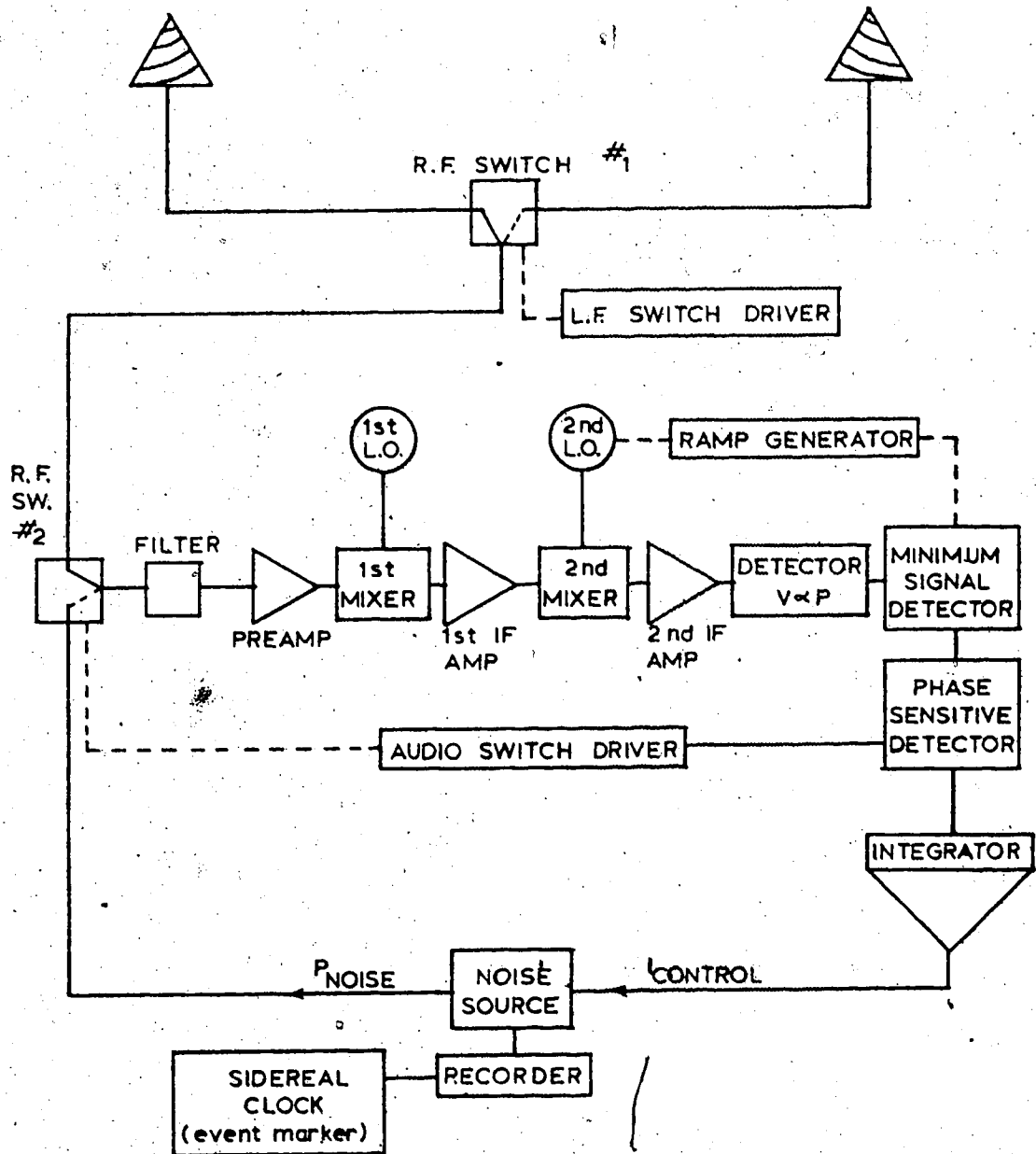
Fig. 3.7 Schematic of the proposed dual-polarized riometer.

than 1.5 dB and a preamplifier with noise figure better than 5 dB are
desirable if the receiver noise temperature is to remain negligible
(< 1%) with respect to the antenna temperature   thus eliminating the
need for corrections in the determination of the sky background
temperature. Placing the preamplifier at the antenna terminals would
also eliminate the noise due to the cable and switches; however, owing
to the severity of weather conditions that can be expected at the
riometer site, it is hoped that this will not be necessary.

The double conversion of the operating frequency was chosen because
of the improved signal-to-noise ratio which can be obtained over the
single conversion format.

3.3.1.1 The Swept Frequency Minimum Signal Detector

Because the cosmic noise signals to be received are very weak,
they can be completely overshadowed by much higher level atmospherics
and man-made interference. With respect to the latter, riometers, like
radiotelescopes are generally located where interference from power lines,
automobile ignition noise, etc., is minimized and they try to use
frequencies which do not correspond with commonly used man-made trans-
mitter signals. However, because of the variability of the reflective
layers in the ionosphere, transmitter signals of frequencies normally
used at great distances from the riometer site may suddenly become
quite prevalent. By the use of a swept frequency second local oscillator
in conjunction with a sample and hold minimum signal detector, this
effect can be minimized. An interference-free channel of bandwidth set
by the second I.F. amplifier is sought within the search band which is
the bandwidth of the first I.F. amplifier. The minimum signal found
within this band is then considered to be the best estimate of the cosmic

noise level. As long as the ratio of the first I.F. amplifier bandwidth to the second I.F. amplifier bandwidth is large, it is likely that at least one interference-free channel will be found.

3.3.2 Switching

Use of the Machin, Ryle, Vonberg receiver replaces the problem of gain stability, with that of accurate, stable switching. The greatest concern is with ▮▮▮dances presented to the receiver when the switches are in either o ▮▮positions. If the impedance levels are not identical ▮▮l of the noise source will not be able to accurately follow the power levels of the antennas and errors will result.

High frequency diodes are ideal for riometer switching purposes, providing reliable, stable and long-life switching as well as low insertion loss ($\sim$ .2 dB) and high isolation loss ($\sim$ 30 dB). An integrated circuit astable multivibrator could then provide a stable and low power driver for the switching diodes. Because the riometer will operate for a long period of time, much of which will be under adverse weather conditions, it is advisable that the switches be periodically checked by replacing the antennas with calibrating noise sources.

The switching frequency of the receiver switch (switch #2 in Figure 3.7) need only be as high as that which will render variations in receiver gain unimportant. In typical riometers this frequency is on the order of a few hundred hertz. The switching rate of the antenna switch (switch #1 in Figure 3.7) should be much less than this; due to the expected difference in power levels of the left and right circularly polarized antennas, sufficient time must be allowed for the power output

of the noise source to stabilize.

3.3.3 Noise Source

Noise sources are available commercially; however, they tend to be expensive, bulky and high power. The noise source is a very important part of the riometer, and aside from its most important characteristics, of thermal stability, linearity and constant impedance, it would be preferable that it also be easily controllable, of low power consumption and small in size.

A noise source meeting all the aforementioned requirements has been sufficiently described in two papers dealing with a riometer used in an Antarctic meteorological expedition [32], [33] and therefore will not be detailed here. It is sufficient to say, however, that this noise source had a power consumption on the order of 10 milliwatts and its output power-versus-controlling current characteristic exhibited linearity with less than 2% change in its proportionality constant over the temperature range $-70°C$ to $+70°C$.

Since the noise source described by Bird et al relies on transistor shot noise for its power, the corner frequency (see Figure 3.8) must be sufficiently below the operating frequency of the riometer if the power out is to be proportional to the collector bias current i.e. $P_n \alpha I_c$. This is not too difficult for an operating
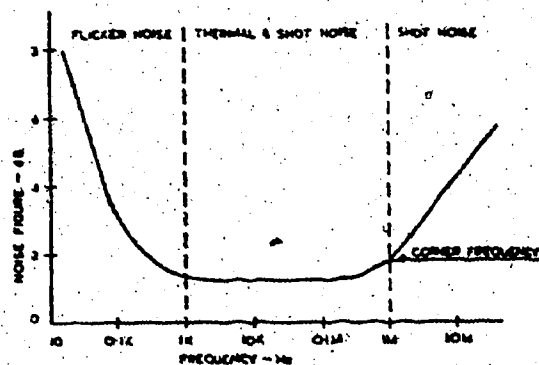
Fig. 3.8 Transistor noise characteristics.

frequency of 30 MHz, which was that used on the Antarctic expedition; however, for 12.4 MHz the acquisition of a suitable transistor may be somewhat of a problem. Power transitors have low corner frequencies but their large structures mean high junction capacitances and a resultant shunt on high frequency collector noise. Germanium signal transistors do not have this problem and their corner frequency is low, but unfortunately, the dependance of their characteristics on temperature makes them unacceptable as well. Owing to the very favorable characteristics of this noise source however it is believed that the acquisition of an appropriate transistor will be well worth the time spent in a search for it.

3.4 Low Power Riometers

Due to the fact that riometers operate at isolated sites year round, it is desirable that they require little attention. This means equipment which is simple, basic and thus reliable. But many sites do not have, and will not have, mains power. Therefore once the problem of equipment reliability has been solved, it is then necessary to optimize this equipment for low power consumption.

Although, perhaps too simple for our purposes (e.g. no minimum detector), the riometer of Bird et al required only 100 m Watts for its operation which was two orders of magnitude lower than the typical power consumption of previous riometers. As they point out, this power consumption could probably have been further reduced if the newer lower power linear microcircuits and CMOS circuits had been used in place of their older linear I.C.'s and TTL circuitry. With such low power equipment solar cells and wind generators become increasingly attractive as

power sources.

3.5 A Data Processing Riometer

As is pointed out by Hargreaves [4], a big step forward in riometer design would be an instrument which not only measured the data but also processed it and produced as a result, a record linear with absorption in decibels as a function of time. With the current microcomputers available it is believed, by the author, that this is entirely feasible. A block diagram for such a riometer is shown in Figure 3.9 where the
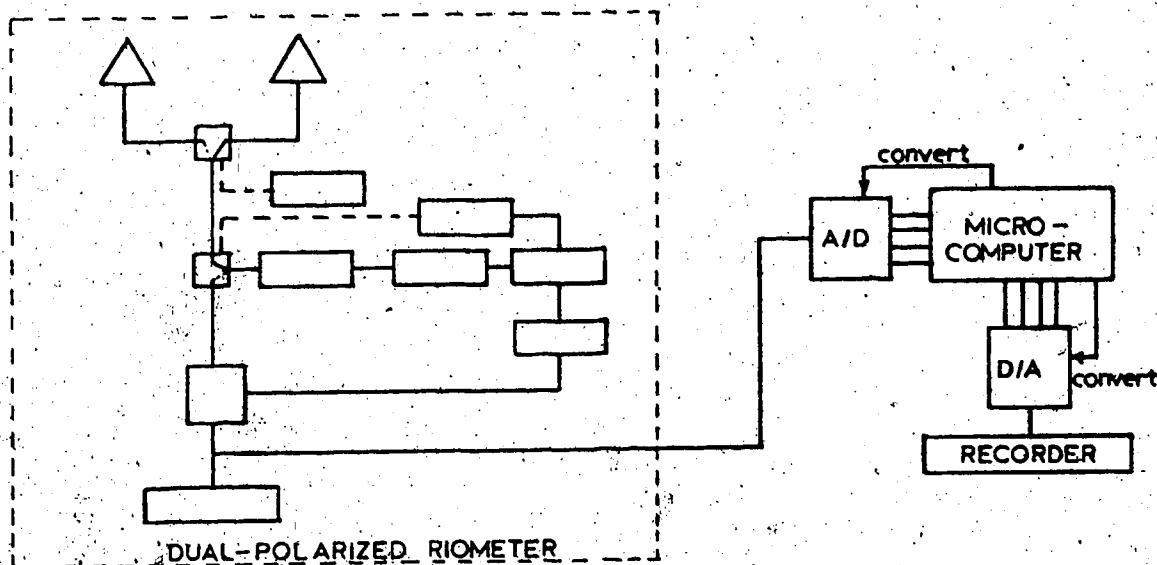
Fig. 3.9 A data processing riometer.

dual-polarized method of riometry is being used. Operation would proceed as follows.

Sampling of a noise source's current which should be proportional to its noise power would be accomplished through an analog to digital converter and would be performed for both the left and right polarizations.

The number of bits in the digitized sample would depend on the accuracy required and the microcomputer used. The sampling rate would depend on the switching frequency between the two antennas which in turn would depend on the time it would take the noise source to stabilize for a given difference in power. Owing to the short cycle time of a micro-processor, which is typically less than 1 μs, sampling could be synchronized to an accuracy of at least ± 10 μs (although the drift characteristics of a microprocessor as a function of temperature have not been considered in this estimate).

The computer could then take samples throughout the sidereal period of interest, say 1 hour, at intervals of perhaps 5 minutes, each set of samples in turn being stored. It then has 5 minutes before the next sidereal period begins to eliminate samples which are not representative of the 1 hour interval (due to terrestrial interference or unusually high absorption), average the samples remaining, convert this average to decibels above reference (by direct calculation or possibly through look-up tables) and store the result in memory locations (two values will actually be stored, one for the extraordinary ray power and one for the ordinary ray power) corresponding to that particular sidereal hour. Sidereal periods less than the 1 hour interval suggested above could be used; however, for a riometer antenna of wide beamwidth the sidereal sky brightness variations would be so slow that this should not be necessary. Shorter periods are also economically unattractive because of the higher cost of implementation due to the greater memory require-ments.

Each hour would similarly be processed and by the end of a month approximately 30 hourly average power levels for both polarizations would

exist for each of the 1 hour sidereal periods. As will be described in greater detail in Chapter 4, the 30 sets of data can then be used to determine the average unattenuated cosmic noise level for the sidereal hourly period to which they pertain. The index n and the true sky temperatures, corrected for any cable or switch losses which might exist, could then be plotted as a function of sidereal time on a recorder, timing signals being generated by the computer.

Memory requirements of such a processing radiometer may be high; this will depend on the size, i.e. the number of bits of the data word (byte) stored. For just the storage of the average powers for both polarizations for a month, the computer would require 2 x 24 x 30 = 1440 bytes of data-memory; scratch pad memory and program memory would also be required.

Once the quiet day curve had been determined, it would be a simple matter to measure the received noise power in the 5 minute interval between samples, convert this value to decibels above reference and plot the result along with the true sky temperature computed to that date for the same sidereal period. Monitoring of the absorption could be limited to periods when this information was desired, whereas updating of the quiet day curve as more data sets are accumulated (resulting in a greater statistical significance) could be an on going venture.

CHAPTER 4

PROCESSING OF THE RIOMETER DATA

The procedure of Little, Lerfald, and Parthasarathy for extracting the unattenuated cosmic noise background levels from the dual-polarized riometer data will now be discussed in detail. An examination into the sources of error to which this technique may be susceptible is given, finally ending in a discussion of the degree of accuracy attainable by this technique.

4.1 Extraction of the Cosmic Noise Background from the Measurement Data

If for the time being, good horizontal uniformity in the ionospheric layers can be assumed (justification for this assumption will be given in section 4.2.4), then from the development of section 2.5, the absorption in decibels for either the extraordinary ray or ordinary ray can be written as

$$A = C f_e^{-\eta} \qquad \text{decibels}$$

where f_e is the effective operating frequency of the particular propagating mode. The absorption for each mode is thus,

$$A_o = C f_{eo}^{-\eta} \qquad\qquad f_{eo} = f + f_L$$

$$A_x = C f_{ex}^{-\eta} \qquad\qquad f_{ex} = f - f_L$$

If now P is the cosmic noise power that would be received in the absence of the ionosphere, P_o is the ordinary ray received noise power,

and P_x is the extraordinary ray received noise power, all measured in

dB's above reference, then

$$A_o = P - P_o$$

$$A_x = P - P_x$$

and for a given operating frequency f,

$$\frac{A_x - A_o}{A_o} = \left(\frac{f_{eo}}{f_{ex}}\right)^\eta - 1 = \text{constant} = -\frac{1}{M} \text{ (say)} \qquad (4.1)$$

or

$$P_o = M(P_o - P_x) + P \qquad (4.2)$$

For electron density height distributions such that the significant

portion of the absorption occurs at levels where $\nu(h) << 2\pi f_e$ (heights

greater than 75 km for f = 12.4 MHz), which may be a valid assumption

for observations made at night, the index η would be equal to 2. If

then the longitudinal component of the gyro frequency f_L was sufficiently

well known, the cosmic noise power for the particular observing time at

which P_o and P_x were measured could be calculated from this one set of

data. However, f_L, which depends on the angle of propagation at the

absorbing levels, is not sufficiently well known, and absorption does

not necessarily occur at levels such that $\nu(h) << 2\pi f_e$.

If several sets of powers P_o, P_x are accumulated for a particular

sidereal period, they may then be plotted according to equation (4.2).

As can be seen from Figure 4.1, the best fit least squares regression

line through the plotted points determines the level of the un-

attenuated cosmic noise power from its ordinate intercept. If measure-

ments are conducted only at night when it is likely that the index n
is equal to 2, an estimation of f_L can also be determined from the
slope. Using this value of f_L an estimation of n can be obtained at
other observing times. The degree to which such estimates are valid
can only be born out by experiment. But both f_L and n are of interest
because of the information which they provide with respect to the
height of absorption.

The effects which may cause scattering in the plot and errors in
the reduced data will now be discussed.
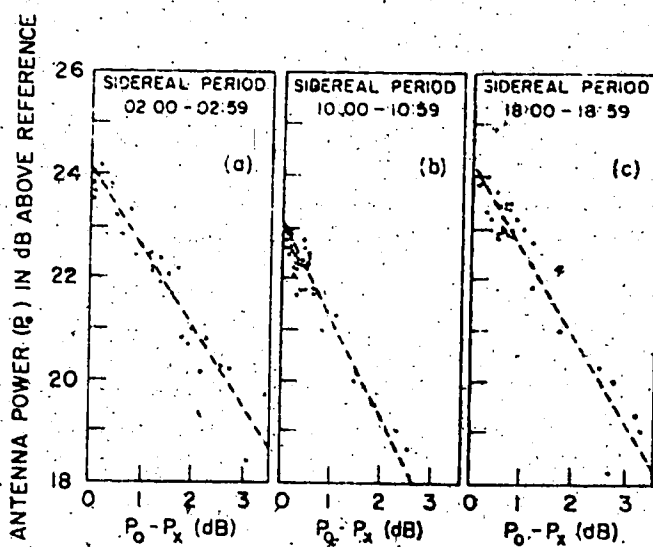
Fig. 4.1 Sample plots of measurement data.

4.2 Sources of Error

4.2.1 Variability in the Height of Absorption

As was mentioned above and explained in detail in section 2.5, the level(s) at which absorption takes place depends on the electron density distribution at the time of observation. The result is that the index η depends on the degree of solar activity and more importantly on the solar zenith angle.

Solar activity will vary with the 11 year sunspot cycle, and except for unusual flare-ups, should exhibit slow enough changes that measurements taken over a 1 to 2 month period should exhibit negligible scatter due to this effect. It would be expected, though, that the average absorption for a solar maximum year would be higher than that for a solar minimum year and this is what is observed [13].

The effect of a rapidly changing electron density distribution during sunrise and sunset is shown in Figure 1.3 (b). Because solar time shifts 4 min per day relative to sidereal time, in 1 to 2 months of observations the solar zenith angle will have shifted $30°$ to $60°$ for the same sidereal time. If during the period of observations measurements are made at a time when the electron density is in a state of rapid change, the index η will change substantially over the sidereal period of interest and a large scattering in the data points will result.

Once the Q.D.C. has been established (i.e. P in eq. (4.2) for each sidereal period within the sidereal day) changes in η will be of value in determining the degree to which heights of absorption vary; however, until the Q.D.C. has been determined these periods of rapid changes in

electron density should be avoided.

4.2.2 Deviative Effects

If high critical frequencies exist, deviative absorption will occur and further scatter in data points in the plot of Figure 4.1 will result. Parthasarathy et al [15] maintain that at 10 MHz deviative effects will be negligible for critical frequencies < 3.5 MHz, will result in an underestimation (<.25 dB) of the derived sky temperatures for critical frequencies in the range 3.5 to 5.0 MHz and will result in an overestimation of the sky temperatures for critical frequencies > 6.0 MHz.

Another deviative and rather unusual effect was observed by Steiger and Warwick [34] in Hawaii (Lat. 21°N) at 18 MHz. They found that even when f_{oF2} was greater than 18 MHz (i.e. all energy incident on the ionosphere below this frequency should be reflected) considerable radiation was still being received. They attributed this phenomenon mainly to cosmic radiation trapped and propagated under the ionosphere, with a possible secondary source being the thermal radiation emitted by the ionosphere itself.

Although deviative effects should, in general, be negligible, (certainly at night) the advantages of having an ionospheric sounder operating simultaneously with the riometer are obvious and the future addition of one at Seven Mile Flat should be looked into.

4.2.3 Sidereal Brightness Variations

Using the data of Andrew [20] for a wide beam aerial centered on declination 52° and operating at 13.1 MHz, sidereal brightness

variations occur at a maximum rate of approximately .4 dB/hr. Since the proposed University of Alberta riometer will also be centered on a declination of approximately 52°, operate at 12.4 MHz and use a wide beam antenna, it would be expected that the brightness variations would also be of this magnitude.

If the records are then broken up into hourly sidereal intervals for which an average value of cosmic noise power is to be determined (the sidereal intervals used in the data reduction can be shorter than 1 hr; however, this should not be necessary due to the slow rate of change of the cosmic noise background when averaged over a wide beam antenna), the points on the plot would be expected to exhibit an additional scattering of at most ± .2 dB, depending on whether the reading was taken near the beginning or end of the sidereal interval. If, however, the readings acquired over the observation period (1 to 2 months) are evenly distributed within this interval, the power determined from the intercept of the regression line through the points so defined, will be the average cosmic noise level for that interval (and thus would be plotted as the mid-hour representative value) and sidereal brightness variations will not be important [15].

4.2.4 Non-Uniformity of Electron Density in the Horizontal Extent

If horizontal patchiness exists it may be possible that the ordinary and extraordinary rays, which in general travel different paths, may each traverse characteristically different regions of the ionosphere. It would be very difficult to determine which observations suffered from such an effect (a clue though would be an extraordinary ray power which was higher than that of the ordinary ray) and therefore the

corresponding data points would introduce errors in the regression line plot which would give an inaccurate intercept.

Yet another effect of horizontal non-uniformity is the reduction in the effective beam width of the antenna due to severe absorption or reflection. As an example, if 20% of the antenna beam intercepts a region which is optically opaque both the E and O modes will appear to have had an additional 1 dB of absorption (window effect). The difference in their powers will still be indicative of the actual absorption; however, the ordinary ray power will now be 1 dB less than what it would be if the layers had been uniform.

Studies of this problem have been conducted [9], [15] and tend to indicate that even for an antenna with HPBW ∿ 60°, uniformity in the horizontal extent is reasonably assured.

4.2.5 Interference

If observations are to be made during the day, one of the most likely sources of interference is the sun. However, evidence [9], [13] suggests that the contribution of signal power from the quiet sun, for wavelengths on the order of 10 meters, is less than 1% of the cosmic noise background when averaged over a broad beam antenna. As observed by Heisler and Hower this may not be the case during solar maximum periods where the contribution to the received power may be as high as 20%. Under such conditions, however, the interference should be obvious from the temporal behavior of the charts and, therefore, the corresponding data should be excluded from those used to determine the regression lines.

Atmospherics, like solar bursts, are easily detectable because of

their high level. Their most serious effect is that they are responsible for the loss of much data, thereby necessitating a longer data acquisition time in order to achieve the same level of statistical significance. Man-made interference can also result in loss of data although it is hoped that this will be minimized due to the use of a minimum signal detector as described in section 3.3.1.1.

The only other source of interference that may be encountered is that due to the decametric radiation from Jupiter. At 20 MHz it has an average flux density of 10^{-21} $Wm^{-2}Hz^{-1}$ [23], which is at least as great as Cassiopeia A, generally the strongest radio source in the sky. Evidence further suggests that the flux increases as frequency decreases, at least down to 10 MHz.

Because the radiation emitted from Jupiter is right circularly polarized (at least at 20 MHz), it may represent an important source of error when it is in the beam width of the antenna despite the broad beam averaging effects. Fortunately, since Jupiter's path lies essentially in the plane of the ecliptic, for an antenna with HPBW ~ 60° its effect, if it has one, should not be observable until approximately 1981 [35]. By that time the riometer should have been in operation for some years, and the cosmic noise background for the sidereal periods, which will then contain Jupiter, should be well known. The additional noise due to Jupiter for each polarization can then be determined and hence, the degree and type of polarization of its non-thermal emissions can be computed. At 12.4 MHz, this knowledge should be of some scientific interest.

4.2 Polarization of the Cosmic Noise Background

If the difference in power received by the left and right

circularly polarized antennas is to truly indicate the difference in absorption between the extraordinary and ordinary modes of propagation, then the incident polarization must be random (i.e. unpolarized). Existing evidence [15] suggests that at high frequencies, when cosmic radio noise is averaged over a broad beam antenna (HPBW ∿ 60°) and a non-zero receiver bandwidth, this is true.

4.2.7 Oblique Rays

Owing to the greater attenuation of oblique rays, the antenna temperature of a riometer will be lower than that which would be recorded if only rays passing vertically down through a horizontally stratified absorbing region entered the beam. Thus there is an "apparent absorption" measured which will be higher than the actual zenithal absorption.

For accurate absorption measurements, the measured absorption must be corrected to zenithal absorption. An example of such a calculation for a vertically directed riometer antenna of beamwidth ± 32° to half power is given by Ecklund and Hargreaves [36].

4.2.8 Thermal Noise from the Ionosphere

Except during periods of high absorption when received cosmic noise powers will be low, the error introduced by assuming a cool ionosphere will be negligible. At 12.4 MHz the equivalent temperature of the unattenuated cosmic noise background will be on the order of 2×10^5 °K and electron temperatures in the absorbing regions should not exceed a few hundred degrees [9], [39]. This latter figure must then be multiplied by the efficiency of the absorbing region which should be

less than 30% under normal observing conditions. Thermal noise due to
the ionosphere thus should be of little consequence.

4.2.9 Errors and Uncertainty Due to Equipment

4.2.9.1 Antenna Axial Ratio

Contamination of the received powers of either the extraordinary
or ordinary mode will occur if when the antenna system is supposedly
responding to only one polarization it is also responding slightly to
the other. A figure of merit in regards to the degree an antenna
responds to polarization of opposite hand is the parameter Q, defined
as

$$Q = \frac{E_L}{E_R} = |Q| \, e^{j\Sigma}$$

where, if $|Q| > 1$ the antenna is said to be left elliptically polarized
(LEP) and if $|Q| < 1$ the antenna is said to be right elliptically
polarized (REP).

For an antenna with a given Q factor, the tip of the electric
vector of the received radiation viewed along the path of the wave would
appear to describe an ellipse with axial ratio (AR) of magnitude

$$|AR| = \frac{1+|Q|}{|1-|Q||}$$

(For a more complete discussion of axial ratio the reader is referred
to section 6.2). For an antenna, then, that is perfectly right
circularly polarized, $Q=0$ and the axial ratio is unity.

Of course, a real antenna has a finite beam width and over that beam width the axial ratio and, hence the degree to which an antenna responds to opposite polarization, changes. An antenna which responds to nearly circular polarization on axis may become extremely elliptically polarized off axis. If for the sake of argument, the left and right polarized beams of the riometer antenna system are each assumed to have an average axial ratio magnitude of 2 over the entire significant portion of their beams, and if the effective collecting area for either polarization is A_e then through the use of Stokes' parameters it can be shown that

$$P_L = (.9\ S_o + .1\ S_x)\ A_e$$

$$P_R = (.1\ S_o + .9\ S_x)\ A_e\ )$$

where

P_L = power received by the left polarized beam

P_R = power received by the right polarized beam

S_o = flux density of the ordinary ray radiation which in the Northern Hemisphere is essentially LCP

S_x = flux density of the extraordinary ray radiation which in the Northern Hemisphere is essentially RCP.

Letting $P_o = S_o A_e$ and $P_x = S_x A_e$ represent, respectively, the ordinary ray and extraordinary ray powers available to the antenna system, which are the powers of interest, then due to the contamination of the opposite polarization, the antenna system described above indicates an ordinary ray to extraordinary ray power ratio of

$$\frac{P_L}{P_R} = \frac{.9\,P_o + .1\,P_x}{.1\,P_o + .9\,P_x}$$

The percent error is thus

$$\text{percent error} = \frac{(P_o/P_x - P_L/P_R)}{P_o/P_x} \times 100 = \frac{10[(P_o/P_x)^2 - 1]}{P_o/P_x(.1\,P_o/P_x + .9)}$$

If the largest difference to be expected between the E and O powers under normal conditions is 3 dB (i.e. $P_o/P_x \approx 2$), then the percent error in the measured ordinary ray to extraordinary ray power ratio is 13.6%.

Since the above development does not take into account the weighting of the received radiation due to the power pattern, which should favor the region of nearly circular polarization on the antenna beam, the error estimate is probably quite pessimistic. However, it does show that for an antenna with poor on-axis axial ratio or one with an axial ratio that drops off rapidly from its zenithal value, polarization effects can be severe. By a similar development as that presented above, it can be shown that if the axial ratio magnitude is less than or equal to approximately 1.2 over the significant portion of the beam (this would give an error on the order of 1%) or the off-axis axial ratio is sufficiently well known so that its effect could be calibrated out, this polarization effect could be neglected. As will be seen in Chapter 7, both of these criteria were achieved through experimentation of model antennas on an antenna test range.

4.2.9.2 Antenna Power Patterns

Except those riometers which have been used in the study of horizontal non-uniformity in the ionospheric layers, riometers have almost without exception used relatively wide antenna beams with half power beam widths on the order of 60°. The reason for this is partially economical as narrower beams require arrays which add to the complexity and, therefore, the cost of the riometer system. It is primarily a practical reason, however, since, as mentioned previously, use of a wide beam aerial results in a galactic background that should appear as a slowly varying function of sidereal time and also results in solar noise contributions which should be insignificant with respect to the level of cosmic noise radiation received. In addition, the dual-polarized riometry technique requires that a wide beam antenna be used in order to ensure that the cosmic radiation when averaged over the wide beam is randomly polarized.

Side lobes are undesirable because of the increased susceptibility of the antenna beam to interference, natural or man-made, and the greater complexity in correcting the observed absorption for oblique rays.

Power patterns which are not identical for both polarizations will result in erroneous power difference measurements because the patterns of the two polarizations will respond to different portions of the sky. By using antennas with identical vertically symmetric patterns this problem will be avoided and if the patterns are also circularly symmetric proper orientation will not be necessary.

At a declination of 52°, circularly symmetric beams are also advantageous in that they should not "line-up" with the plane of the Milky Way Galaxy as a vertically directed fan beam of the same area

could. This should then result in a smoother cosmic noise background to be observed.

4.2.9.3 Antenna and Cable Losses

Antenna and cable losses can be easily measured and the data corrected accordingly. Thermal noise due to the cable should be negligible, however, if this is in doubt it can be measured and thus calibrated out.

If it is felt that ϵ_c the cable's power transmission coefficient, will change more than 1% over the expected temperature range of -50°C to +35°C, or through aging, it may be advantageous to bury the feed cable with an identical length of compensating cable, which would be connected between the noise diode and the switch (see Figure 4.2). Recalling the expression (equation (1.4)) for the power at the receiver input terminals when the switch is connected to the antenna side, as

$$P_1 = \epsilon_{c_1} kT_A B + (1 - \epsilon_{c_1}) T_c kB$$

Then with the compensating cable in place, the power at the noise source side is given by

$$P_2 = \epsilon_{c_2} kT_{ns} B + (1 - \epsilon_{c_2}) T_c kB ,$$

If $\epsilon_{c_1} = \epsilon_{c_2}$, the receiver will record a null only when

$$T = T$$
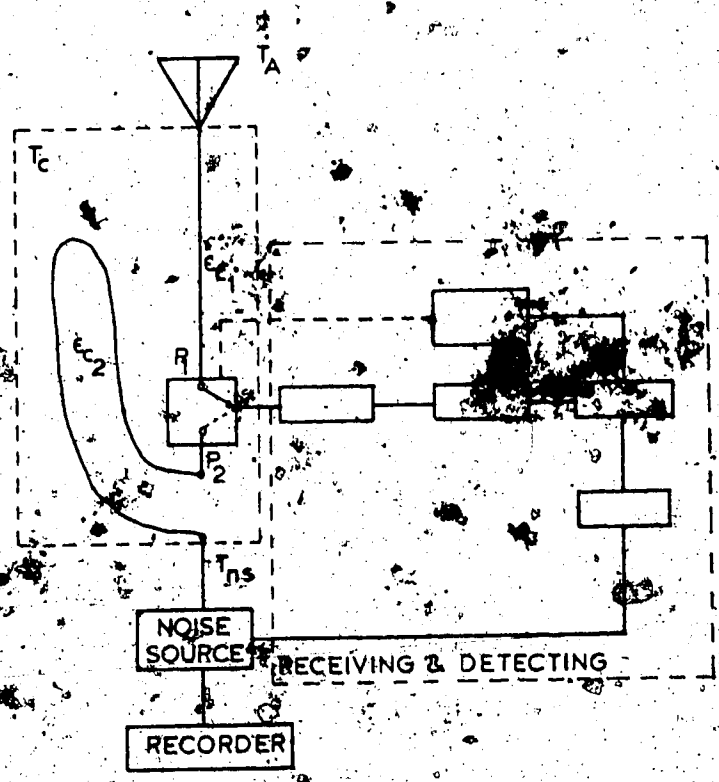
Fig. 4.2 Riometer with temperature compensating cable.

and no errors will result due to uncertainty in the cable transmission
coefficient.

4.3 Attainable Accuracy

4.3.1 Comparison with the Standard Riometry Method

Parthasarathy and Lerfald [ ] ing the dual-polarized method of riometry at 5, 10 and 20 MHz and standard riometry at 30 and 50 MHz, quote the following uncertainties in derived sky temperatures for College, Alaska (Lat. 65°N):

dual-polarized method   5 MHz; ± .5 dB (± 12% and incomplete)

               10 and 20 MHz; ±.25 dB (± 6%)

standard riometry method   30 and 50 MHz; ±.15 dB (± 3.5%).

Their claim is based on the following principal experimental precautions:

a)   identical antenna patterns at all frequencies

b)   dual-polarized method used at lower frequencies

c)   adequate ground mesh to avoid uncertainties due to ground conductivity

d)   an extended period of observation to ensure experimental repeatability of measurements

e)   careful routine monitoring of all system impedances.

They attributed most of the error (±.2 dB) in their 10 MHz data to uncertainty in the degree to which horizontal uniformity in the layers existed and to uncertainty in the levels at which absorption was taking place. Another .05 dB was attributed to antenna cross-polarization effects and all other errors were either calibrated out or negligible.

As a comparison, the data obtained by B.H. Andrew [20] using only the standard riometry method at an observing declination of 52°, lists the following uncertainties in the derived sky temperatures:

10 MHz; ± 15% and incomplete

13.1 and 17.5 MHz; ± 6%

26.5 and   38 MHz; ± 3% .

The improved accuracy at 10 MHz is substantial, especially when it is
realized that the ionosphere at auroral latitudes, i.e. at College,
Alaska, is especially variable in its properties.

4.3.2 Best Accuracy Believed Possible Under Favorable Conditions

4.3.2.1 At Receiver Input Terminals

If the temperature of the ionosphere in the absorbing regions
(altitudes < 100 km) can be assumed to have a maximum value of
$T_{ion} \leq 400°K$ and if its transmission coefficient ε_{ion} is always greater
than .7, the error introduced by assuming a cool ionosphere (i.e. it
does not contribute to T_A, the noise temperature of the antenna),
a sky background temperature of $T_{sky} = 2 \times 10^5 °K$, is

$$\frac{(1-\varepsilon_{ion})T_{ion}}{\varepsilon_{ion}T_{sky}} = .86 \times 10^{-3} \; (@ \; .004 \; dB),$$

and thus negligible as expected.

If now it is assumed that enough measurements have been taken at
night so that it is relatively assured that $f_{o_{F2}} < 3.5$ MHz, (since no
ionospheric sounder will be available), according to the discussion of
section 4.2.2, deviative effects will be negligible (say < .02 dB of
absorption).

As with the measurements taken by Parthasarathy and Lerfald, it

is assumed that the largest error contribution will be due to un-
certainties in the heights of absorption and horizontal uniformity of
the absorbing layers, which will mainly be responsible for the
scattering in the P_o versus $(P_o - P_x)$ plots. This error can be
calculated once the regression line has been determined. However, owing
to the fact that horizontal uniformity should be better at the lower
latitudes and the nighttime absorbing layers should be relatively
constant in comparison to those in the auroral zone, an upper bound of
.1 dB standard deviation should be realistic. Then since polarization
effects for an antenna with AR $\leq$ 1.2 over the significant portion of
its pattern should be negligible, an upper bound on the maximum error
in the sky temperatures measured up to the input terminals of the
receiver is .12 dB (< 3%). If greater accuracy is to be attained
(< 1%) measurements must not only be restricted to the nighttime when
deviative effects are negligible and ionospheric properties relatively
stable, but they must also be taken over a long enough period of time
(at least 12 months) to obtain a greater degree of statistical significance,
thus reducing the errors due to regression line uncertainties to less
than .02 dB.

Thus the dual-polarized method's normally short data acquisition
time is sacrificed in order to attain higher accuracy. It should be
pointed out, however, that for the same level of statistical
significance the standard riometry method would require data acquisition
times at least 2 to 3 times longer. It is also important to note that
although uncertainty due to deviative effects is introduced into both
the standard riometry method and the dual-polarized method, uncertainty
due to non-deviative effects is a problem only of the standard riometry.

method. Almost certainly for solar maximum years, an additional error
of .1 dB is likely, due to this problem, if measurements are conducted
by the standard riometry method.

4.3.2.2 At the Output of the Integrator

Although the receiver itself is a generator of noise, the level
of the noise does not contribute to errors in the measurement of
absorption because like gain fluctuations it affects the noise power
from both the antenna and noise source in the Ryle-Vonberg receiver.
Instead the receiver noise imposes a limit on the sensitivity with
which a given power can be measured because of the inherent statistical
fluctuations in the output of the receiver. For a receiver which is
connected to the signal only half the time, the RMS voltage fluctuations
in the output of the integrator are [22]

$$\Delta v = \frac{2v}{\sqrt{B\tau}}$$

where v = mean value of the detector voltage

B = receiver noise bandwidth

τ = post-detection (integrator) time constant.

Thus for output fluctuations on the order of 1% (.04 dB) and a
receiver bandwidth of 10 KHz, τ must be approximately 4 seconds. Since
the riometer employs a minimum detector it should not be necessary to
keep τ small so that recovery from high level interference is rapid.
A time constant of 4 seconds should therefore not be prohibitive and
if large changes of absorption occur on the order of minutes, this
value can be further increased with a resultant drop in detector

voltage uncertainty.

4.4 Conclusions

It is apparent from the discussion of the preceding sections of this chapter, that despite the optimization of equipment and the numerous corrections for its deficiencies, the measurement of ionospheric absorption by any method still suffers from a basic lack of knowledge of the ionospheric properties at any given time, at any given frequency, above any given observing location.

The dual-polarized method has, at least at auroral latitudes, proven itself to be more accurate than the standard riometry technique. But even whether this method is capable of measuring ionospheric absorption to within is not known. If all investigations cited had been made on the above Seven Mile Flat and at 12.4 MHz, a much more reliable estimate of accuracy could be obtained. However, assumptions must be made with the information available. The validity of these assumptions can only be born out once the equipment is built and in operation. If the dual-polarized method is found to be unsuitable, reversion to the standard riometry technique is not so much an equipment modification as it is a data processing change.

CHAPTER 5

THE CONICAL LOG SPIRAL ANTENNA

Selection of a suitable antenna for use in the dual-polarized riometer, was based on the following criteria:

a) good response to circular polarization over most of the beam width

b) HPBW on the order of 60° with a single element

c) symmetrical pattern (and preferably circularly symmetric)

d) no side lobes

e) simple to construct.

As was mentioned in Chapter 1, the conical log spiral, in comparison to the other antennas considered (crossed dipoles and helices), met the first four of these characteristics admirably well, and in addition, displayed a certain degree of frequency independence which would be of value in multifrequency riometry experiments. It's one major fault, however, was its height ($\sim$ 30 meters) and ways of reducing it were investigated.

It was known that this height could be reduced by about 2/3 through truncation with only minor changes in pattern and slight degradation of the on-axis axial ratio. What effect truncation would have on the off-axis axial ratio, however, was not known. With the aid of an antenna test range, this parameter could be determined and possibly at the same time, ways could be found to further reduce the height or at least change the shape (e.g. pyramidal) to facilitate construction. This was the approach taken. The design, construction and operation of the antenna test range will be discussed in following chapters.

5.1 Geometry and Defining Equations

The defining equations of the 2-arm conical logarithmic spiral antenna are:

$$\rho = \rho_o \exp[\pi b(\phi - \delta)/180]$$

$$b = \frac{\sin\theta_o}{\tan\alpha}$$

where the symbols are as shown in Figure 5.1 and all angles are in degrees. The parameters θ_o, α and δ are referred to, respectively, as the cone angle, angle of wrap and the angular arm width.

The truncated cone height h can be found from

$$h = \frac{D - d}{2 \tan\theta_o}$$

and the total length of one spiral arm is given by

$$L_s = \frac{(D-d)\sec\alpha}{2\sin\theta_o} = \frac{h \sec\alpha}{\cos\theta_o}$$

For $\theta_o = 90°$, these equations reduce to those of the planar logarithmic spiral antenna.

5.2 The Standard Antenna Model

Modelling is a very useful engineering tool in the investigation of the radiating properties of an antenna whose characteristics would be very difficult if not highly impractical (e.g. aircraft antennas) to
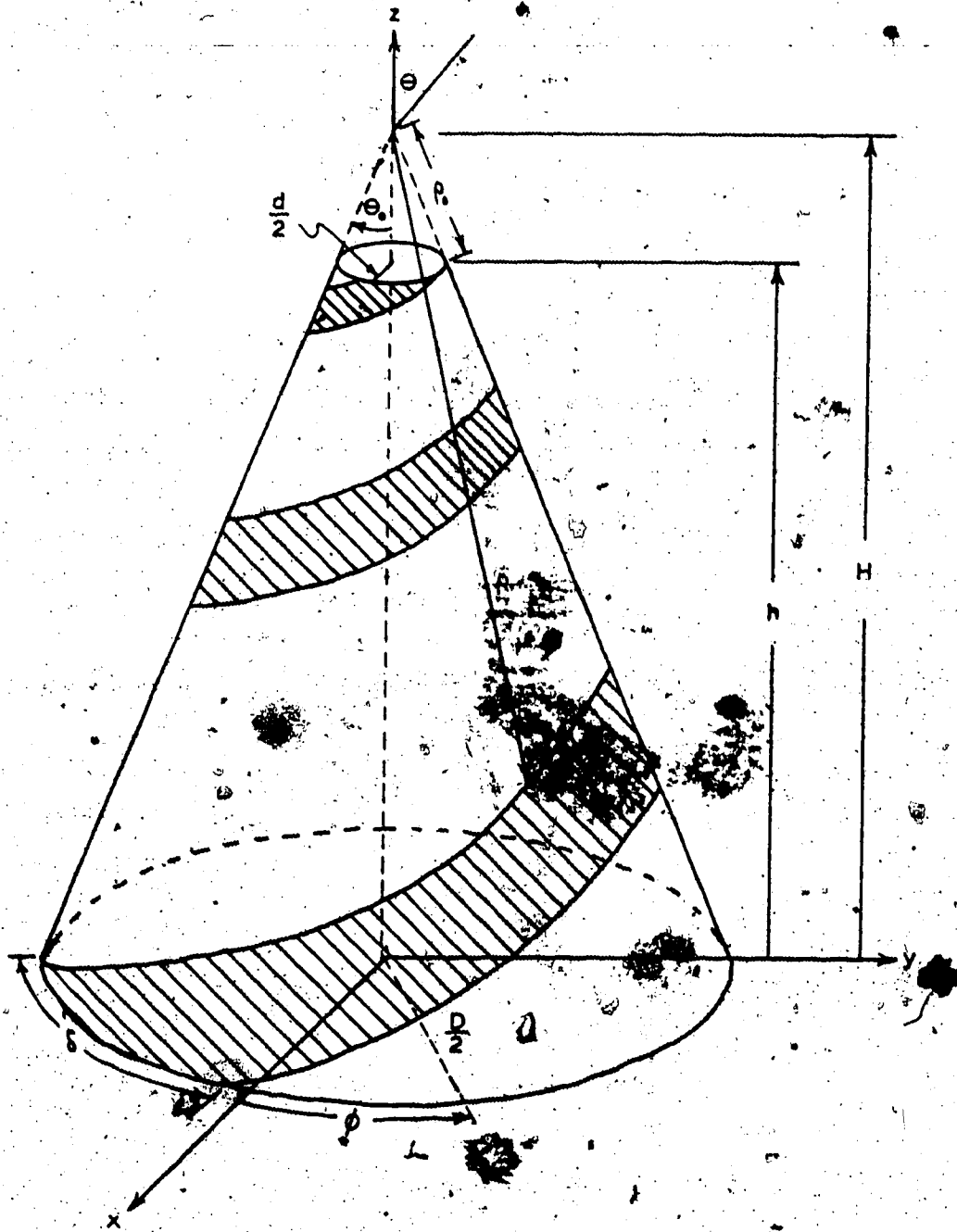
Fig. 5.1 The conical log spiral and its parameters.

measure on the full-size structure. Such was the case here since it

was not desirable to build a structure which had dimensions on the order

of tens of meters and then put a great deal of effort into measuring its properties, only to find they were not suitable.

Reduced versions of the antennas under consideration would, therefore, be tested on the antenna test range. Their only requirements were that they be exact geometrical scale models of the corresponding full-size antennas and that nonlinear media (e.g. ferromagnetic material) be absent from their construction and in fact from any part of the range [39]. Such models are, therefore, capable of giving direct information on those properties of an antenna which do not depend on power level such as polarization and relative power pattern, the quantities of interest here. A geometrical model antenna which has been scaled down by a factor of m must then be operated at a frequency m times that of the full-size antenna in order that its radiating properties be equivalent.

For calibration of the test range, an antenna whose off-axis axial ratio and radiation pattern were well known, was required. For our purposes, Dyson [17], [40] had sufficiently defined these parameters for a 2-arm conical spiral antenna with cone angle $\theta_o = 10°$, angle of wrap $\alpha = 80°$, and arm width $\delta = 90°$. Hence, this was the standard used.

5.2.1 Design

From Figure 5.2 which shows the relative amplitude of the near fields along the surface of the cone (the designations a_{10}, a_{15}, etc., refer to the radius of truncation at the relative near-field amplitude indicated by the subscript), it can be seen that truncation at 30 dB down points will introduce negligible changes in the radiation pattern; therefore let
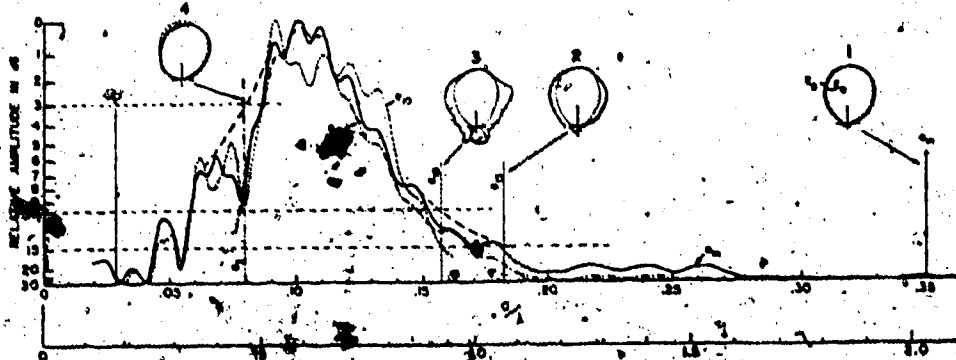
Fig. 5.2 The near fields of a conical log spiral antenna
($2\theta_0 = 20°$, $\alpha = 80°$, $\delta = 90°$) and the effects of truncation on
its far-field pattern [18].

$$\frac{d}{2} = .03\lambda \quad \text{and} \quad \frac{D}{2} = .3\lambda$$

The remaining parameters of the antenna are determined as

$$H = 1.70\lambda \qquad \rho_0 = .173\lambda \qquad L_s = 8.96\lambda$$
$$h = 1.53\lambda \qquad b = .0306$$

5.2.2 Specifications and Characteristics

The electrical properties of the spiral so defined (i.e. $2\theta_0 = 20°$,

$\alpha = 80°$, $\delta = 90°$), as measured in free space, are from Dyson's curves,

HPBWθ = 72° ± 4°

HPBWϕ = 76° ± 4°

Front to Back Ratio = 17 dB

Axial Ratio ($\theta = 0°$, 30°, 60°) = (1.0, 1.2, 1.8)

Z_{in} = 110Ω (infinite balun feed)

Z_{in} = 150Ω (on axis feed) . .

The method of feed for a conical spiral antenna will be discussed in section 5.2.4.

The specifications above refer to an antenna which is operated in free space. Operation over a ground plane with the metal arms bonded to the plane apparently narrows the beam width somewhat but does not deteriorate the general pattern [17]. No information was available on the effect a ground plane would have on the axial ratio although because of the small back lobe, it was expected that it would be slightly poorer.

As pointed out by Dyson, conical spirals do not exhibit a unique center of phase. However, over a portion of the main beam an "apparent center of phase may be defined" which for the high angle of wrap ($\alpha \geq 80°$) antenna described above would be approximately half-way up the structure along the axis.

For conical spirals with parameter $b \leq .05$ the pattern is essentially rotationally symmetric.

Typical conical spirals exhibit an axial ratio change of approximately 15% for a 90° change in azimuth position [17].

All conical spiral antennas appear to require a base diameter of at

least λ/n for efficient operation and only minor radiation pattern changes relative to those spirals formed on extended conical structures. It is of note that this diameter corresponds to a base circumference of λ which is a dimension characteristic of efficient radiators.

5.2.3 Fabrication

The arms of the antenna described above, are defined by the equation

$$\rho = .173\lambda \, \exp[\pi \, .0306 \, (\phi-\delta)/180]$$

The edges of the first arm are defined by ρ when $\delta=0°$ and $\delta=90°$. The edges of the second arm are defined by these same values of δ, but after ρ has been multiplied by $e^{-b\pi}$, i.e. the second arm is identical to the first but shifted 180°. This type of conical spiral (with $\delta=90°$) results in a conical surface with equal portions of dielectric and metal arms and, hence, is called a self-complementary antenna. It has been found by Dyson that these self-complementary antennas exhibit the best radiating properties.

Now that the equation for the antenna has been determined, it then becomes a simple matter to plot points (ρ as a function of ϕ) on a conical structure with the appropriate cone angle. This was considered to be a rather crude method of determining the position of the arms for a test standard, and certainly also time consuming. A computer program was, therefore, written for this purpose and is described in more detail in Appendix A. With the aid of a digital plotter, the computer drew out a pattern (see Figure 5.3) which when cut out, folded into
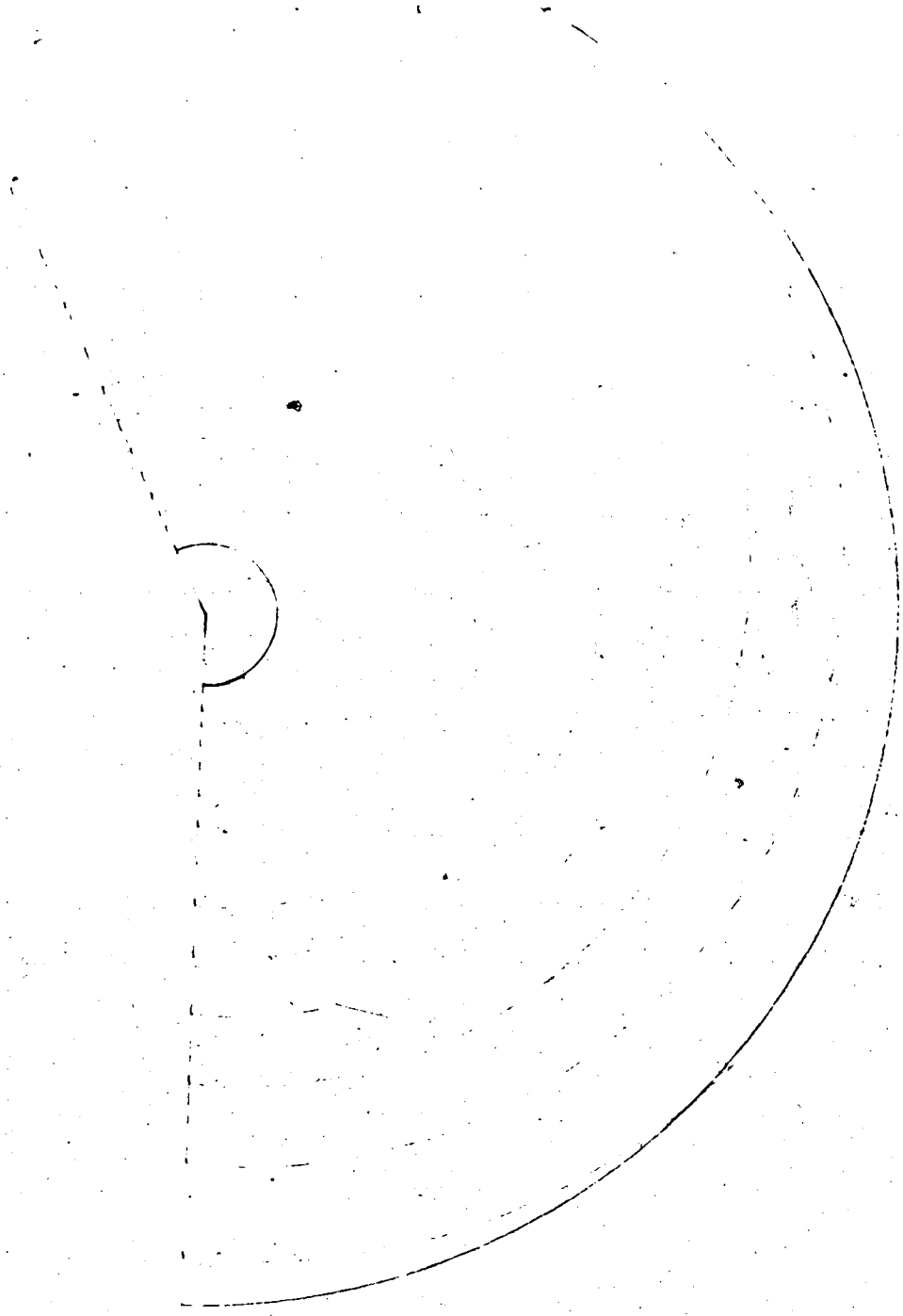
Fig. 5.3 Sample computer plot of conical spiral fabrication
pattern with parameters $2\theta_o=70°$, $\alpha=85°$, $\delta=0°$.

the desired conical structure with the appropriate spiral arms (each a different color) marked on it. The program was interactive; therefore, new values of θ_o, α, ρ_o, ρ_{max} ($H/\cos\theta_o$) and δ could be entered on each run, allowing for the rapid design of any of a number of different conical spiral antennas.

The pattern, thus achieved, was then transferred to a piece of thin cardboard, which acted as a form, onto which the metal arms, made out of 3 mil brass shim, were attached. (The 3 mil thickness of the arms represented eighteen "skin depths" at 1 GHz.) The planar cardboard pattern was then formed into a cone and the metal ends soldered together.

5.2.4 The Feed System

There are two main methods of feed for conical spiral antennas. One method is to bring a balanced transmission line up from the base along the axis of the cone to the apex where one wire is connected to each arm. According to Dyson, the balanced line may be shielded or placed inside a metallic cylinder as long as the diameter of the cylinder is no more than 1/3 the diameter of the cone at any point along its axis. Conversion to an unbalanced coaxial feeder cable may be made through the use of a balun or coaxial hybrid; however, except in very large structures, i.e. where the transforming device's size is relatively insignificant, this transition should be accomplished outside the antenna.

The second method of feed is to bring the coaxial feeder cable along one arm up to the apex where its center conductor is then connected to the outside sheath of a "dummy cable" attached to the other arm.

The outside sheath of both the dummy cable and the feeder cable, then, become part of the spiral arms. As long as the arms at the base of the antenna do not carry appreciable antenna currents the feed terminals are isolated from ground in a balanced manner. This method, devised by Dyson, is termed the "infinite balun feed" and has been found to be the most effective method of feed, especially in regards to preserving the large inherent bandwidth of the antenna. It was, therefore, the method used on the standard conical spiral.

5.2.5 Cable-Arm Version

If the width of the spiral arms of the standard conical spiral fed by the infinite balun method is reduced until only the cable remains, the antenna is found to have, generally, the same radiating character-istics as the complementary antenna, although the input impedance is slightly lower. These antennas are referred to as cable-arm conical spirals and were built to test the truncation properties of the spirals since turns could be easily removed from both top and bottom. Because cable-arm conical spirals are far easier to construct than their metal-arm counterparts it was likely that this type of conical spiral, which used coaxial cable for its spiral arms, would be the type used in the full-scale antenna. Thus the results of test range measurements on such antennas would be directly applicable to the full-scale antenna.

Fabrication of this type of model was accomplished by transferring the appropriate pattern onto a styrofoam form cut to the proper cone angle. The feed cable (RG - 59/U) was then wrapped around the form up to the top of the cone where the center conductor was attached to the outside sheath of a second (dummy) cable, which then spiraled down the

cone to the base.

A photograph of the cable-arm version of the standard conical spiral next to its metal-arm counterpart is shown in Figure 5.4.

5.3 Wide Cone Angle Conical Spirals

An example of a wide cone angle conical spiral antenna with cable arms is shown next to the standard conical spiral in Figure 5.5. As shown by Dietrich and Long [19], the advantage of using wide cone angles ($2\theta_o \geq 45°$) is that a base of circumference λ could be retained, making the structure an efficient radiator but without the excessive height of the smaller cone angle structure. (Dietrich and Long built two oppositely polarized 37 meter high conical spiral antennas, operated as an ionosonde over the frequency range 2 to 20 MHz.) This method of height reduction was therefore of interest and models such as that shown in Figure 5.5 were built to be tested on the antenna test range.

These cable-arm models, owing to their very small size used RG-174/U miniature coaxial cable as the feed cable and cardboard as the form. The computer plot of Figure 5.3 is one of the patterns used in the fabrication of these wide cone angle antennas.
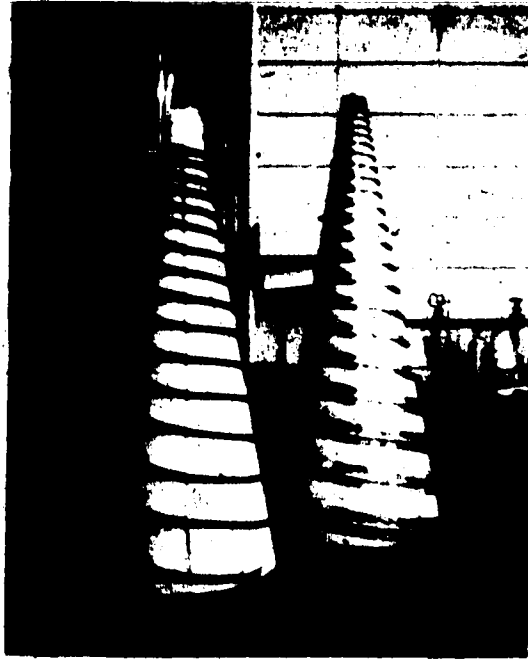
Fig. 5.4 The cable-arm version (left) of the standard
conical spiral ($2\theta_0 = 20^\circ$, $\alpha = 80^\circ$, $\delta = 90^\circ$), shown next to its
metal-arm counterpart.
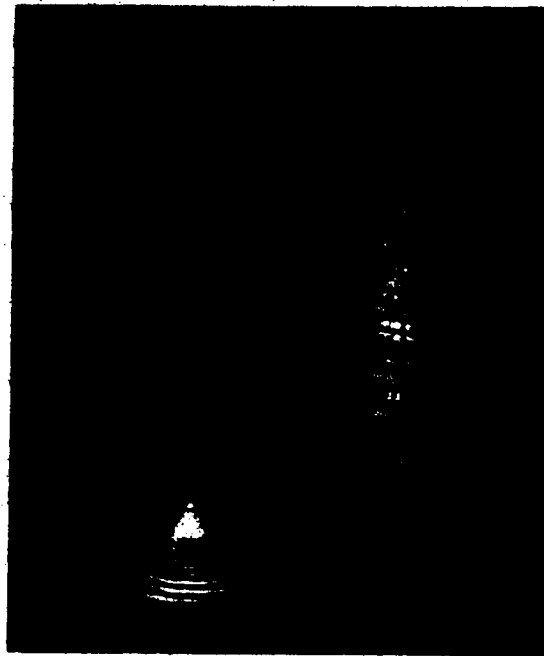
Fig. 5.5 One of the wide cone angle cable-arm antenna
models ($2\theta_0 = 70^\circ$, $\alpha = 87^\circ$), shown next to the much
taller standard conical spiral.

CHAPTER 6

THE MICROWAVE ANTENNA TEST RANGE:

DESIGN AND CONSTRUCTION

As has been pointed out in Chapter 5, many of an antenna's propert-
ies can be determined by conducting tests on a geometrical scale model
of the actual antenna. The reduced size of the antenna under test then
allows measurements of its radiating properties to be conducted at a
reduced distance. The radiating properties to be determined by the
test range described in the following sections were the antenna's axial
ratio and power pattern.

Unlike most test ranges, which are concerned with the far-field
radiation pattern of the test antenna, the primary function of the
range described here was the determination of the polarization response
over the beam area of the antenna under test. It was hoped that in the
process the power pattern could also be determined to a reasonable
accuracy. However, because the patterns of the antennas to be tested
were fairly well known and since it was expected that the full scale
antenna would have its pattern measured at the observing site, this was
of secondary concern.

6.1 The Test Site

For obvious reasons, test ranges must be located in minimum radio
interference areas and where the effects of reflections from obstacles
could either be neglected or readily calculated. Indoor ranges are
expensive because of the large amount of high quality absorbing material
required even for a small test room. Because the beam of the riometer's
antenna would be directed at the zenith, the models to be tested would

be oriented such that their maximum radiation would also be vertically directed. If then, a test site could be found outdoors such that most of this radiation would be emitted harmlessly into space, thereby not contributing to stray reflections, much less absorbing material would be required and thus the cost minimized. For this reason and because of its accessibility, the roof of the Electrical Engineering Building was chosen as the test site.

The north, east, south, and west views from the test site are shown in Figures 6.1, 6.2, 6.3, and 6.4, respectively. Adjacent buildings were relatively distant from the test site, the closest being on the north side and representing an obstacle 20 feet high at a distance of approximately 210 feet from the proposed location of the transmitting antenna. As can be seen from the photographs, ventilating ducts, the metal hand rails on the entrance ladder, and metal sheeting which bordered the roof provided more immediate obstacles.

6.2 The Measurement of Axial Ratio

6.2.1 Polarization Ellipse and the Poincaré Sphere

In section 2.3.1, the particular case of a wave propagating with circular polarization was discussed. It can be shown [22] that the electric field vector of the wave, with components in the wave-front given by

$$E_x = E_1 \sin(\omega t - \beta z)$$

and

$$E_y = E_2 \sin(\omega t - \beta z + \Delta) \ ,$$

Fig. 6.1 North view from test site.

Fig. 6.2 East view from test site.

Fig. 6.3 South view from test site.

Fig. 6.4 West view from test site.
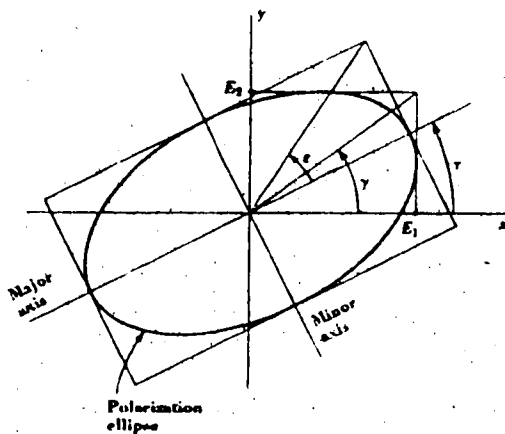
Fig. 6.5 The polarization ellipse and its defining parameters.

In general, describes an ellipse characterized by the angles γ, ϵ, and τ (see Figure 6.5). These angles are defined by the equations

$$\gamma = \tan^{-1} \frac{E_2}{E_1} \quad 0° \leq \gamma \leq 90°$$

$$\tau = \frac{\tan^{-1}(\tan 2\gamma \cos \Delta)}{2} \quad 0° \leq \tau \leq 180°$$

$$\epsilon = \frac{\sin^{-1}(\sin 2\gamma \sin \Delta)}{2} \quad -45° \leq \epsilon \leq +45°.$$

The angle ϵ is also related to the axial ratio by the equation

$$AR = \cot \epsilon,$$

where if AR < 0 the wave is right polarized and if AR > 0 the wave is left polarized.

The various polarization states that a wave may have can be represented on what is known as the Poincaré sphere, one-eighth of which is depicted in Figure 6.6. Any point on the sphere represents a particular polarization state $M(\varepsilon, \tau)$ with coordinates,

2ε = Poincaré latitude

2τ = Poincaré longitude.
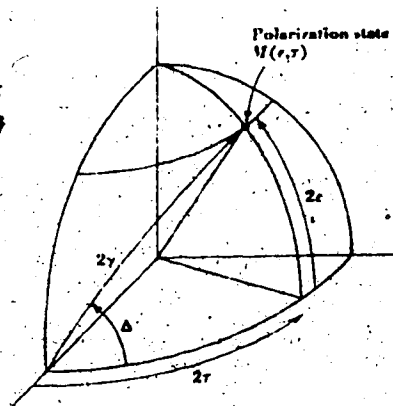
Fig. 6.6 Section of Poincaré sphere.

It is also possible to show that the great circle distance $M_1 M_2$ between any two points, $M_1(\varepsilon_1, \tau_1)$, $M_2(\varepsilon_2, \tau_2)$ on the sphere, is given by [40]

$$M_1 M_2 = \cos^{-1}[\sin 2\varepsilon_1 \sin 2\varepsilon_2 + \cos 2\varepsilon_1 \cos 2\varepsilon_2 \cos(2\tau_2 - 2\tau_1)] . \tag{6.1}$$

6.2.2 Practical Aspects

6.2.2.1 Extraction of the Axial Ratio from Power Measurements

The practical measurement of axial ratio can be accomplished by the use of a dipole rotated in the plane of polarization of the wave. According to Kraus [22], the voltage received by this dipole is

$$V = E \ell_e \cos \frac{M_w M_a}{2} \qquad (6.2)$$

where

$E = \sqrt{E_1^2 + E_2^2}$ = the magnitude of the electric field vector in the wave-front

ℓ_e = the dipole's effective length

$M_w M_a$ = the great circle distance between the polarization state of the wave $M_w(\varepsilon_w, \tau_w)$ and the polarization state of the dipole antenna $M_a(\varepsilon_a, \tau_a)$ on the Poincaré sphere.

Thus, as a linear dipole antenna rotates, its polarization state on the Poincaré sphere, as can be seen from Figure 6.7, moves along the equator $(\varepsilon_a = 0)$ and, therefore, by equation (6.1)

$$M_w M_a = \cos^{-1}[\cos 2\varepsilon_w \cos(2\tau_a - 2\tau_w)] .$$

Thus using equation (6.2), when $\tau_a = \tau_w$ (see Figure 6.8 (a)) the voltage received is a maximum and equal to
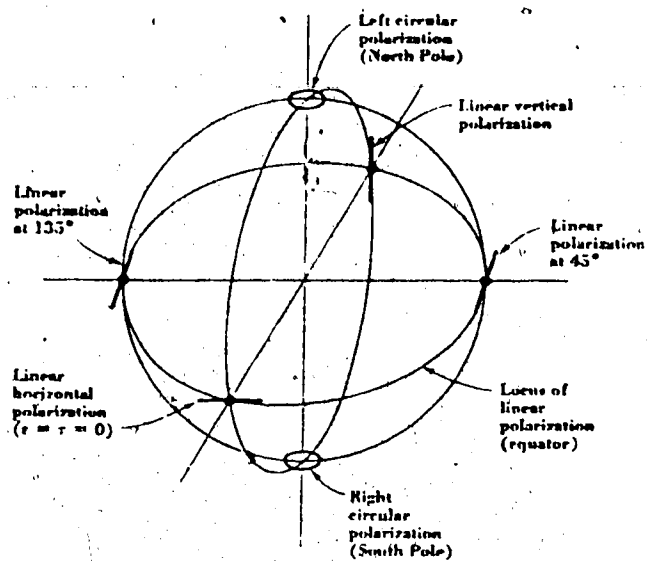
Fig. 6.7 Some polarization states on the Poincaré sphere.

$$\tau_a = \tau_w$$

(a)

$$\tau_a = \tau_w + 90°$$

(b)
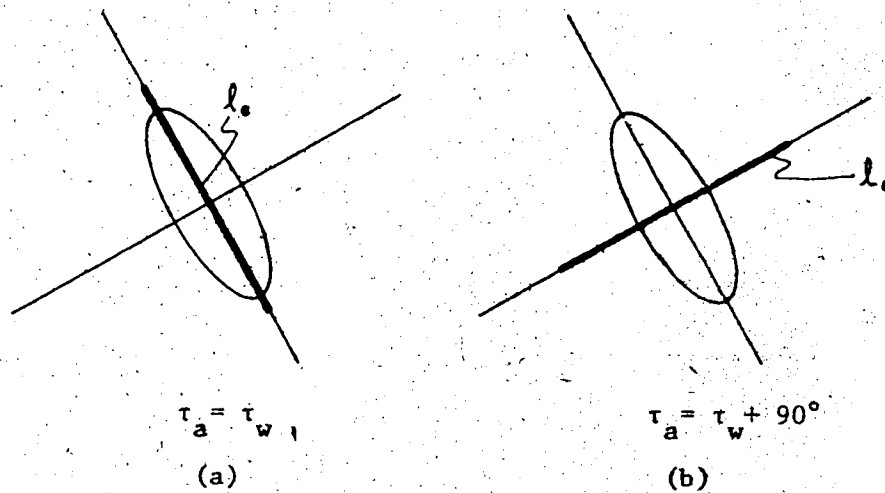
Fig. 6.8 Relative orientation of a linear dipole antenna with respect to the wave polarization ellipse.

$$V_{max} = E\ell_e \cos \epsilon_w$$

and when $\tau_a = \tau_w + 90°$ (see Figure 6.8 (b))

$$V_{min} = E\ell_e \sin \epsilon_w$$

and hence,

$$\frac{V_{max}}{V_{min}} = \cot \epsilon_w = AR .$$

As will be seen later in the section on the receiver, the voltage detected will be proportional to the square of the voltage at the antenna terminals, i.e. proportional to the received power. Therefore,

$$\frac{V_{DET_{max}}}{V_{DET_{min}}} = (\frac{V_{max}}{V_{min}})^2 = (AR)^2$$

and thus,

$$|AR| = \sqrt{\frac{V_{DET_{max}}}{V_{DET_{min}}}}$$

Also the total power in the wave front is proportional to the sum of the detected voltages, i.e.

$$P_T \propto (V_{DET_{max}} + V_{DET_{min}}) .$$

It should be pointed out at this time, that although the above development has assumed that the antenna whose polarization response is to be measured is the transmitter and the rotating dipole is the receiver, by reciprocity the results should be identical if the roles were reversed. Owing to the stability requirements of the oscillator (which will be discussed in section 6.6.4.1) supplying power to the transmitting antenna, it was not desirable to have it located outdoors and if it was inside, it was not feasible to have it feed the rotating dipole due to the length and inflexibility of the cable that was required. (RG-213/U was used to minimize power loss.) Hence, the antenna under test was the transmitter and the rotating dipole the receiver.

6.2.2.2 Maintaining the Plane of Polarization

If the axial ratio over the pattern of the antenna under test is to be accurately determined, the dipole's rotation must always remain in the plane of polarization of the wave. This plane would always be perpendicular to the radial drawn between the phase centers of the two antennas. Hence, the easiest method of maintaining the proper orientation was to have the rotating dipole traverse a circular path. Then for test antennas which radiated in only one hemisphere, the entire polarization response could be measured using a quarter circular arc as shown in Figure 6.9 and allowing the antenna under test, placed at its focus, to rotate in azimuth.
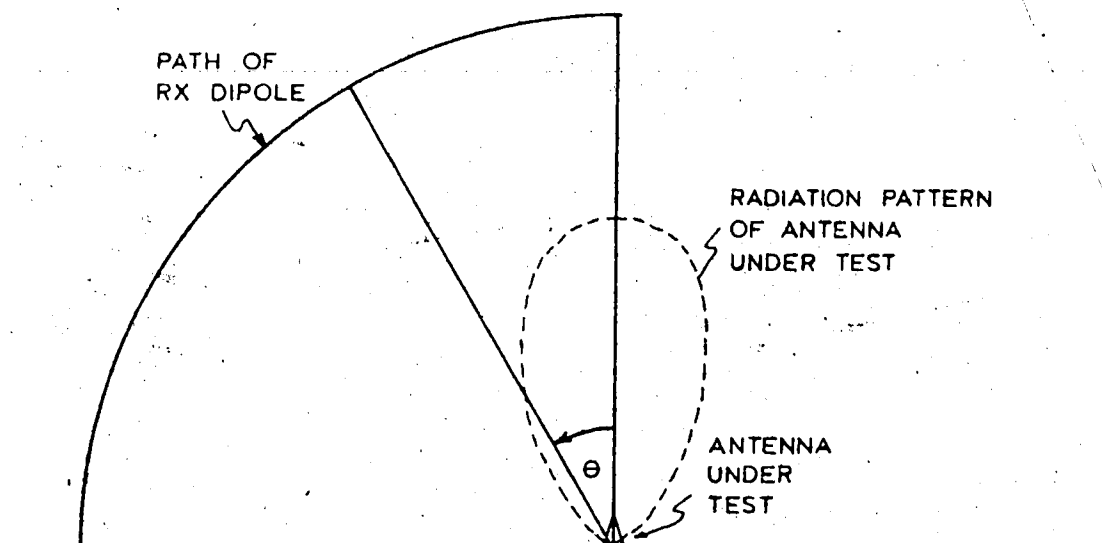
Fig. 6.9 Example of one method of carrying out axial ratio
measurements.

The radius of the dipole's path need not be excessive. Dietrich
and Long [19] have shown that satisfactory far-field axial ratio
measurements could be carried out on conical spirals at only one
antenna height above the apex of the cone. It was expected that the
tallest antenna to be tested would have a cone height of 1.5λ; the
minimum test distance could, therefore, be $\sim 3\lambda$ above the ground plane
(assuming the probe was small enough so that it did not perturb the
field).

Since it was believed that this was not a widely accepted distance
for carrying out axial ratio measurements, the measurement distance was
tentatively and somewhat arbitrarily set at 10λ. Further criteria
for determining this distance would come from the requirements for

measuring the far-field power pattern.

6.3 Measurement of the Far-Field Power Pattern

As can be seen from Figure 6.10, if r the distance from the center
of phase on the antenna under test (in this case a conical spiral) to
the point P where the field is to be measured is large, then R~r for
any source distribution on the antenna structure. Under these conditions
the field at P appears to be due to a point source located at a distance
r from the point where the field is measured. The point P is then said
to be in the far-field of the antenna.
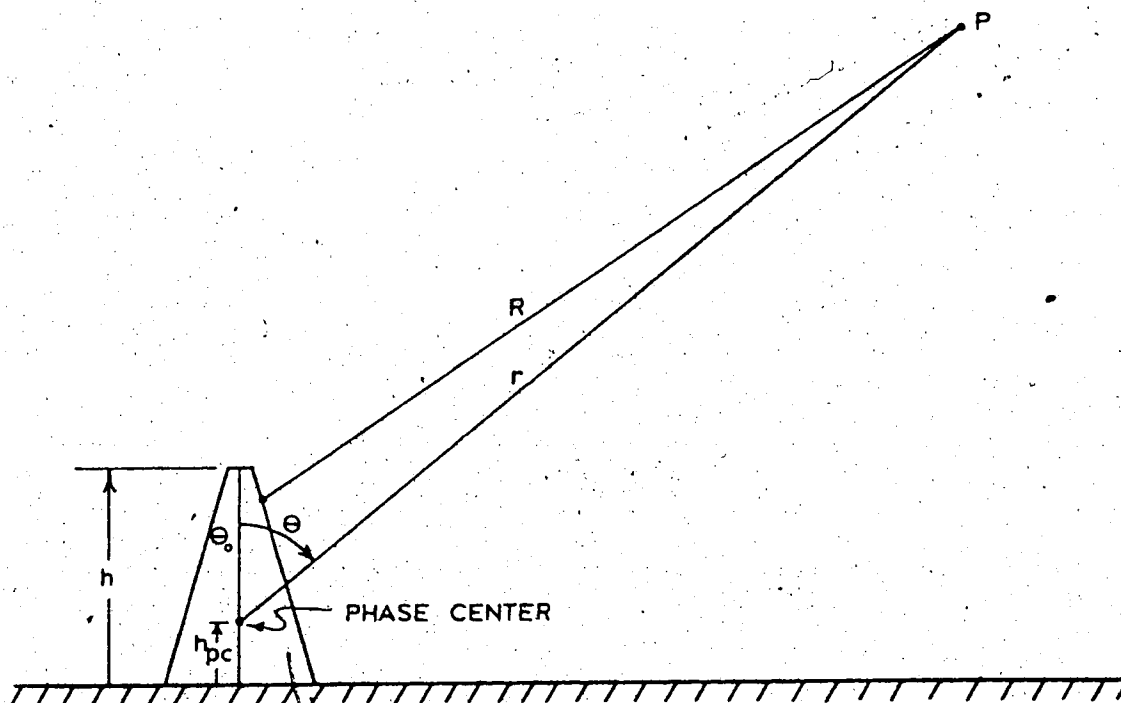
Fig. 6.10 A source distribution contributing to the field at point P.

There are two general criteria for establishing where approximately, this far-field region begins. One of these criteria concerns itself with the error in the magnitude of the field contribution due to a particular source on the antenna structure and the other with its phase. It can be shown that the worst case magnitude error occurs when $\theta=0°$ and the worst case phase error when $\theta=90°$. Under these conditions, the criteria for determining the far-field region become,

$r \geq 5d_e$ for less than 10% error in magnitude

$r \geq \dfrac{2d_e^2}{\lambda}$ for less than $\dfrac{\pi}{8}$ (22.5°) error in phase.

Since the conical spirals tested would all be located above a ground plane, d_e the maximum effective dimension of the antenna would in this case be 2h. Thus, since the tallest antenna to be tested would have a height of $h \sim 1.5\lambda$,

$r \geq 15\lambda$ for less than 10% error in magnitude

$r \geq 18\lambda$ for less than $\dfrac{\lambda}{8}$ (22.5°) error in phase.

It was expected that the test range would be operating at a wavelength of $\lambda \sim 1$ foot (f=985 MHz); therefore, satisfactory far-field pattern and axial ratio measurements could be conducted if $r \geq 18$ ft. It was decided, however, that owing to the weight and awkwardness of the structure required to guide a dipole through a 90° arc, an upper bound to its radius of curvature would be 16 feet. Allowing 1' for the finite

dimensions of the receiver housing and the equipment used to rotate the dipole, an effective radius of curvature for the dipole was $15' = 15\lambda$. This distance would be sufficient for the majority of antennas as far as pattern measurements were concerned and more than sufficient for all antennas as far as AR measurements were concerned.

6.4 The Design of a Zone of Minimum Interference (Quiet Zone)

If power measurements between a given transmitting and receiving antenna are conducted such that no stray reflections are incident on the receiving antenna, accurate measurements can be attained. The region so defined will be referred to here as the "quiet zone" of the antenna test range.

Design of the quiet zone proceeded with the idea in mind that unwanted reflections should not only be attenuated but, where possible, also directed away from the region where measurements were being made, in this case the quarter circular path travelled by the receiving dipole. It was, therefore, decided to surround the test area with reflectors (see Figure 6.11) made of microwave absorbing material, oriented in such a manner that any radiation not absorbed would be directed harmlessly into space.

An estimate, using ray theory, of the best orientation for the reflector/absorbers and the determination of the resultant quiet zone is developed below.

Figure 6.12 shows a plan of the roof where the test range was to be built. The locations of objects which could be responsible for un-wanted reflections are shown in the plan along with their respective heights above the base of the roof. Because of the availability of an

existing anchoring frame in the southeast corner which would be

useful in the setting up of the 90° measurement arc (see section 6.5.1),
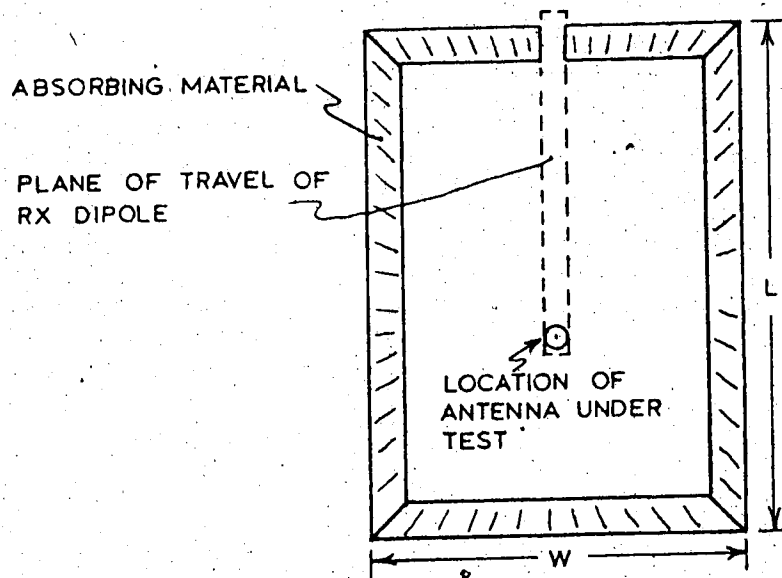
Fig. 6.11 General layout of test range viewed from above.

the range was oriented as shown in the diagram.

For operational considerations (height of the turntable used to

rotate the transmitting antenna in azimuth, limited radius of curvature

of RG-213/U cable feeding the transmitting antenna, possibility of

water and snow on the roof) the base of the range was raised 16 inches

above the gravel base of the roof. The base of the test range would

represent the ground plane for the antennas to be tested.

Referring, now, to Figure 6.13, the ray paths which will help to

determine the proper orientation of the reflector/absorbers which en-

close the test range are shown.

38′

h=33″

h=38″ o

28′

o h=10″

h=46″

33′

h=65″

14′

METAL
FLASHING   73′
h=24″

2′

h=36″

h=33″

31′

h=15″

o h=2″

73′
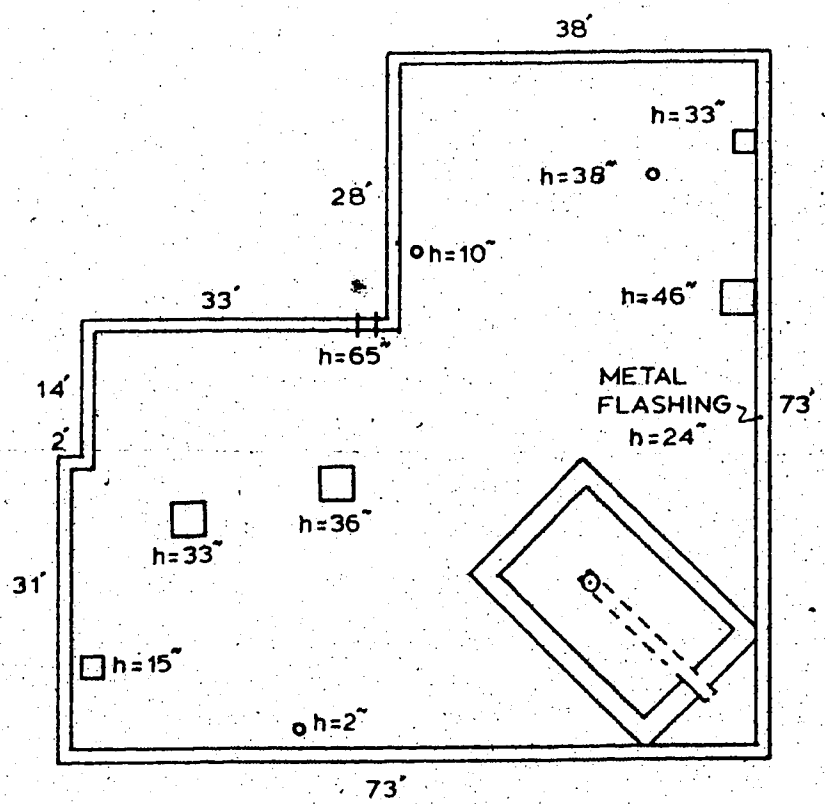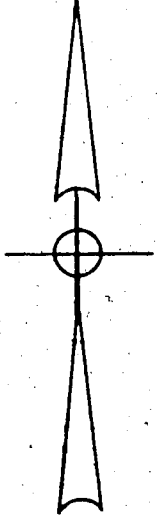
SCALE   1″=20 FEET

Fig. 6.12 Plan of roof of Electrical Engineering Building showing

obstacles and location of test range.
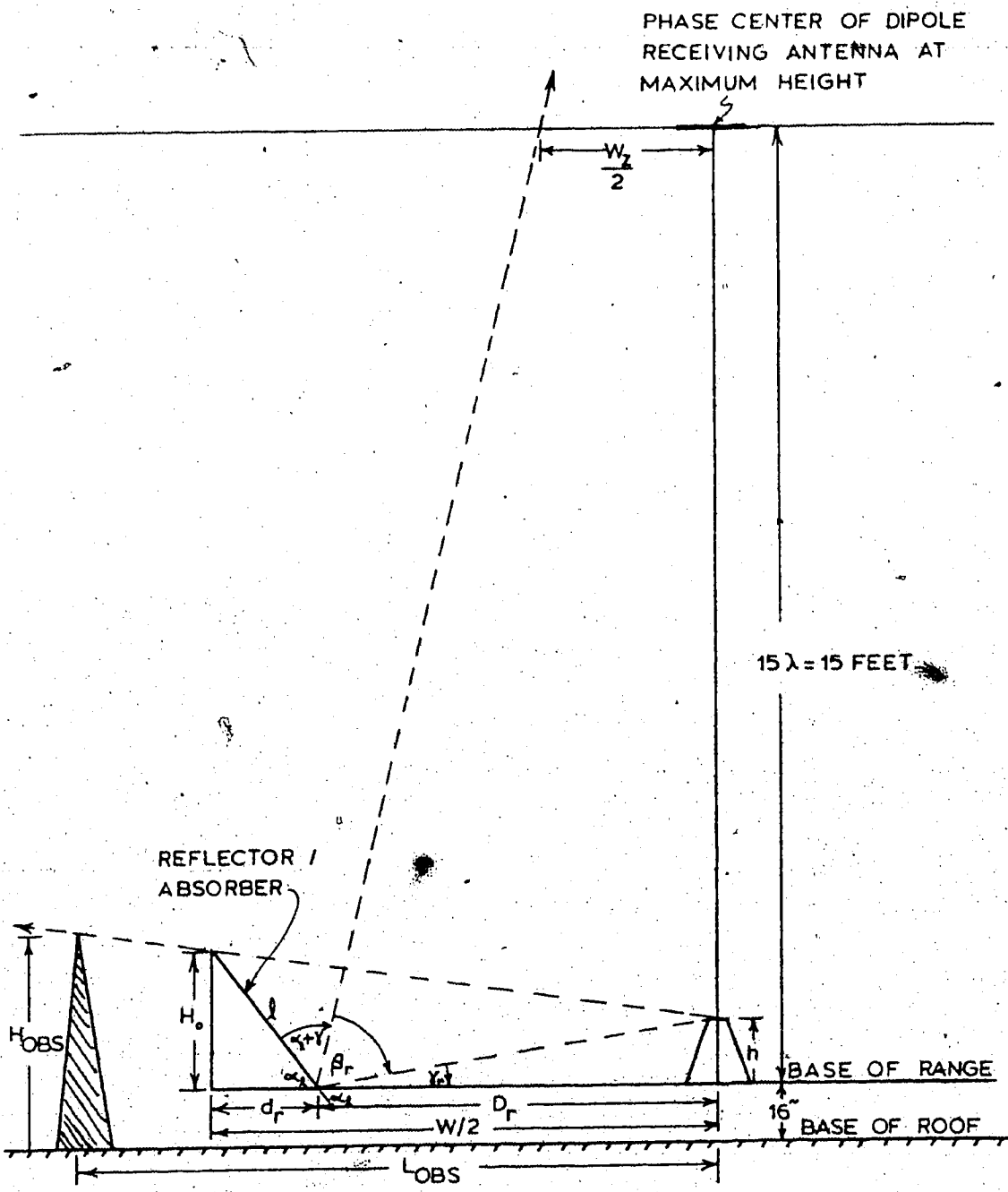
Fig. 6.13 Ray paths for determination of quiet zone.

The transmitting antenna will not "see" the obstacle if

$$\frac{H_o - h}{W/2} > \frac{H_{OBS} - 1.33 - h}{L_{OBS}} \tag{6.3}$$

where all dimensions are in feet. It was found that the maximum value of the right side of equation (6.3) was set by the adjacent building on the north side (H_{OBS}= 20 ft, L_{OBS}= 210 ft), with the result that (the tallest antenna to be tested would have a height of 1.5λ, and at a range frequency of 985 MHz this meant that h=1.5 feet)

$$\frac{H_o - h}{W/2} > .082 .$$

Owing to the particular dimensions of the absorbing material, and since it was not desirable to cut it, the reflecting surface dimension ℓ was fairly well constrained to be 3 feet. Also, since only a limited amount of the material was available, restrictions on the physical area of the reflecting/absorbing surface placed the width W at approximately 16 feet and the length L at approximately 28 feet. Therefore

$$H_o - h \gtrsim .65 \text{ feet}$$

or

$$H_o \gtrsim 2.15 \text{ feet}$$

and thus

$$\alpha_\ell \gtrsim \sin^{-1} \left(\frac{H_o}{\ell} \right) \sim 45° .$$

With the reflector/absorber orientation angle α_ℓ set, the minimum zone of interference can now be deduced. Referring again to Figure 6.13,

$$D_r = W/2 - \ell \cos\alpha_\ell = 5.9 \text{ feet}$$

$$\beta_r = 90° - 2\gamma_r$$

$$\gamma_r = \tan^{-1}(h/D_r) = 14.2°$$

Therefore,

$$W_z = 2(D_r - 15 \tan\gamma_r) = 4.2 \text{ feet} = \text{width of quiet zone at height of } 15\lambda.$$

The quiet zone up to the maximum measurement height of 15λ should be at least as wide as that depicted in Figure 6.14. It widens as either the antenna height shrinks or D_r is increased or both. It should thus be possible to carry out measurements anywhere along the 90° measurement arc without interference from unwanted reflections.

6.5 Construction

A picture of the completed test range is shown in Figure 6.15. The details of the construction of its various components will now be discussed.

6.5.1 The Measurement Track

In order to guide the rotating dipole throughout its 90° measurement arc, a track was constructed, along which a carriage (see section
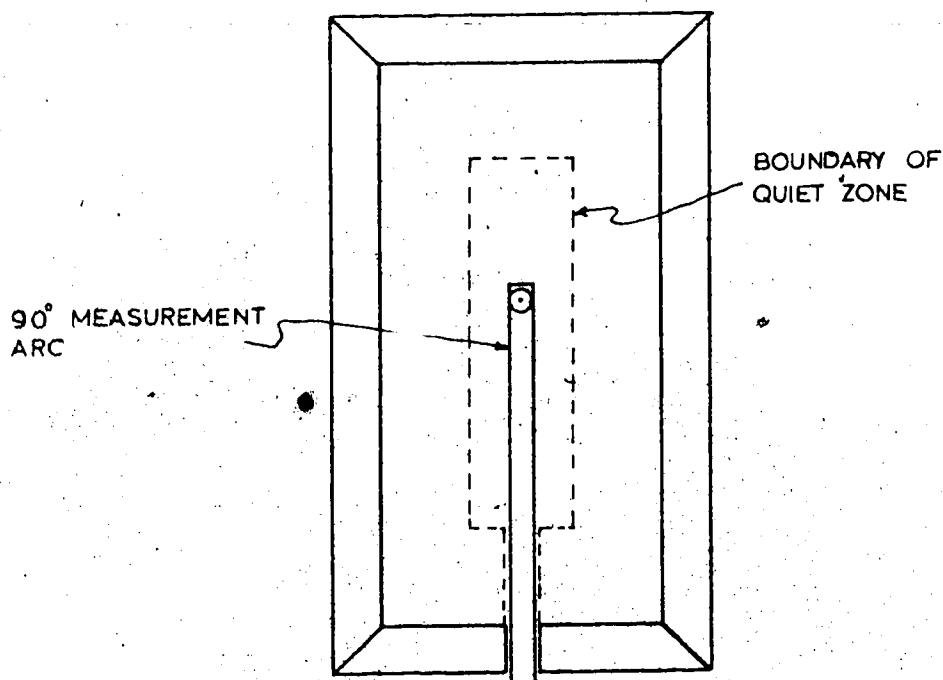
Fig. 6.14 The quiet zone within the range.

6.5.3), carrying the receiving equipment and dipole, travelled.

The track consisted of two T-shaped sections, each section constructed from laminations of 1" poplar plywood cut to the proper radius of curvature (see Figure 6.16). Having the track in two sections would aid in its construction, handling and future storage. The radius of curvature of the track was 16 feet as specified in section 6.3.

Once the two sections of the track had been raised to the test site on the roof, they were bolted together using ten 1/2" diameter steel bolts (non-metallic bolts had been made which could replace the steel bolts once the track was in position and ready for measurements — it was found, however, that the steel bolts contributed negligible reflections and the practice was discontinued). One end of the track was

Fig. 6.15 The microwave antenna test range structure.
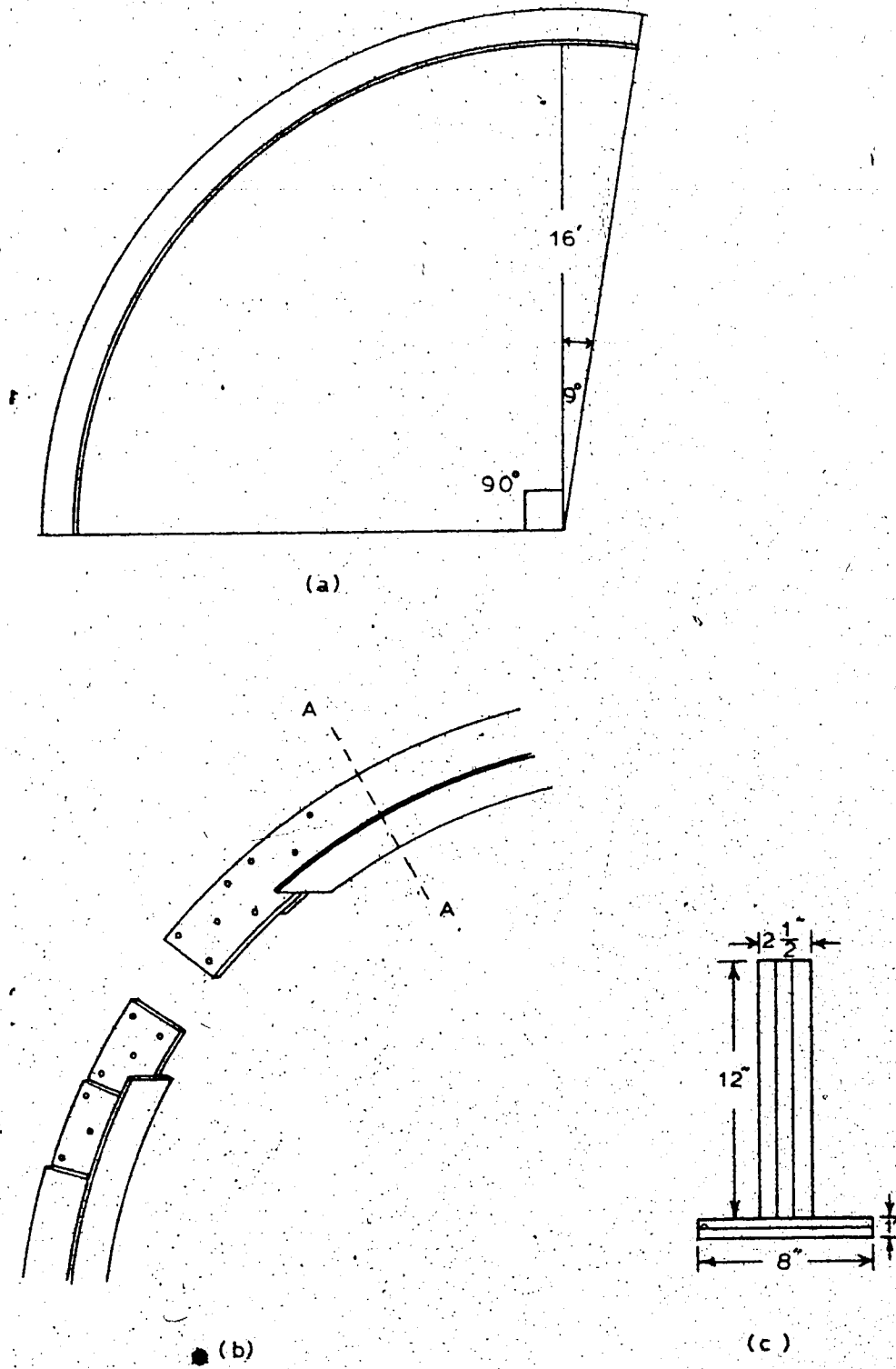
Fig. 6.16 The measurement track showing (a) its arc length, (b) joint between the two sections, (c) its T-shape (cross section A-A).

then anchored by a hinge attached to an existing frame in the southeast corner. The track could then be raised to its operating height using a gin pole and power pull arrangement, also located in the southeast corner. Once up, a wooden triangular structure was moved into place to support its free end.

The arc was actually 9° over its required 90° angular length, partially so that the height of its focus relative to its hinged base could be adjusted yet still retain at least 90° of arc for measurements, and partially to allow for the support structure at either end.

The track could not be constructed from steel because of the severe reflections that would result. It was felt, however, that a fairly good compromise between weight and strength had been achieved. The total weight of the track, i.e. both sections, was approximately 300 lb.

The surface area of the track and its support structure was kept to a minimum in order to avoid excessive wind loading. The track in its "up" position has withstood winds gusting to 65 km/hr and has been used in test range measurements in winds up to 32 km/hr with negligible vibration effects being observed on the recordings.

6.5.2 Dipole Rotation Assembly

The rotation of the dipole was performed through a gear arrangement shown in Figure 6.17 which was driven by a 2-phase 400 Hz induction servo motor. The position of the dipole was monitored by placing a voltage across a 10 k potentiometer, the top voltage of which was arranged to vary linearly and synchronously with the rotation of the dipole. This voltage would supply the X-input of the recorder used in the axial ratio measurements, the experimental procedure of which will

POTENTI-   ROTATIONAL
OMETER   COUPLER   IDLER MOTOR
GEAR   GEAR   GEAR   DRIVE
                                  GEAR

1 : 1   3 : 1   1 : 1
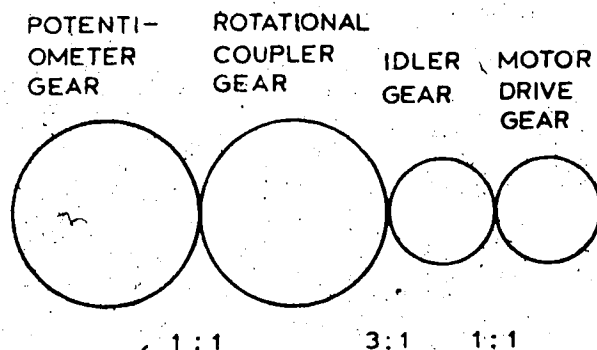
Fig. 6.17 Gear arrangement of dipole rotation assembly.

be detailed in Chapter 7.

For information on the induction motor and its 400 Hz power supply, the reader is referred to Appendix B.

6.5.3 The Receiver Carriage

The receiver, dipole, and dipole rotation assembly were transported along the measurement track by a carriage constructed of 3/8" acrylic material, and using four ball bearings as rollers. Regardless of the zenith angle at which measurements were being taken, the rollers of the carriage always remained in contact with the track surface, owing to a spring arrangement of 2 ball bearing rollers on the opposite side. By adjustments available on the ball bearing casings, the carriage could be tilted sideways or up and down to allow for fine

adjustment of the receiving antenna. Because of the low gain of the dipole used, these adjustments were not found to be necessary.

The angular position of the dipole above the ground plane of the test range was monitored with the aid of a 25 k, ten-turn potentiometer attached to the receiver carriage. The potentiometer, in turn, was geared to a spool of known circumference. A cable was then attached at one end of the track, wrapped once around the spool and fastened to the other end of the track. As the carriage moved, the spool rotated. Thus, knowing the ratio of spool turns to potentiometer turns (10.3:1) a voltage V could be placed across the potentiometer such that its tap voltage would indicate degrees along the track when fed into a digital voltmeter. It is not difficult to show that this voltage is given by the expression

$$V = \frac{150 \ CG \ 10^n}{\pi \ R} \qquad \text{Volts}$$

where

C = circumference of spool in inches

G = the gear ratio between spool turns and pot turns

R = radius of curvature of imaginary arc travelled by the spool in feet

n = positive or negative integer which determines the decimal place of the recorded voltage.

Using this method, the dipole's indicated height could be read to a precision of .1° and was found to repeat to within .5° as the carriage was moved from the base of the track to the top.

6.5.4 Altitude Drive

A drive mechanism had been devised to position the dipole remotely anywhere along the measurement track. It was found, however, to be too slow, too inaccurate and too unreliable. Hence, it was abandoned.

Time did not allow for the design and construction of a new remote positioning mechanism; therefore, the dipole's position was set manually through the use of a cable and pulley system. For future use of the range, it is suggested that a winch, located below the ground screen, be used to remotely alter the position of the dipole along the arc.

6.5.5 The Reflector/Absorbers

Supports for proper orientation of the absorbing material were constructed entirely out of wood, using glue and wooden dowels for bonding purposes. Each support had a reflecting surface area of 6' x 3' and fourteen were made.

Since there was only a limited amount of the absorbing material that was desired (CH type), two types were used:

Eccosorb CH; reflectivity - 20 dB at .94 GHz ; 4" thick

Eccosorb FR-330; reflectivity - 20 dB at 2.3 GHz ; 2" thick.

Because of the expected poorer reflectivity of the FR type , it was placed in the lower 1/3 of the reflecting/absorbing surface and two layers were used. Power radiated at these low elevation angles was expected to be at least 20 dB down from the zenithal level.

The final arrangement of the absorbing material which encompassed the test area is shown in Figure 6.18.

MEASUREMENT
TRACK

METAL MESH
GROUND PLANE

REFLECTOR / ABSORBERS
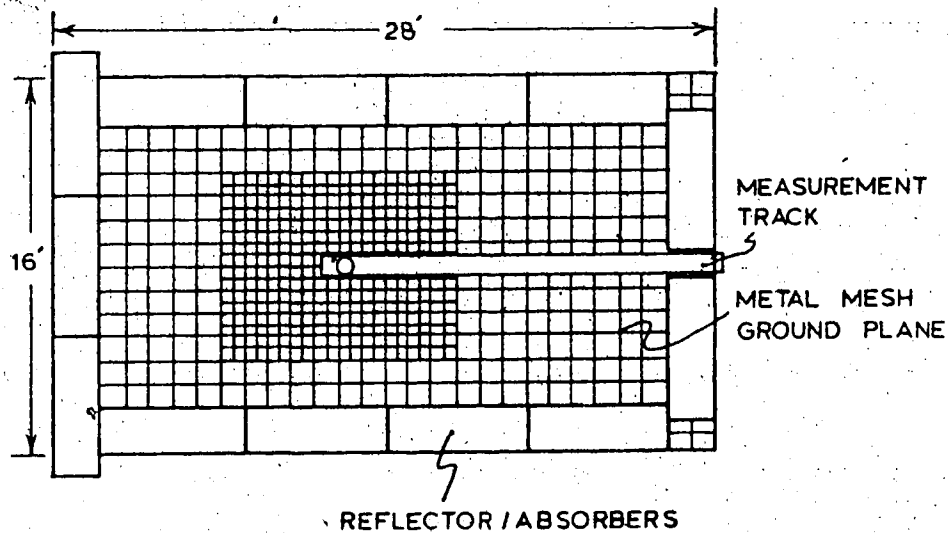
Fig. 6.18 Final layout of the test range.

6.5.6 The Ground Plane

A 16' x 28' frame constructed of 2 x 4's raised the antenna test

range approximately 16 inches above the gravel base of the roof. On

top of this frame was placed 2" galvanized metal mesh. Within a

radius of about 4 feet of the transmitting antenna's location, another

layer of metal mesh was placed in such a manner that the resulting mesh

had a 1" by 1" spacing. At the location of the transmitting antenna

(it is apparent that the mesh could not be placed over this region if

the turntable was to be used) a 2 foot diameter copper plate, bolted

to the turntable, began where the mesh left off. As will be pointed

out in section 7.4.6 this ground plane satisfactorily represented a

uniform.perfectly conducting ground plane.

6.5.7 The Azimuth Positioner

Rotation of the transmitting antenna in the ϕ direction was

accomplished remotely using a Scientific-Atlanta azimuth positioner.

The instrument was capable of quite accurate positioning (within a

few minutes of arc) and provided trouble free operation.

A complete list of its specifications can be found in Appendix C.

6.6 The R.F. Section

6.6.1 Operating Frequency

Up until now, design of the test range has proceeded under the

assumption that the operating frequency would be approximately 985 MHz.

This frequency was chosen as a good compromise between too low a

frequency, which would make measurements on a compact range less

accurate, and too high a frequency which would make construction of the

model antennas difficult. Unfortunately, 985 MHz fell into the radio-

navigation band; hence, the lower frequency of 959 MHz (λ=12.4"), which

was open to space research on an experimental basis, was used.

6.6.2 Noise Considerations

If the transmitting and receiving sections of the test range can

be represented as shown in Figure 6.19 , and assuming that the pre-

amplifier's gain is high enough so that noise contributions following

$T_A = T_S + T_{NS}$

$G_{RX} = 1.64 \ (2.15 \ dB)$

$\lambda / 2$ DIPOLE

```
50Ω ─┤ CABLE, BALUN, FILTER,   PREAM-    SQUARE   D.C.
      │ MATCHING  NETWORK      PLIFIER   LAW      AMPLI-
      │   ε₁, T₁               F, G₂, T₂  DETECTOR FIER
RECEIVER
```


$G_{TX} \sim 10 \ (10 \ dB)$

CONICAL SPIRAL

```
50Ω ─┤ CABLE,         ATTENUATOR    POWER
      │ MATCHING                    OSCILLATOR
      │ NETWORK                     f = 959 MHz
```
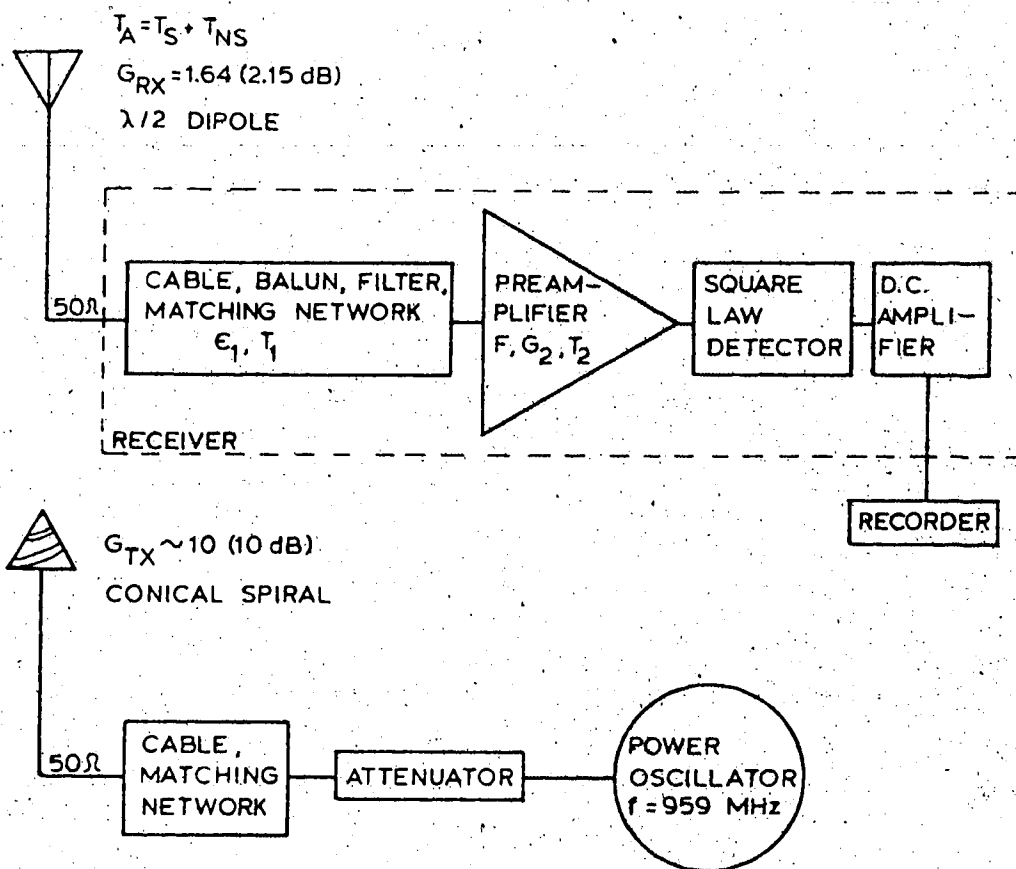
Fig. 6.19 Representations of the transmitting and receiving sections.

it are negligible, then the total power (i.e. signal and noise) at the terminals of the detector is,

$$P_T = G_2 \epsilon_1 k T_T B = G_2 \epsilon_1 k (T_S + T_{NS})B + G_2 \epsilon_1 T_1 kB + G_2 T_2 kB \qquad (6.4)$$

where

k = Boltzmann's constant

T_T = total equivalent temperature (signal and noise) of system

T_S = equivalent temperature of received signal power

T_{NS} = equivalent temperature of artificial noise power in environment

$T_1 = \dfrac{(1-\epsilon_1)}{\epsilon_1} T_{phys}$ = equivalent noise temperature of first stage

$T_2 = (F-1)T_o$ = equivalent noise temperature of second stage

$T_o = 290°K$ due to IEEE definition of noise figure

B = predetection noise bandwidth of system.

Equation (6.4) can also be written in terms of equivalent temperatures as

$$T_T = T_S + T_N = T_S + T_{NS} + T_1 + \frac{T_2}{\epsilon_1}$$

where T_N is the total noise power equivalent temperature.

In an urban environment the power density of the artificial noise per KHz bandwidth is on the order of 10^{-14} Watts/m^2 [41]. For a $\lambda/2$ dipole ($A_{eff} \sim 13 \times 10^{-3}$m^2 at 959 MHz) this results in $T_{NS} \sim 10^{4}°K$. Then if the attenuating first stage has a power transmission coefficient ϵ_1 = .5 and a physical temperature of T_{phys} = 300°K, and the preamplifier has a worst case noise figure of $F = 4$ (6 dB),

$$T_N = 10^4 + \frac{(1 - .5)}{.5} .0300 \times 10^4 + \frac{(4-1)}{.5} .0290 \times 10^4$$

$$= 1.2 \times 10^4 \; °K .$$

If, now, a minimum signal to noise ratio of 100 is desired,

$$T_{S_{min}} = 1.2 \times 10^6 °K .$$

Thus the transmitter must transmit enough power such that under minimum signal conditions an equivalent signal power of $P_{S_{min}} = kT_{S_{min}} B$ is available at the dipole.

6.6.3 Power Considerations

For a system noise bandwidth of (say) B = 100 MHz and recalling from the previous section that $T_{S_{min}} = 1.2 \times 10^6 \, ^\circ K$, then

$$P_{S_{min}} = kT_{S_{min}} B = 1.38 \times 10^{-23} \times 1.2 \times 10^6 \times 10^8 \sim 1.7 \times 10^{-9} \text{ Watts.}$$

Now, for a transmitting antenna of gain $G_{TX} = 10$ and a maximum test range distance of 15λ (from section 6.3), the ratio of the power received to the power transmitted under the conditions of best pattern orientation is

$$\frac{P_{RX}}{P_{TX}} = a \, G_{RX} G_{TX} \left(\frac{\lambda}{4\pi R} \right)^2 = a \, 4.6 \times 10^{-4}$$

where the factor a will depend on the polarization of the wave transmitted, and the orientation of the dipole relative to that polarization. For a linear dipole receiving circular polarization, a = 1/2; therefore, the minimum transmitted power must be

$$P_{TX_{min}} = \frac{P_{S_{min}}}{P_{RX}/P_{TX}} = 7.1 \mu W \; (\sim -21 \text{ dB}_m).$$

Then, if it is desired to measure the power pattern to 40 dB below its maximum value, yet retain a signal to noise ratio of 100, the power transmitted must be at least

$$P_{TX} = 71 \text{ mW} \qquad (\sim 19 \text{ dB}_m) \; .$$

6.6.4 The Transmitting Section

6.6.4.1 The Power Oscillator

Using the value of P_{TX} arrived at in the previous section and assuming that cable and mismatch losses are on the order of 10 dB (remembering that the power must be transmitted from the laboratory up to the roof of the Electrical Engineering Building), then the power oscillator (or oscillator-power amplifier combination) must be capable of supplying a power of .71 Watts.

Tube oscillators available in the department could do no better than supply a power 10 dB below this requirement at the operating frequency of 959 MHz. Although it is possible that this would have been sufficient, preliminary tests indicated that even under controlled conditions, their stability was questionable.

Power oscillators were, of course, available commercially; however, they were expensive and their specifications generally far exceeded those required.

Fortunately, there were excellent papers available [42], [43], [44], on the design of low cost microstrip power oscillators. This was, therefore, the approach taken. The design equations and circuit schematic of the power oscillator are given in Appendix D; only the

oscillator's relevant properties will be presented here.

The power to the transmitting antenna must remain constant over the time that measurements are being taken (approximately 4 to 5 hours) and the frequency must remain sufficiently stable so as not to enter a significantly different region of the frequency response of the filter primarily responsible for setting the system bandwidth. (The filter is discussed in section 6.6.5.3). Measurements carried out on the microstrip oscillator when fed from a regulated supply, indicated that the power output changed by less than 4% and the frequency by less than .05% over a 12 hour period. Spikes and discontinuities evident on the strip chart recording of indicated power but totally absent from the recording for frequency, suggested that, perhaps, the strip chart channel recording power was not functioning properly and therefore the power stability was better than indicated. Unfortunately, the strip chart recorder broke down shortly thereafter, and it was not possible to check this out further. This was of little consequence, however, since the power and frequency stabilities were sufficient.

The oscillator was tuned to a frequency of 959.0 MHz and its supply voltage was adjusted until the power into 50 Ω was 1 Watt. Throughout the experiments, the power and frequency of the oscillator were continuously monitored, although, except for the initial stability tests, not continuously recorded.

6.6.4.2 The Attenuator

A 3dB power attenuator was initially placed in front of the power oscillator so that power could be boosted for more accurate measurements at low zenith angles without changing its power supply voltage. It

was, eventually, replaced by a 10 dB and sometimes 20 dB power attenuator (depending on the radiating efficiency of the antenna under test) so that the detector in the receiving section would remain in the square law region of its characteristic.

6.6.4.3 The Transmitting Antenna Feed Cable

The transmitting antenna, located on the roof of the Electrical Engineering Building, was fed from the Radio Astronomy Laboratory, located two floors down, through approximately 70 feet ($\sim$ 6dB) of RG-213/U cable. Specifications for this cable and other types used in the experiment can be found in Appendix E.

6.6.4.4 The Matching Network

Depending on the angle of wrap, the method of feed, the arm width and the cone angle of the conical spirals tested, their input impedance was expected to be real, and to vary between 100 and 200 ohms [18]. For this reason $\lambda/4$ matching sections of cable with characteristic impedance 73 ohms (RG=59/U) and 93 ohms (RG-67A/U) were constructed which could then match loads of 107 ohms and 173 ohms, respectively, to 50 ohms.

6.6.5 The Receiving Section

6.6.5.1 The Dipole Antenna

A resonant $\lambda/2$ dipole constructed out of 1/16" diameter ($Z_{o_{avg}} \sim 500$ at 959 MHz) brass rod was used as the receiving antenna. It was matched to a length of RG-58A/U ($Z_o = 50\Omega$) cable by cutting the ends of a $\lambda/2$

dipole until the return loss at the operating frequency of 959 MHz was maximized.

The transformation from the balanced antenna to the unbalanced feed line was accomplished by the use of a balun built into the feed axis of the antenna (see Figure 6.20). Two $\lambda_g/4$ sections of 1/4" copper tubing were placed over a length of RG-58A/U cable and shorted to the outside sheath of the cable a distance $\lambda_g/4$ below the feed point. ($\lambda_g = \lambda/\sqrt{\epsilon_R}$, where ϵ_R, here, is the dielectric constant of the PVC jacket of the coaxial cable.) Currents flowing on the outside of the outer sheath of the coaxial cable would then have high impedances presented to them whether they originated from the top or bottom. Thus a balanced feed should result.

The entire feed arrangement was then encased in acrylic for rigidity, and a BNC connector was attached at the bottom for connection to a rotational coupler.

6.6.5.2 The Rotational Coupler

The permanently fixed cable and amplifying sections of the receiver must in some fashion be connected to the rotating dipole. This connection is made by a rotational coupler. Within the limits of the measuring equipment (resolution, .05 dB) the loss in the coupler was found to remain constant as its one end was rotated. This insertion loss was measured to be on the order of .1 dB for any frequency between 650 MHz and 1.2 GHz.

6.6.5.3 The Band-Pass Filter

The system bandwidth was primarily set by a band-pass filter placed

1/16" BRASS ROD

COPPER TUBING

ACRYLIC

COAXIAL CABLE DIELECTRIC

CENTER CONDUCTOR

OUTER SHEATH

PVC OUTER JACKET

10"
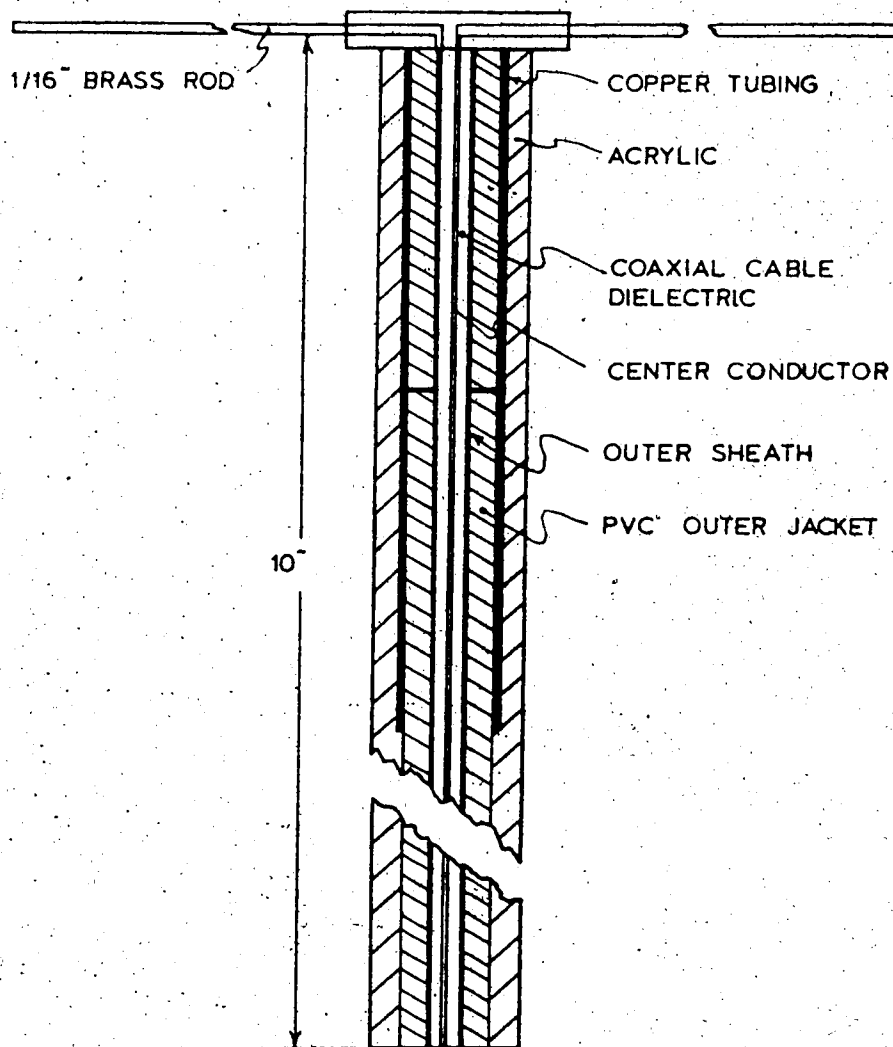
Fig. 6.20 Receiving dipole with built-in balun.

in front of the preamplifier. The filter, shown in Figure 6.21, consisted of 2 microstrip resonators formed from 2.8 mil copper, etched on a 1/32" thick polyethylene board.

The filter had a   dB bandwidth of 42 MHz centered on 964.8 MHz and a return loss of better than 25 dB at 959 MHz. (Note that in section 6.63, which determined the transmitter power required for a signal to noise ratio of 100, a bandwidth of 100 MHz was assumed.) The mid-band insertion loss of the filter was approximately 3 dB; however, this was considered tolerable and could only be reduced at the expense of increasing the bandwidth.

As can be seen from Figure 6.22, higher modes are present and are responsible for the second peak in the filter response at 1.74 GHz. This, however, presents no problem since the bandwidth of the pre-amplifier, which follows it, is high frequency limited at 1 GHz.

For more details on this filter, the reader is referred to Appendix D.

6.6.5.4 The Preamplifier

Preamplification of the signal was accomplished immediately after the band-pass filter in order to minimize the noise power due to cable loss between the filter and preamplifier. Hence, the preamplifier was mounted on the receiver carriage which moved up and down the measurement track. It therefore had to be small, lightweight, and capable of operating over a wide temperature range. The Watkins-Johnson 6201-342 wide band (5 MHz to 1 GHz) amplifier met these requirements handsomely. Its measured gain versus frequency characteristic is shown in

Fig. 6.21 The 2 resonator microstrip band-pass filter,
shown outside its casing.
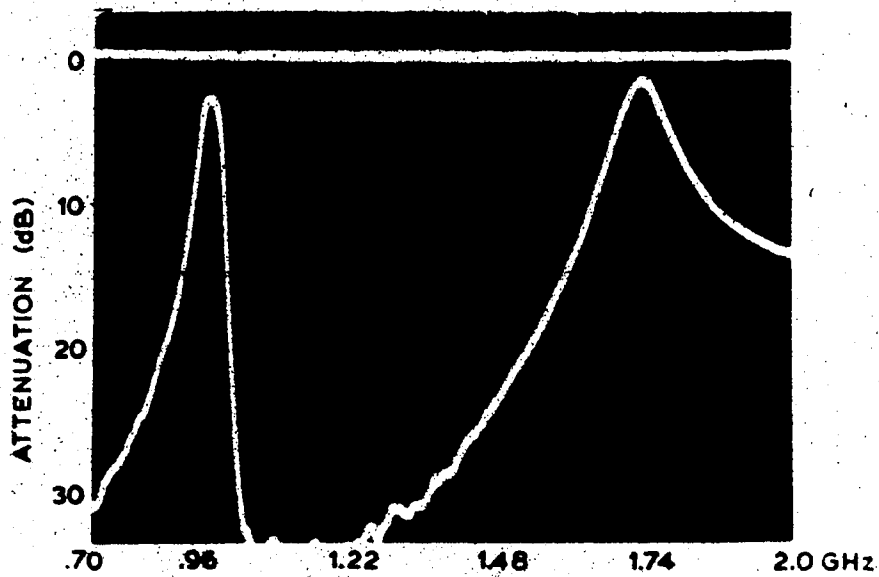
Fig. 6.22 Filter response from .7 GHz to 2.0 GHz.

Figure 6.23 and a detailed list of its specifications follows:

Guaranteed Specifications of WJ6201-342 wideband amplifier at 25°C

Noise Figure = 4 dB

Gain = 27 dB

Gain Flatness(5-1000 MHz)= ±1.5 dB

VSWR(input and output) = 2.5:1

Power Output = +6 dB$_m$

Supply Voltage(nominal) = 15V

Current (typical) = 33mA

Temperature Range = -54°C to + 71°C.

6.6.5.5 The Square Law Detector

By converting the microwave power of the preamplifier to D.C. power at the receiver carriage, the heavy and semi-rigid R.F. cable that would have been required to transmit the microwave power to the laboratory for conversion was avoided. In addition, the R.F. cable losses (∿ 10 dB) that would have resulted in this cable, had it been required, were eliminated. (The D.C. losses were negligible.)

For detection, an HP423A negative voltage square law crystal detector with optimum load resistor was used. Up to an output voltage of 50 mV, its characteristic does not deviate from square law by more than ± .5dB when using the optimum load resistor. At 1GHz it has an SWR of better than 1.2 and its sensitivity is, typically, greater than .1mV/μW.

Because drift in the D.C. amplifier, which had a gain of approximately 100, set the minimum recordable voltage at approximately 1mV and deviation of the detector from square law set the maximum recordable
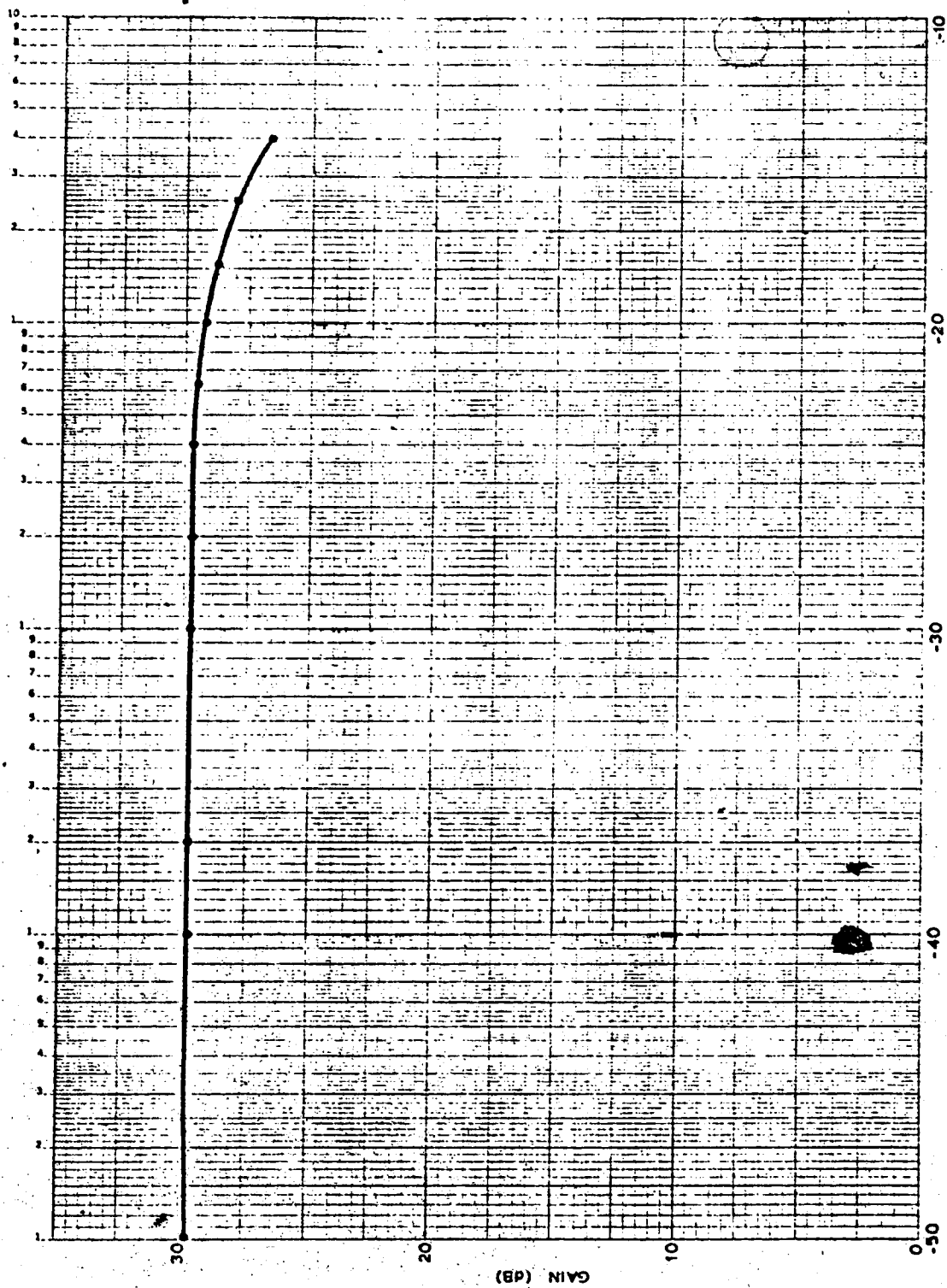
Fig. 6.23 Measured gain versus input power characteristic of preamplifier.

voltage at approximately 5V measurements could be carried out over a dynamic range of approximately 37dB. The error over this range would primarily be set by the crystal detector and be on the order of .5dB. By correcting measurements taken at detector output levels greater than 50mV for non-square law operation the measurement range could be extended to 40dB where now the high level limit is set by the 100mW maximum CW input power to the detector. If the detector's D.C. voltage output versus microwave power input characteristic could be determined to a sufficiently high accuracy, all measurements, high and low level, could be corrected for deviation of the detector from square law operation and thus obtain an accuracy better than .5dB.[b] This was not considered necessary and such corrections were not made.

6.6.5.6 D.C. Amplification

The detected voltage was raised to a recordable level by two stages of D.C. amplification (each x10). As a precaution against small interfering voltages that may enter into the cable transmitting the D.C. voltage to the laboratoty, a preliminary stage of D.C. amplification was carried out at the receiver carriage. This first stage consisted of a µA 741 linear I.C. amplifier operating in the non-inverting mode. No special circuitry was added to the typical application circuit shown in Figure 6.24; however, it was shielded by placing the amplifier in a 1/2" diameter length of brass tubing. In order to minimize the effects of temperature variations, the tubing was then filled with an epoxy of low thermal conductivity. BNC connectors, attached to the ends of the tubing, completed the structure. The output voltage of this first stage was then
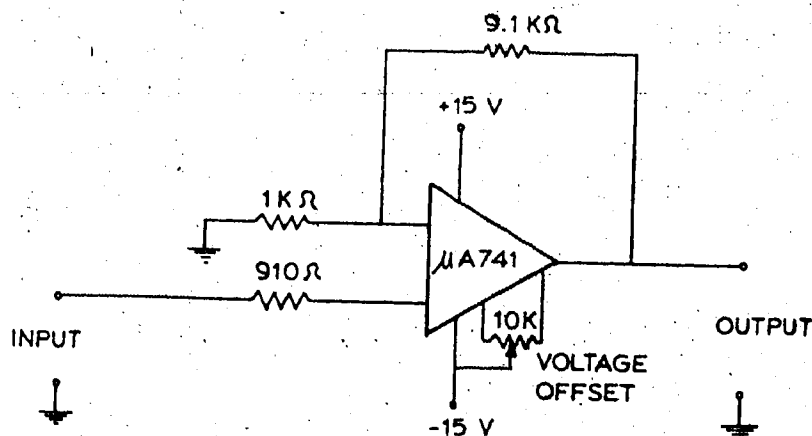
.Fig. 6.24 Schematic of first stage of D.C. amplification.

transmitted down to the laboratory through a shielded cable where it underwent further amplification.

This second stage of D.C. amplification was performed by the very stable amplifier of an analog computer. Any voltage offset.due to the first stage could be easily monitored on the computer's built-in digital voltmeter and easily corrected by introducing an equal voltage of opposite polarity into the second stage. The DVM of the computer was also of use during measurements in that it provided a digital readout of the voltage being recorded.

Since the minimum power to be received was on the order of $-60dB_m$ the minimum voltage to be recorded was on the order of 1mV. If the drift of the D.C. amplifier combination was severe enough, an error would be introduced in the axial ratio measurement. However, these low power levels occurred only at high zenith angles ($\theta > 70°$) where the AR was large (i.e. the polarization almost linear) and hence the error

unimportant. Nevertheless, accurate AR measurements could be made at

these high zenith angles by boosting the transmitted power by 10 or 20 dB

as discussed in section 6.6.4.2. If this approach was not desirable, the

D.C. amplifier combination could be zeroed just prior to the recording

of a low power measurement. The results thus achieved were quite

accurate for most purposes since the total drift, over the entire

period that measurements were being made (4 to 5 hours), rarely exceeded

3mV.

6.6.5.7 Receiver Prototype

The completed receiver is shown attached to the underside of the

receiver carriage in Figure 6.25. The various components in the

photograph can be identified by comparing it with the diagram of Figure

6.26. The recorder voltage as a function of the microwave power at the

input to the rotational coupler of the receiver prototype is shown in

Figure 6.27. As can be seen, the voltage versus power characteristic

remains within .5dB of square law at least up to 5V.

The complete receiver package including the receiver carriage,

receiver, dipole and dipole rotation assembly weighed approximately

20 lbs.

6.6.6 The Measurement and Control Center

All power required for the monitoring of position, operation of

the receiver, rotation of the dipole and rotation of the azimuth

turntable originated from the area referred to as the measurement

and control center. In addition, the microwave power feeding the

transmitting antenna was sent from this area. All positional feedback
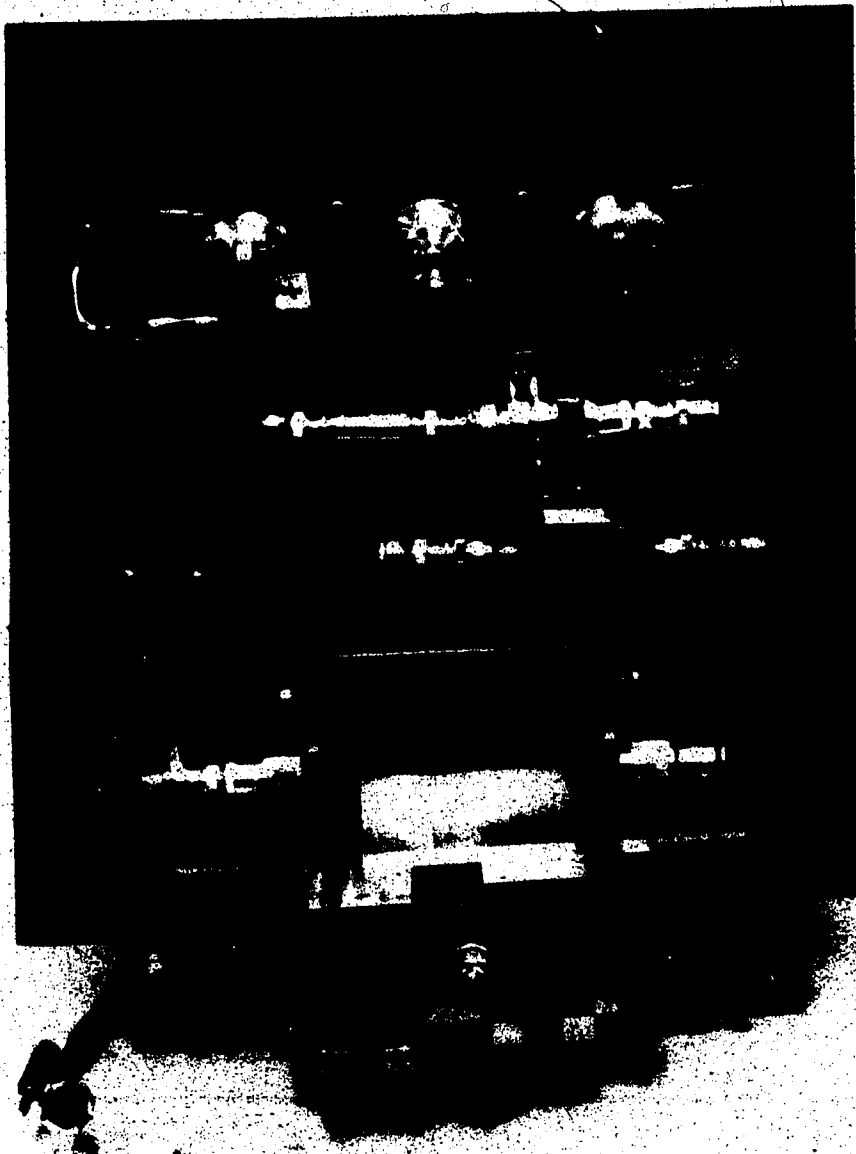
Fig. 6.25 Photograph of prototype receiver shown attached to the underside of the receiver carriage.
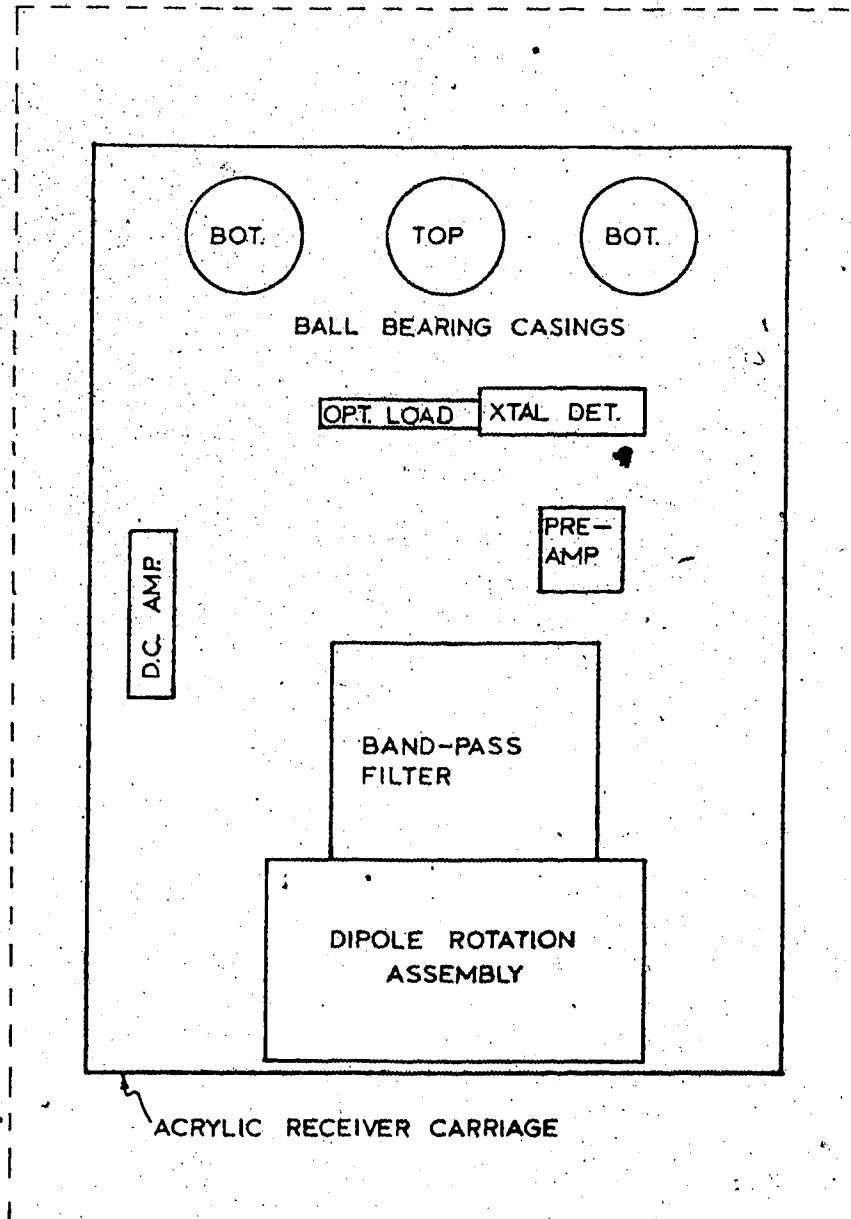
Fig. 6.26 Diagram identifying various receiver components shown in photograph of Figure 6.25.
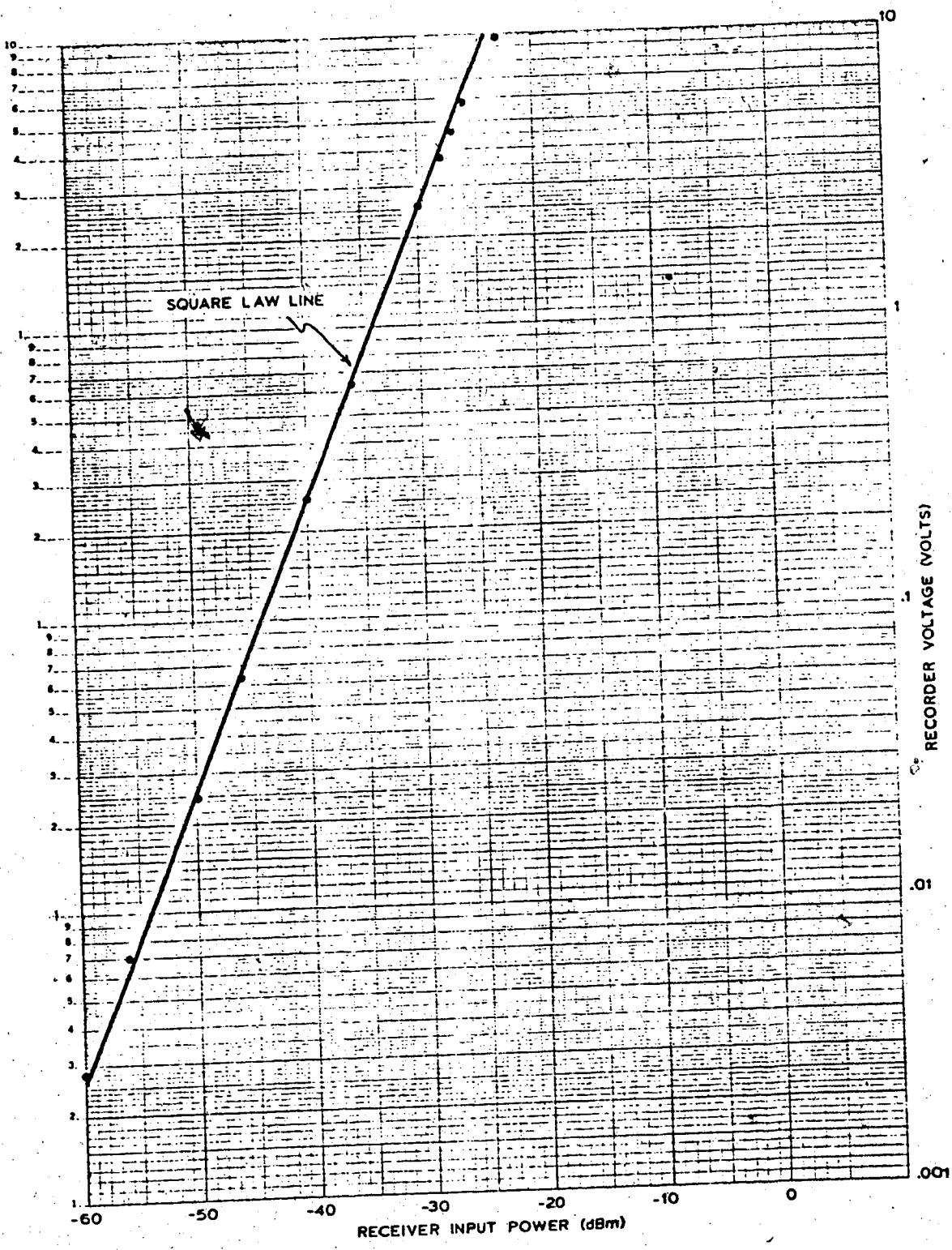
Fig. 6.27 Recorder voltage versus receiver input power characteristic.

voltages and the detected voltage of the receiver were received at this center.

A control box was built which provided patching facilities and control switches for the operation and monitoring of the various devices used in the range. A schematic of the equipment required in the measurement and control center for a typical experiment is shown in Figure 6.28.
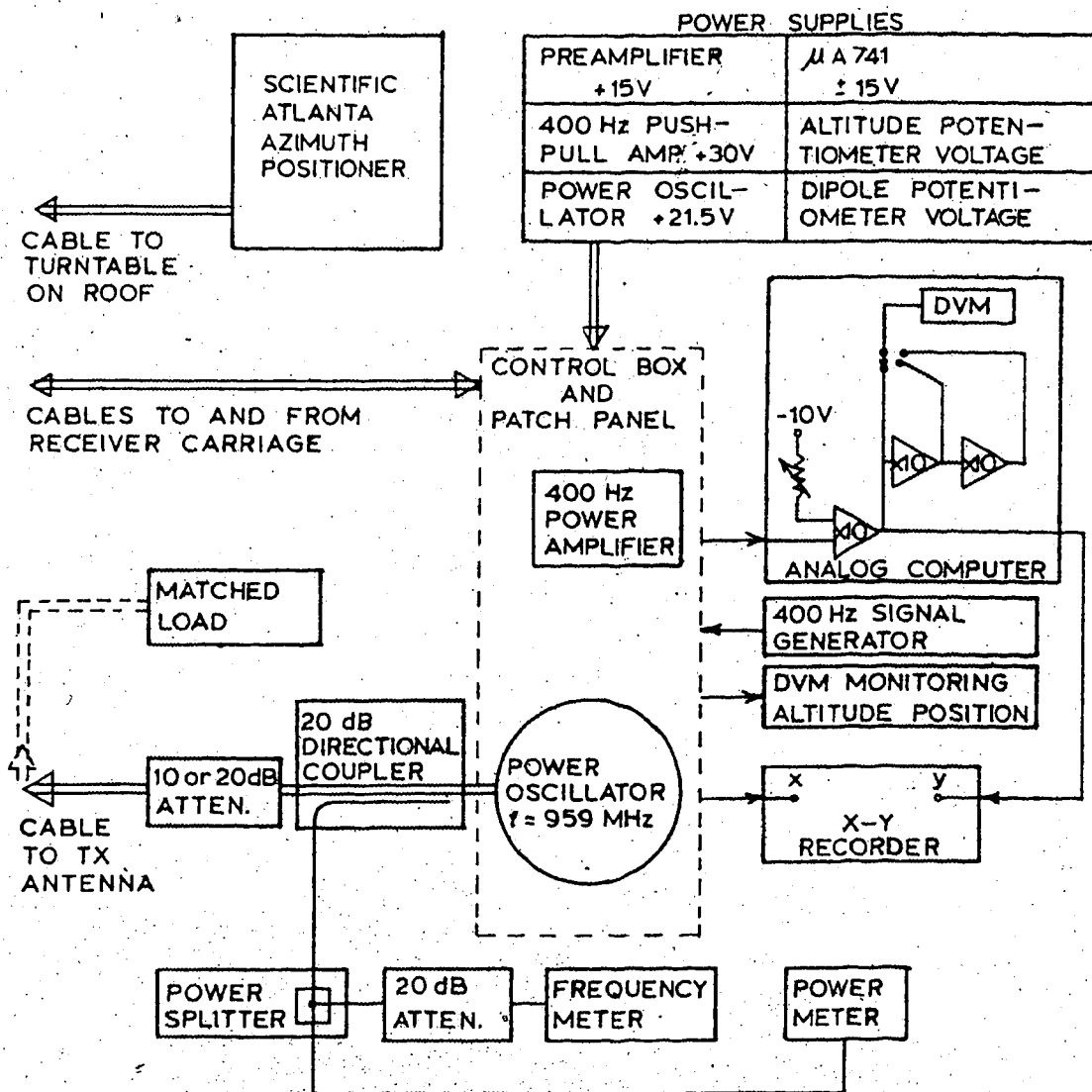
Fig. 6.28 Equipment schematic of measurement and control center.

CHAPTER 7

THE MICROWAVE ANTENNA TEST RANGE:OPERATION

The method and results of measurements taken with the test range described in Chapter 6 will now be presented. Errors introduced into the measurements because of constructional problems and design shortcomings will be discussed. Solutions to the various problems and improvements in the design will be offered. Finally, after analysing the data with the deficiencies of the test range taken into account, a design will be presented for the most suitable conical spiral for use with the riometer.

7.1 Positioning of the Track and Turntable

The measurement track could be raised or lowered by the use of a gin pole and power pull arrangement. Once raised a wooden triangular structure was moved into place to support its free end. By moving the base of the triangular structure either in or out the height of the measurement track could be adjusted so that the center of the top of the turntable, which was assumed to be the position of the center of phase for all antennas tested, was at the focus of the curved track.

Because of the expectation of high winds, the measurement track was frequently set up and taken down. Fortunately, either operation could be accomplished by one person in approximately 15 minutes.

7.2 Test Procedure

At the test site the antenna to be tested was attached to the turntable of the azimuth positioner. The receiver was then placed at the top of the track, i.e. past the zenith position, where measurements would

begin.

In the laboratory all instruments were turned on and allowed to warm up for 10 minutes. The power oscillator was also turned on; however its output was fed through approximately 10 feet of cable and a 10 dB attenuator into a matched load (see Figure 6.28). With zero power being fed to the transmitter the D.C. amplifier's offset voltage was adjusted to give a reading of zero volts ± 1 mV. By amplifying the output of the D.C. amplifier combination sufficiently and monitoring the result on the analog computer's digital voltmeter, this offset voltage could be zeroed to within ± .1 mV. However, except when very low powers were being recorded, this fine a zeroing was not required. Throughout the measurement period, the zero level was checked and adjusted. It rarely exceeded 3 mV which represents less than .2% error for most antenna measurements to half power.

When all equipment was ready for measurements the matched load (but not the attenuator) was removed and the power oscillator was connected to the feed cable of the transmitting antenna. The dipole was then rotated through 360° as the detected voltage as a function of dipole angle was recorded on the X-Y recorder (see Figure 7.1). If a measurement at a different azimuth angle was required, the transmitting antenna was remotely oriented accordingly, and the dipole again rotated.

Recalling from section 6.2.2.1 that the total power in the wave is proportional to the sum of the detected maximum and minimum voltages, and the AR is the square root of the ratio of maximum to minimum detected voltages, it can be seen from Figure 7.2 that rotation of the transmitting antenna has little effect on the total received power; however, the axial ratio does change by approximately 13%. As pointed
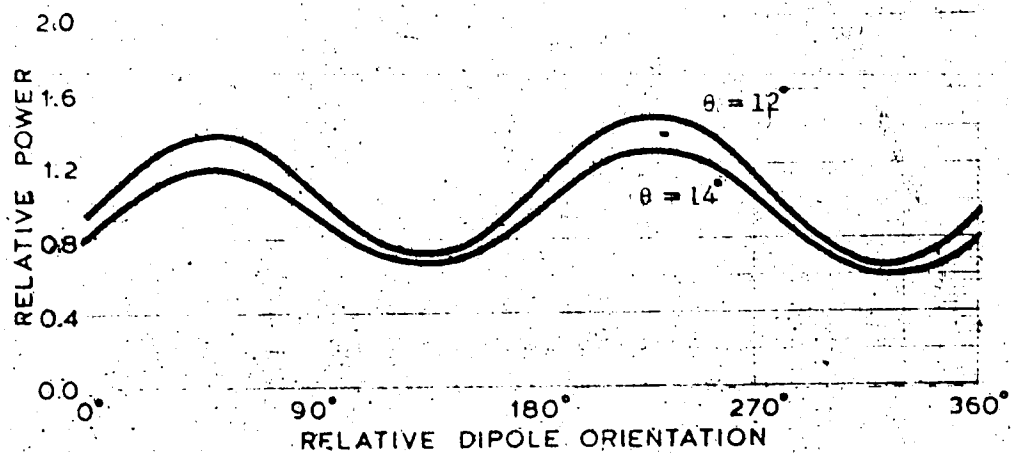
Fig. 7.1 Typical recordings for a conical spiral antenna at two different zenith angles.
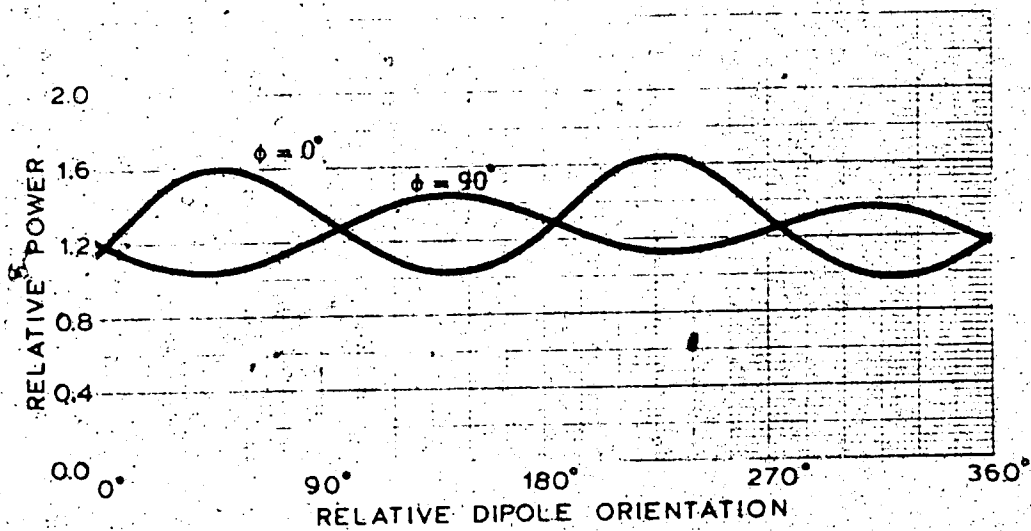
Fig. 7.2 Typical recordings for a conical spiral antenna at two different azimuth angles.

out in section 5.2.2, an axial ratio change of 15% for a 90° change in

azimuth position is typical of conical spirals. The trend of axial

ratio as a function of zenith angle, however, remains the same for a

given azimuth orientation [17]. For this reason and the fact that the

total power does not change significantly (less than 5% in Figure 7.2)

with rotation, measurements were generally conducted at only one

azimuth angle. Spot checks were occasionally made and revealed that

the power and axial ratio variation generally remained within the limits

defined above.

It is interesting to note the shift in the curve of detected voltage

versus dipole orientation angle as the azimuth angle is changed. This

is an indication of the close association between the angular orientation

of the major and minor axes of the polarization ellipse, represented

by the positions of the maxima and minima on the linear recording, and

the physical orientation of the antenna. As long as most of the radiation

emitted by an antenna is nearly circular, the phase of the emitted wave

can be changed by a mechanical rotation of the antenna structure. This

is a useful property in phased arrays using conical spiral elements [45].

Although the above discussion has been limited to the normally

circularly polarized conical spirals, a linearly polarized antenna was

also tested. A $\lambda/2$ dipole, $\lambda/4$ above a 2λ diameter copper ground plate

was used to test the validity of the far-field assumptions used in the

design of the range. At the zenith the cross-polarization between this

antenna and the receiving dipole was better than 27 dB. Obviously, then,

axial ratio measurements were of little value; the antenna was to all

intents and purposes linearly polarized as would be expected. However,

its power pattern was of value, although the measurement procedure used

to determine it was slightly different from that of the conical spirals.

At the zenith the dipoles were oriented for maximum power. Because

the dipole would not be rotated, the potentiometer monitoring the

dipole orientation angle was disconnected from the X-input of the X-Y

recorder. In its place the voltage representing the zenith angle of the

dipole was applied. Therefore, allowing the receiver carriage to move

down the track, a plot of received power (detected voltage) versus

dipole zenith angle was recorded.

7.3 Data Reduction

The measurement records obtained for the linearly polarized dipole

transmitting antenna were essentially already in the desired form. The

records just had to be normalized with respect to the maximum power

level recorded, and the results plotted on a polar diagram. Because

the dipole records were continuous functions of zenith angle, care was

taken to prevent any loss of detail in the transfer from the continuous

records to the discrete point plots of the polar diagrams.

Power measurements on the conical spirals, however, were not

continuously recorded as a function of zenith angle but were made at

discrete intervals along the measurement arc. The trends in power

response and axial ratio as functions of zenith angle were not

immediately obvious from the records. The measurement data, therefore,

had to be reduced to a more readable form.

The total power in the received wave was proportional to the sum of

the maximum and minimum voltages detected, and the axial ratio was

determined from the square root of the ratio of the maximum to minimum

voltage detected. As can be seen from the examples of the measurement

records, there are two maxima and two minima recorded for each zenith angle. Normally, it would not matter which maximum or minimum was used in the determination of the total power and axial ratio. However, because the receive dipole was found to have a tilt in its pattern, probably due to a feed imbalance, the two maxima or two minima differed by approximately 6%. Care thus had to be taken in choosing which maximum was related to which minimum. For all measurement records the convention used was that the total power and axial ratio would be determined from the larger maximum and minimum voltages. Axial ratios determined from the smaller maximum and minimum voltages differed by less than 2% and the normalized power patterns so determined were indistinguishable from those evaluated from the other set of extrema.

7.4 Calibration and Evaluation of the Range

The standard conical spiral and a $\lambda/2$ dipole were used in a series of tests to evaluate the performance of the test range. The data from these tests, and the height reduction experiments on the conical spirals which followed them, were not analysed until all experiments had been completed. This was done so that as much information as possible could be gathered before operations would have to be shut down due to the impending winter.

7.4.1 Measured Pattern and Axial Ratio of the Standard Conical Spiral

As has been pointed out in section 5.3, the HPBW, axial ratio and other radiating characteristics of the conical spiral antenna with $2\theta_o = 20°$, $\alpha = 80°$, and $\delta = 90°$ were well known. This antenna was therefore

chosen as the calibration standard for evaluation of the test range. The first measurements to be made were to determine its power pattern and polarization response so that these could be compared with the expected values.

For these initial measurements a microwave absorbing material with better than -20dB reflectivity at 450 MHz completely covered the receiver carriage but the gin pole used to raise the measurement track and the cables feeding the receiver carriage were exposed. The power pattern and axial ratio measured for the standard conical spiral under the above conditions are shown in Figure 7.3 and 7.4, respectively.

The power pattern is seen to be quite ragged. However, the average power pattern drawn midway between its maximum and minimum envelopes is believed to be the true far-field pattern. This will be discussed further in section 7.4.5. It is of note that all dashed curves identify a HPBW of approximately 70°. For an identical antenna but not mounted over a ground screen, Dyson's curves indicate an average HPBW of approximately 74° ± 6°, where the variation in the HPBW is due to the fact that the pattern changes slightly over the bandwidth of the antenna [18]. It is known that on a conical spiral the beam width increases as the operating frequency approaches the low frequency limit of the structure. As the frequency approaches its high frequency limit, the beam width decreases slightly, then increases again. Since the standard conical spiral was designed to be well above the low frequency limit not at the high frequency limit, it seems likely that it would be at most 74°. Adding to this the fact that the antenna was mounted on a large ground plane, a modification which is known to produce a narrower beam [17], a HPBW of 70° appears to be a very likely result.
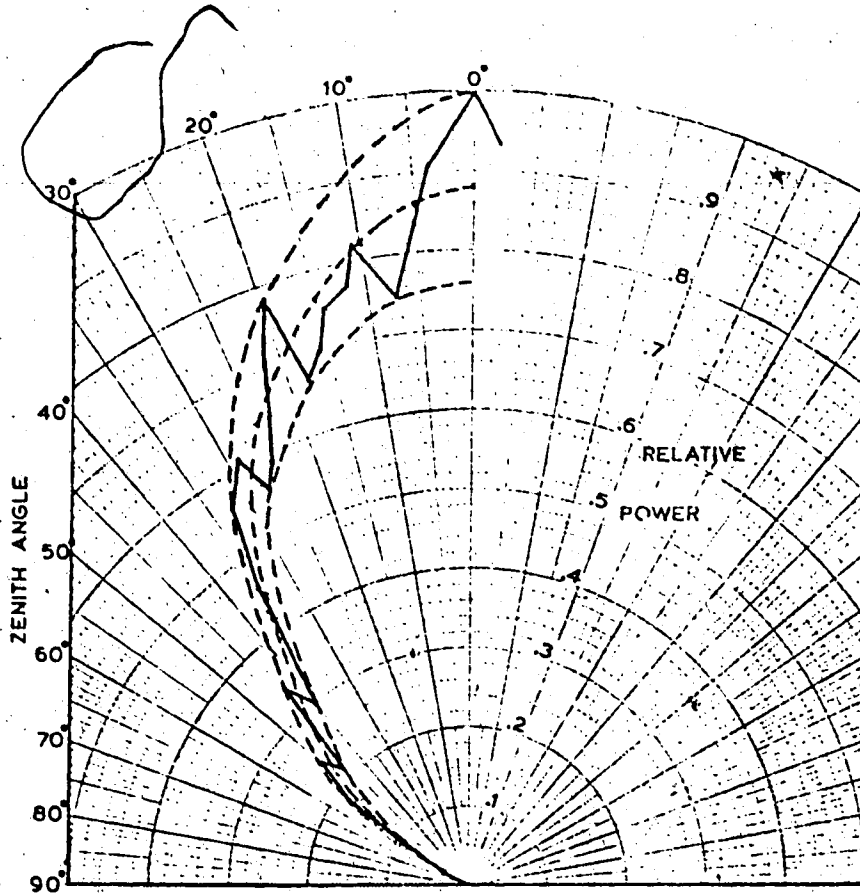
Fig. 7.3 Measured power pattern of the standard conical spiral $(2\theta_0 = 20°,$ $\alpha = 80°, \delta = 90°)$ (solid), with maximum,minimum and average curves superimposed (dashed).
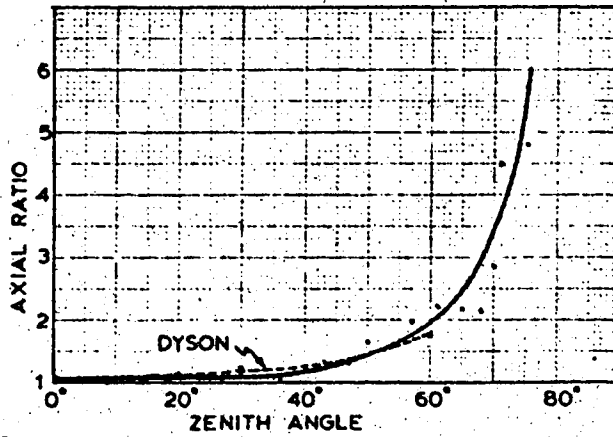
Fig. 7.4 Measured axial ratio of antenna of Figure 7.3 with curve of

Dyson [18] for comparison (dashed).

Looking now at the axial ratio measurement results shown in Figure 7.4, it is seen that, again, good agreement exists between Dyson's results and those taken by the author. It is not known whether Dyson checked the axial ratio at zenith angles of 0°, 30°, and 60° only, but these, with the appropriate curve drawn through them, were the only points plotted in his 1965 paper. At this point it was believed that, certainly, as far as the measurement of axial ratio was concerned, the range was functioning satisfactorily.

7.4.2 A Check for Reflections from the Gin Pole and Receiver

Feed Cables

As was mentioned in section 7.4.1, the gin pole used to raise the measurement track, and the cables feeding the equipment on the receiver carriage were not covered in the first test of the standard conical spiral. Up until now it has been assumed that these objects were not responsible for any serious measurement errors. It will now be shown that this was a valid assumption.

For these measurements an additional piece of absorbing material was placed on top of the absorber that had previously existed on the receiver carriage. This was done in order to cover a small section of the dipole rotation assembly which had previously been exposed and which could cause a slight perturbation in the receiving dipole pattern. This effect could be checked as well, by comparison with the measurements of the first test.

Measurements with the pole and cable exposed as in the first test were again conducted on the standard conical spiral. However, the azimuth orientation of the antenna was not necessarily the same as that

in the first test. The gin pole and receiver cables were then covered

by placing absorbing material all along the measurement track with only

a small slot left uncovered through which the dipole could protrude. In

order to obviate any unforeseen effects due to temperature or humidity,

these measurements were conducted immediately after those tests with

the pole and cable exposed. This also ensured that the conical spiral's

azimuth orientation was the same for both measurements. As was pointed

out in section 7.2, for a given zenith angle the total power may change

by 5% and the axial ratio by 15% for a 90° rotation in azimuth.

The measurement results are shown in Figure 7.5. It is first

immediately obvious that no drastic changes occur in either the power

pattern or axial ratio measurements. Considering that the measurements

were made at discrete intervals and many records were difficult to read

due to overlapping curves, the differences are reasonable. Throughout

the remaining experiments, however, the gin pole was always covered with

the microwave absorbing material.

Now comparing the power patterns measured with that of Figure 7.3, it

is seen that a narrowing has taken place. This could be due to a small

section of the dipole rotation assembly which was exposed to the

receiving dipole in the first test as was mentioned earlier. However,

it is more likely that this is due to different azimuth orientations

of the transmitting antenna which can alter the beam width by 4° to 5°.

As will be described in section 7.4.4 an improved measurement set up

was later used and the standard conical spiral was retested; in fact the

HPBW and axial ratio results are very similar although definite improve-

ment is noted in the uniformity and regularity of the pattern structure.
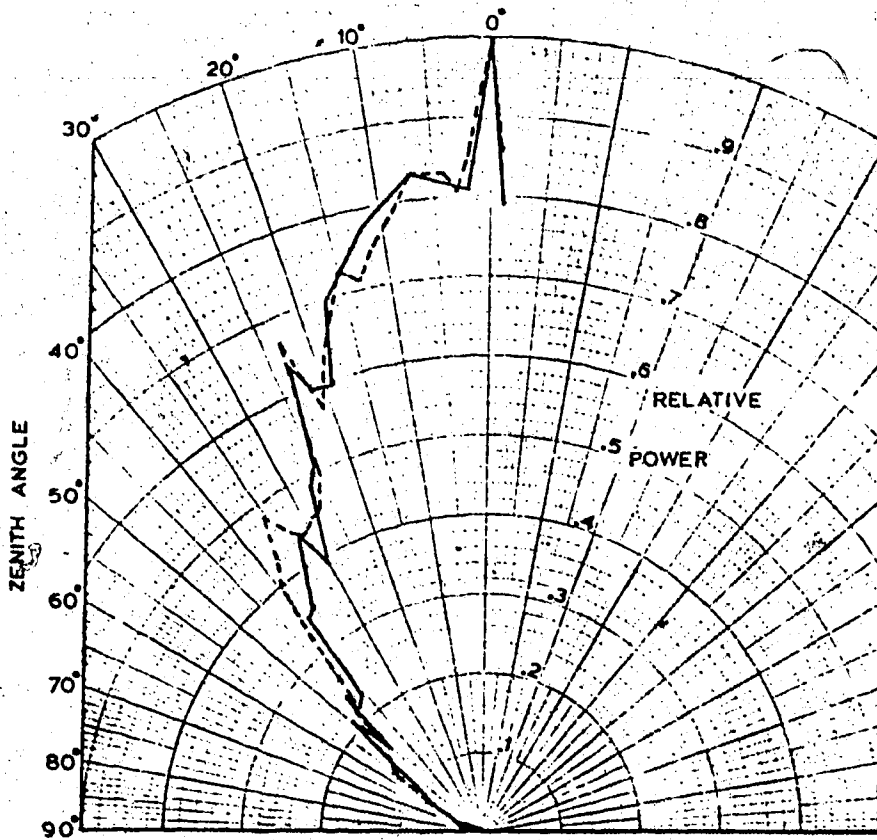
(a)
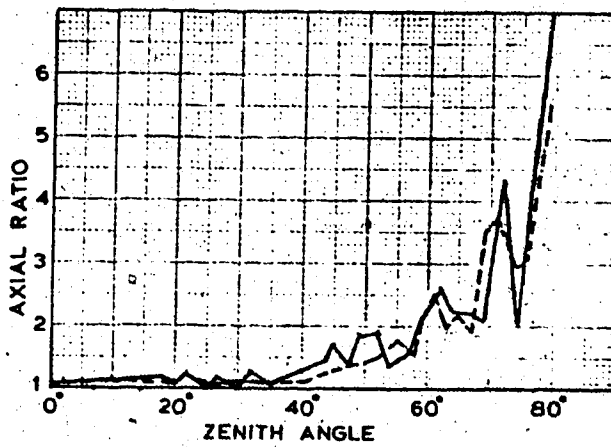
(b)

Fig. 7.5 Power pattern (a) and axial ratio (b) measurements on the standard conical spiral with (dashed) and without (solid) absorbing material covering the gin pole and receiver feed cables.

7.4.3 Effect of Receiver Carriage Sideways Tilt

Provision had been made on the receiver carriage to allow it to be tilted approximately 5° to either side. For a direct comparison measurements were first taken without tilt in the receiver carriage, then cet. par, measurements were repeated with the carriage tilted.

Because of the degree of tilt, the carriage could not fit through all the absorber holders which were still attached to the measurement track from the previous experiment. However, it is believed that the data gathered, sufficiently illustrates the effect of sideways tilt on the receiver carriage.

The results of the measurements are shown in Figure 7.6. It is seen that even with this excessive tilt, representing a shift of approximately 15 inches in the measurement focal point, the power pattern and axial ratio are not affected dramatically. This is to be expected since the receiving dipole has such a broad beam.

This test was felt to be important since the measurement track exhibited sideways deviations of ± 2° over its length. Measurement errors due to this deviation should, therefore, be insignificant.

7.4.4 A Retest of the Standard Conical Spiral on an Improved Set Up

The results of section 7.4.2 showed that if reflections from the gin pole and receiver carriage cables affected measurement results, it was a very small effect. However, in an attempt to obtain the most accurate measurements possible without undue expense or additional set up time, an effort was made to completely render the effects of reflections from either the gin pole or receiver feed cables negligible.

As far as the gin pole was concerned, the solution was simple since

(a)

(b)
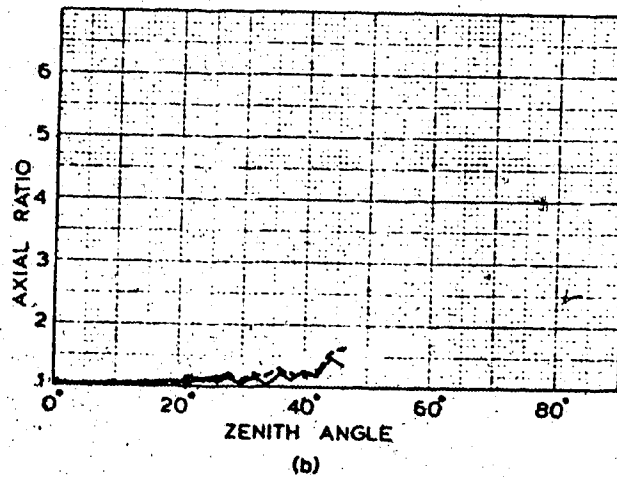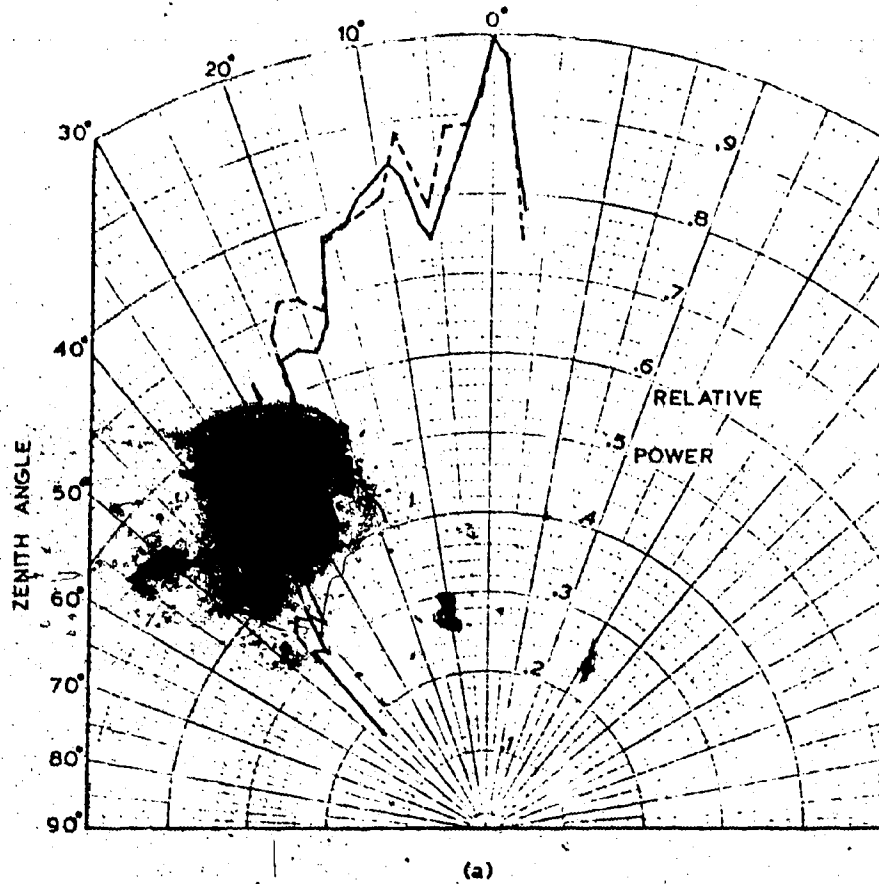
Fig. 7.6 Power pattern (a) and axial ratio (b) measurements on the
standard conical spiral with (dashed) and without (solid) sideways
tilt on the receiver carriage.

it could be covered with absorbing material yet still perform its function of raising or lowering the measurement track when it was being set up or taken down.

Covering the cables which trailed behind the receiver carriage as it moved up and down the measurement track was not so simple a task but instead was an involved process which required many hours to complete. It required the placement of absorbing material all along the measurement track yet allowing a slot through which the dipole could protrude. However, these cables which had a combined diameter of approximately 3/4", when uncovered, represented a reflecting surface which was always normal to the incident radiation and thus the reflected energy should never enter into the aperture of the receiving dipole. This would almost certainly apply if the absorbing material covering the receiver carriage extended sufficiently beyond the ends of the dipole. Hence, all subsequent measurements were conducted with a 2'x2'x4" piece of microwave absorber placed over the receiver carriage. A 1" hole cut in its center allowed for the connection of the $\lambda/2$ receiving dipole. Thus the absorbing material extended at least 9" beyond the arms of the dipole, regardless of its orientation.

This method of eliminating reflections from the receiver carriage cables was not only desirable because of the reduced set up and take down times, but also because, unlike its alternative which placed absorbing material all along the track, this method did not add significantly to the weight and wind loading factor of the measurement track.

The results of measurements taken on the standard conical spiral, using the improved set up described above, are shown in Figure 7.7.

(a)

(b)
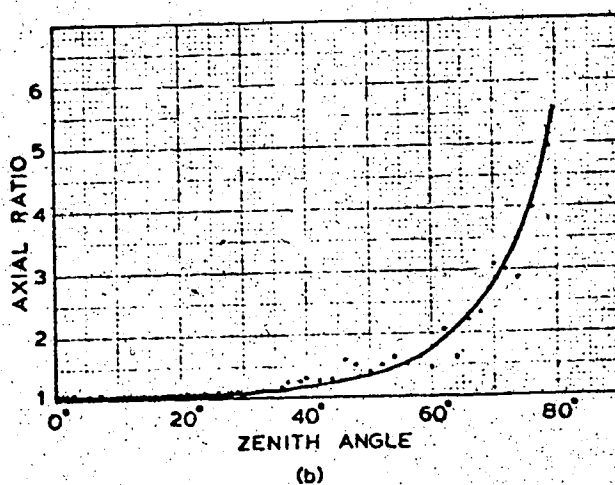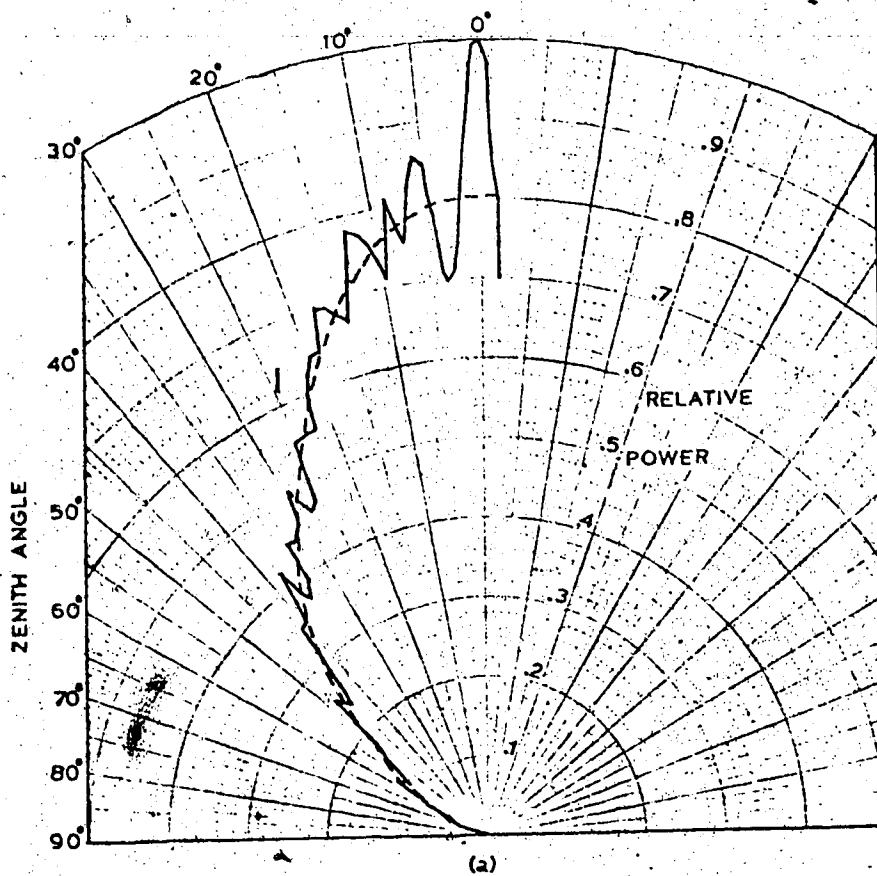
Fig. 7.7 Power pattern (a) and axial ratio (b) measurements on the standard conical spiral using the improved measurement set up.

The measured power pattern is much more uniform and its peaks occur approximately every 4°. The HPBW determined from the dashed smooth curve shown, which attempts to define the average power pattern, is approximately 70°. This is the same value of HPBW arrived at in the first test of the standard conical spiral although the measured power pattern in that test was not nearly as well defined. The axial ratio appears to have improved slightly in its general trend but this could be due to different azimuth orientations of the transmitting antenna between this test and the first test.

Because of these favourable results, the improved measurement set up was used on all subsequent tests and the results of this section are believed to best represent the characteristics of the standard conical spiral.

Justification will now be given for drawing smooth average curves through the measured axial ratio and power pattern results and determining the characteristics of the antenna under test, from these smooth average curves.

7.4.5 The Measured E and H Plane Power Patterns of a Simple Dipole

The standard conical spiral mounted over a ground plane represented an antenna with maximum dimension of 3λ and was the largest antenna tested on the range. Because of the compactness of the range, which had a measuring distance of only 15λ, from the discussion of section 6.3, measurements were possibly not made in the far-field. Thus the ripples on the measured power pattern could be due to a near-field effect.

To test this a $\lambda/2$ dipole, $\lambda/4$ above the ground plane was constructed and tested. If the ground plane appeared infinite to the dipole, the

dipole-ground plane combination could be represented by a two dipole array which would have a maximum dimension of $\lambda/2$ and thus its measured pattern should closely resemble its far-field pattern. The far-field pattern for this antenna can be easily calculated and it has a HPBW of 64° in the E plane and 120° in the H plane. These calculated values can thus be compared with the measured values.

The measured E and H plane power patterns of a $\lambda/2$ dipole, $\lambda/4$ above the ground plane are shown in Figures 7.8 and 7.9, respectively. It is immediately noted that the patterns are in the proper sense; that is, the H plane pattern is considerably broader than the E plane pattern. If, as shown, smooth average curves are drawn through the peaks of the measured patterns, a HPBW of 65° in the E plane and 118° in the H plane is obtained. These values are in good agreement with those calculated for the far-field patterns. The ripples are still present, however, and are far worse in the H plane than the E plane. The fact that the ripples still exist and occur approximately every 4° as on the conical spiral power pattern, suggests that they are not due to a near-field effect as supposed. Because of the small size of the dipole the ripples in both planes should have been reduced compared to those on the conical spiral power pattern. Also it would be unlikely that they would occur at the same interval since the near fields of a conical spiral and linear dipole should be substantially different, and thus if the measured fields are due to a near-field effect, they too, should be different.

It was then suggested that perhaps the ripples on the power pattern were due to the non-infinite ground plane. If currents flowing within the ground plane had not been reduced to zero by the time they reached
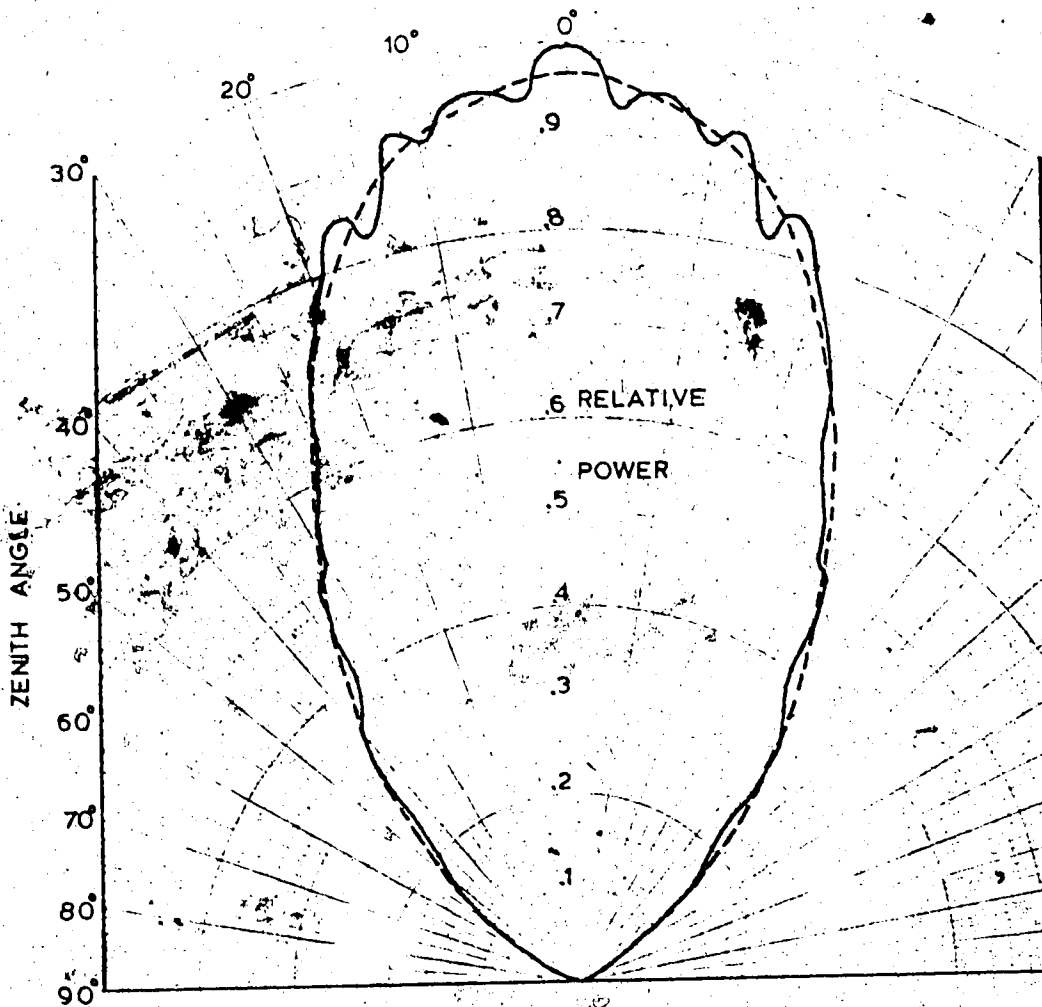
Fig. 7.8 Measured E plane power pattern of a λ/2 dipole, λ/4 above a ground plane with average of pattern superimposed (dashed).
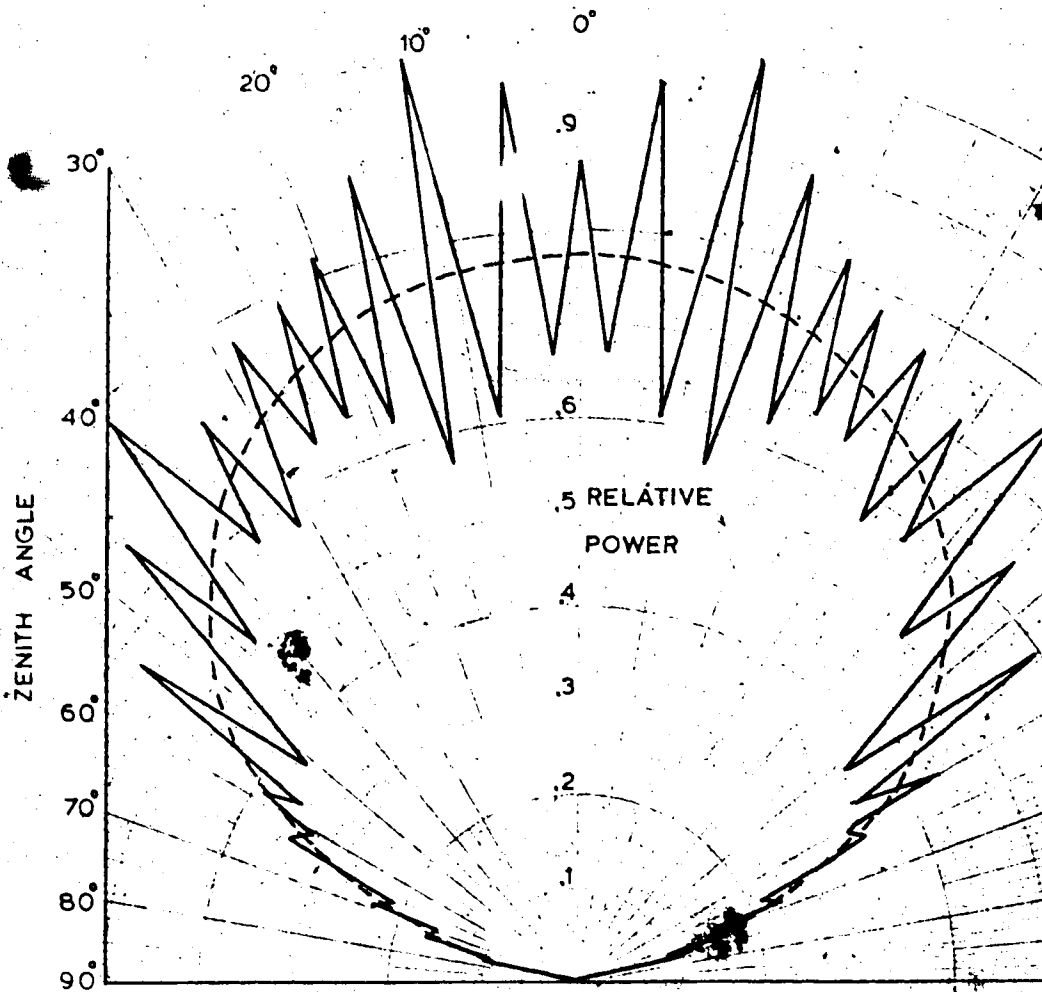
Fig. 7.9 Measured   H plane power pattern of a λ/2 dipole, λ/4 above
a ground plane with average of pattern superimposed (dashed).

its edges, the ground plane would very closely resemble a radiating aperture antenna and rapid peaks similar to those observed would occur. It can be shown that for an aperture antenna, the interval between peaks depends on the aperture size [25], in this case, the size of the ground plane. Thus if the ground plane was physically reduced to, say, one tenth its original size, the interval between peaks should increase by a factor of 10, i.e. the peaks should occur at a much slower rate, with zenith angle. This was tested but absolutely no change in the interval between peaks was observed. It was therefore concluded that the ripples on the measured power patterns were not due to a ground plane edge effect.

The only other explanation that could be realistically considered was that stray reflections were entering into the aperture of the receiving dipole and thus the quiet zone, that had been determined in section 6.4 using ray theory, was not as good as had been hoped. Since the gin pole was always covered with absorbing material, and from section 7.4.2 the cable was known not to be responsible for any serious reflections, the only other obvious metallic reflector was the metal flashing which bordered the roof. Although it was not possible to cover all the flashing because of the limited amount of absorbing material available, approximately 30 feet of flashing, in either direction from the corner of the roof bisected by the range, was covered. The H plane pattern of the dipole was again tested. Although the peaks occurred at precisely the same intervals as those of Figure 7.9 the peak to peak magnitude was reduced by approximately 1/2 while the average power pattern remained virtually unchanged.

The fact that the ripples could not be entirely eliminated suggests that the reflection problem is a complex one involving reflections not

only from the flashing but perhaps from adjacent buildings, the wooden structures, and even the absorbing material itself. If radiation incident on the reflector/absorbers, which had a power reflectivity of only - 20 dB, was high enough and if they did not direct the reflected energy harmlessly away as had been hoped, they alone could account for the observed ripples, i.e. power pattern variations on the order of 20%. Thus, for an antenna that radiates high power levels at high zenith angles, i.e. at the zenith angles corresponding to the elevation of the reflector/absorbers and flashing located behind them, one would expect the measured pattern to display stronger interference variations than those on the pattern of an antenna which radiates primarily in the direction of the zenith. This would explain why the H plane pattern, which is very broad, displays interference variations which are much greater in magnitude than those of the narrower E plane pattern or the power pattern of the standard conical spiral.

Since it seemed logical to assume that the stray reflections would alternately add in phase and out of phase with the actual field of the antenna, it was equally logical to assume that their average should closely approximate this actual field. Thus, drawing a smooth curve through the average of the peaks seems a very likely method of estimating the pattern in the absence of these stray reflections and explains why the average power patterns of the dipole and conical spiral agreed so well with their expected values.

The effect that these reflections would have on the axial ratio measurements was not immediately obvious. However, a close examination of the axial ratio results for any of the conical spiral antennas tested reveals their effect. From Figure 7.10, which is just the axial ratio
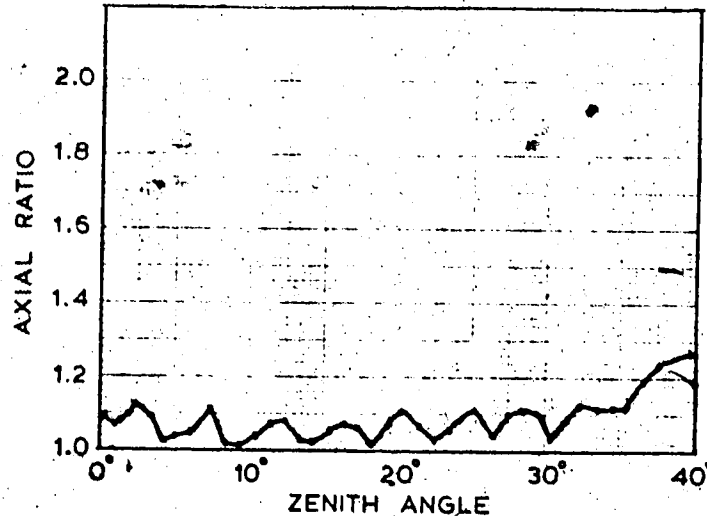
Fig. 7.10 Expanded view of axial ratio measurements of Figure 7.7(b).

results of Figure 7.7(b) up to a zenith angle of 40°, plotted on a larger scale, the axial ratio is seen to vary periodically with zenith angle at precisely the same rate as the interference peaks on the measured power patterns. Thus by taking the average through these peaks as well, it is believed that a good estimate of the axial ratio is achieved. The excellent agreement with Dyson's results in section 7.4.1 corroborates this theory. Since variations from the average curve of either the axial ratio or power pattern generally did not exceed 10%, the average values are believed to be at least this accurate. As long as the antenna test range is operated at sufficiently low power levels so that the D.C. voltage output of the crystal detector in the receiving section always remains proportional to its input power (discussed further in section 7.4.7), stray reflections should be the limiting source of error.

Thus the microwave antenna test range should be capable of axial ratio

and power pattern measurements to within 10% although this can change,

depending on the directivity of the antenna under test.

7.4.6 A Check on the Conductivity of the Ground Screen Mesh

The degree to which the galvanized metal mesh ground plane, described

in section 6.5.6, represented a uniform perfectly conducting ground

plane was of interest. If at the operating wavelength of approximately

1 foot the metal mesh was quite lossy, the measured patterns and AR

would not be indicative of an antenna above a perfectly conducting

ground plane.

Because the pattern of the $\lambda/2$ dipole with its large back lobe

should be the most severely affected by a lossy ground plane, it was

remeasured with overlapping aluminum metal sheets replacing the metal

mesh ground plane. The results were virtually identical with those of

Figure 7.8 and 7.9 and will not be presented here. But this was to be

expected since all measurement results obtained to this point, when

properly interpreted have agreed well with the expected values, i.e. of

antennas above a perfectly conducting ground plane. It is quite possible,

however that the equivalence of the two measurements (those using metal

mesh and those using metal sheets) was due largely to the fact that all

antennas, including the $\lambda/2$ dipole, were mounted on a 2λ diameter

ground plate and that this plate, by itself, sufficiently represented

an infinite ground plane.

7.4.7 Operation of the Range at High Power Levels

If the transmitting antenna radiates too high a power level, gain

saturation of the preamplifier and non-square law operation of the

crystal detector may result. Axial ratio measurements will therefore

be in error due to different preamplifier gains and diode characteristic

changes, as the dipole rotates. Errors in the power patterns will

result because the normalizing factor, which is always the maximum

power received, will be too low.

A .5 dB reduction in the gain of the preamplifier was found to occur

at an output power level of + 7 dBm. The crystal detector used, operates,

typically, within .5 dB of square law up to input power levels of - 3 dBm.

Since the crystal detector immediately followed the preamplifier stage,

significant deviations from its square law characteristic would occur

at preamplifier output power levels on the order of 10 dB below those

which would indicate significant gain saturation. Thus if the detector

could be kept in its square law region; preamplifier gain saturation

would not be a problem. For a typical crystal detector sensitivity of

. 1 mV/μW and recalling that the D.C. amplifier combination had a total

gain of approximately 100, recorded voltages of 5V or less should give

power measurements which have errors less than .5 dB due to the effects

of high power levels.

Experimentally it was found that for recorded voltages less than 7V,

less than 10% error occurred; less than 5V, less than 5% error occurred;

and less than 3V, less than 1% error occurred in the axial ratios measured.

All measurements had recorded voltages less than 7V, and most were

below 3V.

7.4.8 Evaluation

Summarizing, the range, as designed, is quite capable of giving reliable axial ratio and power pattern measurements as long as the characteristics of the antenna under test are identified with the average of the measured parameters.

Before the range is used again, it is suggested that an electric winch be placed beneath the ground plane to remotely position the receiver carriage in altitude. With the winch in place, it should also be possible to position the carriage more accurately and reliably. (The receiver carriage and its drive are discussed in sections 6.5.3 and 6.5.4 respectively).

All recorded voltages should be kept below 3V to ensure proper square law operation of the crystal detector and to prevent gain saturation from occurring in the preamplifier of the receiving section.

Experiments were carried out successfully over the temperature range $-20°C$ to $+25°C$. It is not recommended that the lower end of this range be exceeded. If it is, breakage in the receiver carriage cables may result and the turntable may cease to function.

7.5 Using the Test Range to Determine a Suitable Riometer Antenna

7.5.1 Size Reduction by Truncation of Small Cone Angle Conical Spirals

All conical spirals considered by Dyson [16], [17], [18] had included cone angles of $2\theta_o \leq 45°$. He showed that a fairly well-defined active region existed on these antennas and that if an infinitely long conical spiral structure was truncated such that only this active region remained, the resultant antenna displayed essentially the same radiating character-

istics as that of its untruncated form.

The antenna which exhibited the radiating properties required by
the riometer was the conical spiral with included cone angle $2\theta_o=20°$
and angle of wrap $\alpha=80°$. As was mentioned in Chapter 5, the cable-arm
versions of the conical spirals exhibit essentially the same radiating
properties as the complementary antennas, i.e. those antennas with
angular arm width $\delta=90°$, but are much simpler to construct. The full-
scale antenna would, therefore, likely be a cable-arm conical spiral.
It would also be in its truncated form in order to keep its height to
a minimum. However, the degree to which the antenna could be truncated
without substantially degrading its axial ratio and power pattern,
had to be determined. Simply, by removing turns from either the top or
bottom of the cable-arm version of the standard conical spiral, previously
shown in Figure 5.4, truncation could be simulated. This antenna, as
with all conical spiral antennas tested, was fed by the infinite balun
method, and since it was tested above a ground plane its spiral arms
at its base were fastened to the ground plane, as per instructions by
Dyson.

The power pattern and axial ratio of the cable-arm version of the
standard conical spiral were virtually identical to those of its metal-
arm counterpart and thus will not be shown here. The effect of not
connecting the spiral arms to the ground plane, however, is shown in
Figure 7.11. This upward shift in the axial ratio curve is apparently
due to reflections from the ends of the spiral arms which set up fields
with polarization opposite to that of the primary field [19]. These
small cone angle conical spirals were thus always tested with their arms
fastened to the ground plane.
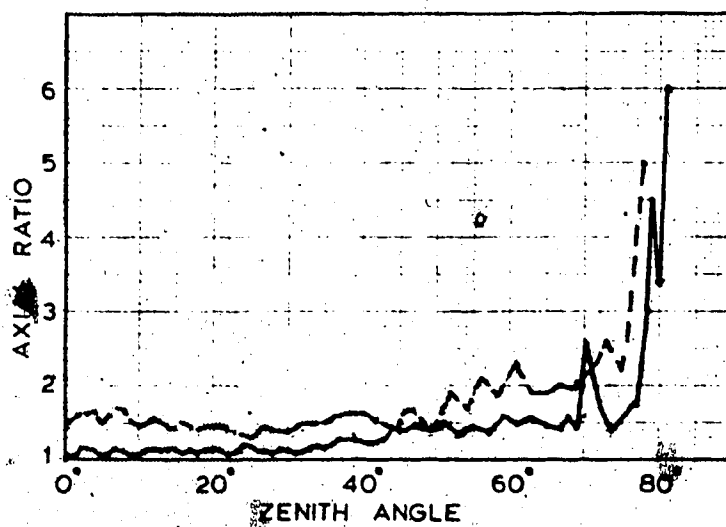
Fig. 7.11 Axial ratio of the cable-arm version of the standard

conical spiral antenna with (solid) and without (dashed) the

spiral arms attached to the ground plane at the base.

Truncation experiments were carried out until the height of the antenna had been reduced to .75λ or about 1/2 the height of the original structure. Although its power pattern was still essentially that of the untruncated standard conical spiral its axial ratio on axis was already at a value of 1.4 and further truncation produced unacceptable pattern and especially, axial ratio changes. This was to be expected since the structure was physically approaching the limits of the active region. It was, therefore, decided that the height reduction technique of Dietrich and Long, i.e. the use of wide cone angle conical spirals, would be tried.

7.5.2 Size Reduction by the Use of Wide Cone Angle Conical Spirals

All conical spiral antennas generally require a base diameter of at least λ/π for efficient operation. Antennas so designed exhibit essentially the same radiating characteristics as one built on a cone which extends to infinity. By placing the spiral arms on a conical structure with wide cone angle, this base diameter requirement can be retained but the height of the resultant antenna is considerably reduced. The broadening of the beam width which normally accompanies such an increase in cone angle can then be compensated by wrapping the arms very tightly on the structure.

The above is essentially a summary of the size reduction technique of Dietrich and Long, outlined in their 1969 paper. Because their results were uncorroborated and since their antenna exhibited a rather unusual beam reversing phenomenon when the angle of wrap was only slightly changed, this height reduction technique was initially abandoned. It was only after the failure of the truncation method to satisfactorily

reduce the antenna size that this technique became attractive.

One of the reasons the technique is so successful is the use of a so-called "radiating ring" at the base of the antenna structure. Because the active region on these structures lies very near to the base, if the fields at the ends of the spiral arms have not sufficiently died out reflections will cause the axial ratio to be degraded. Artificially attenuating these fields by terminating the spiral arms in a resistor does improve the axial ratio but also has the effect of dissipating some energy which would normally be radiated. By wrapping the spiral arms very tightly ($\alpha \sim 90°$) in the base region, the fields apparently die out along the spiral arms due to the enhanced radiating efficiency of the antenna in this region, i.e. due to the radiating ring.

A wide cone angle antenna with parameters $2\theta_o = 70°$ and $\alpha = 85°$ was constructed using RG-174/U miniature coaxial cable for the spiral arms. An antenna similar to this and displaying a radiating ring was shown in Figure 5.5, next to the standard conical spiral. The radiating ring consisted of four turns of the miniature coaxial cable, wrapped as tightly as the diameter of the cable would allow. The height of the structure was $\lambda/4$ ($\sim 3"$) and its base diameter, as required, was $\lambda/\pi (\sim 4")$. The height, to which the spiral arms could be wrapped, was limited by the physical size of the cable in the apex region. It was approximately 3/4" below the apex of the cone, and therefore well above the active region which lies near the base on these structures. As with all antennas tested, this antenna was mounted with its base on a 2λ diameter copper ground plate.

Measurements were begun on this antenna; however, it soon became apparent that it did not possess a satisfactory axial ratio versus

zenith angle characteristic and measurements were halted. The antenna
and measurement set up was checked to make sure that all connections
were good and the results were not due to equipment malfunction.
Everything was found to be in order and an explanation of the results
was sought.

It was felt that if a large back lobe existed the fields in the
base region would be so large, that even with the radiating ring,
reflections would occur from the ends of the spiral arms and the axial
ratio would be degraded. To check this the copper ground plate was
replaced by a 2' x 2' square of absorbing material and the antenna
was again tested.

A comparison of the axial ratio measurements from the two tests
are shown in Figure 7.12. As expected, the energy of the back lobe
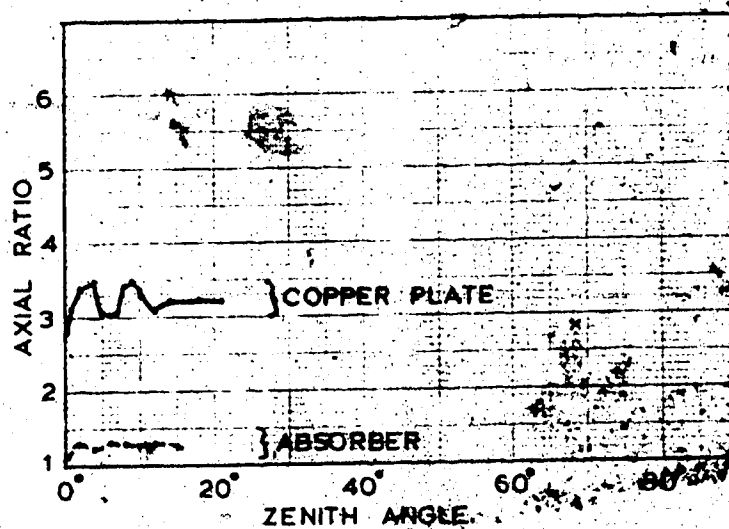
Fig. 7.12 Axial ratio of the cable-arm, wide cone angle antenna
($2\theta_o$=70°, α=85°) when mounted over a 2λ diameter ground plate (solid)
and a 2λ x 2λ piece of absorbing material (dashed).

apparently was dissipated in the absorbing material and therefore did not contribute to reflections which could degrade the axial ratio. It was also noted that the received power levels when the antenna was mounted over the copper ground plate were almost three times the levels when it was mounted over the absorbing material. This would tend to indicate that most of the radiated energy was concentrated in the back lobe.

At first it was thought that this method, too, could not be used to reduce the antenna height. However, closer inspection of the Dietrich and Long paper indicated that by increasing the angle of wrap by just $2°$ to $\alpha=87°$, it was possible that this back lobe could be largely eliminated. This was done, and the measurement results are shown in Figure 7.13.

The power pattern does not exhibit any sidelobes and was found to be essentially circularly symmetric. Average curves for the power pattern and axial ratio are superimposed on the measured values. From the discussion of section 7.4.5, these average curves are believed to best represent the characteristics of the antenna under test. The HPBW as determined from the average curve is approximately $66°$. The average axial ratio is approximately 1.2 on axis and remains less than 2 up to $70°$ off axis. Although the antenna of Dietrich and Long was constructed to operate over a range of frequencies, their patterns did not exceed a HPBW of $80°$ and the axial ratio at midband was approximately 1.1. They did not measure the trend in off-axis axial ratio as far as the author knows.

This antenna, therefore, exhibited all the characteristics desired; i.e. low axial ratio over the significant portion of its beam, a HPBW of approximately $60°$, no side lobes and low height. It is, however,
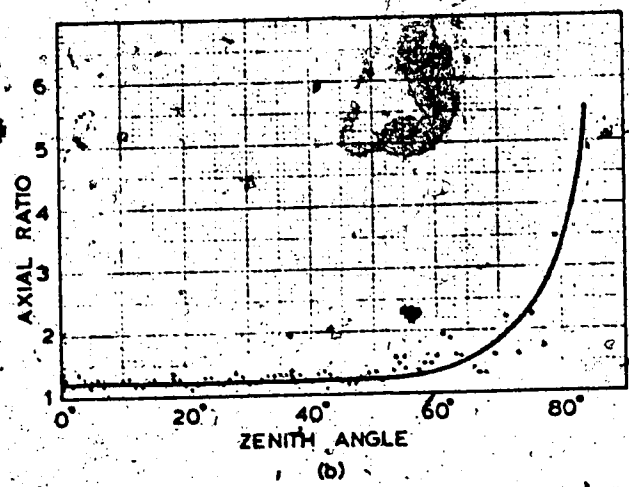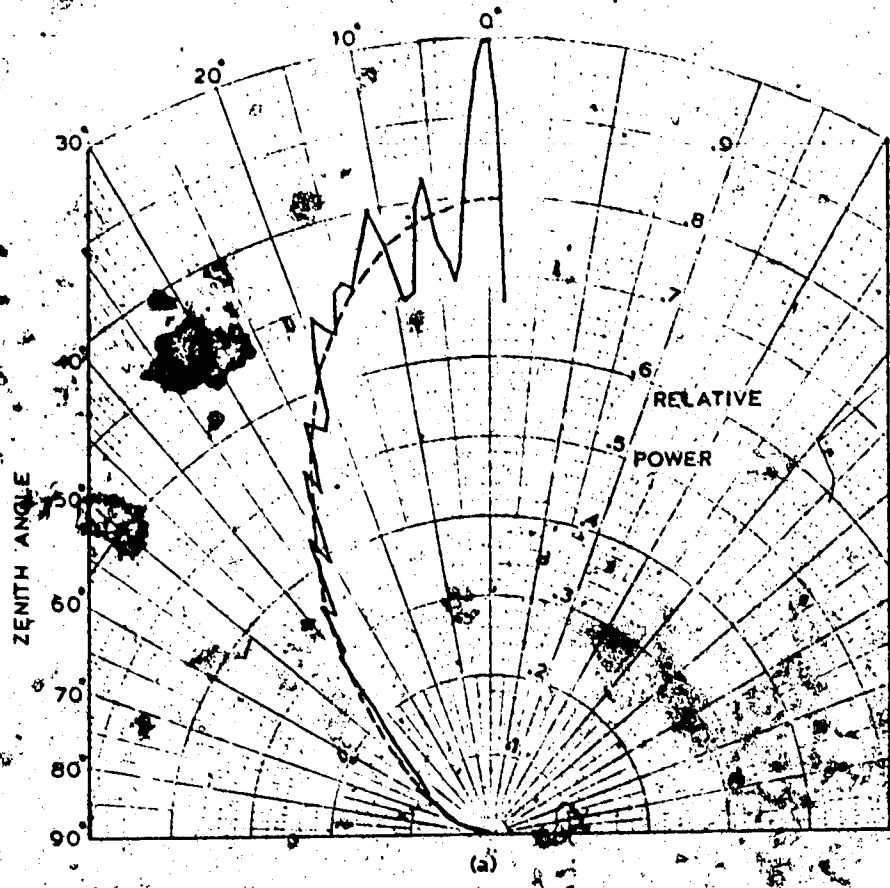
Fig. 7.13 Power pattern (a) and axial ratio (b) measurements on the cable-arm, wide cone angle conical spiral with $2\theta_o = 70°$, $\alpha = 87°$.

only a model and certain design changes may be desirable on the full-scale version. These will be discussed in the next section.

7.6 Design Considerations of the Full-Scale Riometer Antenna System

Two antennas will be required for the riometer - one to receive right circular polarization and one to receive left circular polarization. The antennas will be identical except with respect to the direction of wrap; a right hand (clockwise) opening spiral radiates (and therefore receives) predominantly a left circular wave.

From the measurements conducted on the antenna test range, the most suitable conical spiral was found. With an included cone angle $2\theta_o = 70°$ and angle of wrap $\alpha = 87°$. The base diameter must be at least λ/π for efficient operation.

The spiral arms can be formed from cable, in which case this cable may also be used to feed the antenna (see section 5.2.4). They may also be formed from wire as long as the gauge of the wire is such that the resistance per wavelength is negligible, as was the case on the models. At the riometer frequency of 12.4 MHz, a wire size of 20 gauge or larger should be sufficient. It may be obvious at this stage, that the arm width on a cable-arm conical spiral, relative to the rest of the physical structure, is considerably less on the full size antenna than on its equivalent model. This should not be a problem, however, since a small arm width has only minor effects on the radiation pattern, causing it to broaden somewhat (<5°), and does not affect the axial ratio. It primarily affects the input impedance, causing it to increase as the arm width decreases. However, as has been shown by Fisher, a wide arm width can be simulated by 3 wires; two defining the arm edges

and one down the center.

If the spirals are not fed by the infinite balun method but instead use the on-axis method of feed, the unbalance-to-balance transformation should be performed at the base of the antenna and preferably below the ground plane, if possible. A shielded balanced line can then be brought from this transformation up to the apex, along the axis of the cone. Because of the small diameter of the cable relative to the rest of the structure, its presence, on axis, will not perturb the fields existing within the cone.

The conical spiral elements need not be difficult to construct. Using the method of Dietrich and Long, nylon ropes could be extended to ground from the top of a central pole, the height of which corresponds to the $\lambda/4$ height required of the conical spiral elements. The ropes, which would be placed at least at $30°$ intervals, thus generate the desired conical structure. The cable or wire arms could then be spiraled down these ropes. By premeasuring the position of the spiral arms relative to the nylon ropes and attaching them accordingly, the entire assembly could then be raised in one motion. As mentioned in section 5.2.4, as long as the diameter of a metallic cylinder on axis does not exceed 1/3 the diameter of the conical structure anywhere along its axis, the fields within the cone will not be disturbed. Thus a metallic central pole may be used in the structure.

Coupling may occur between the two elements, although Dyson [16] has shown that for element to element spacings greater than $\lambda/2$, this coupling is less than -30 dB. For such spacings only minor changes occur to the radiation pattern and axial ratio due to the presence of another element, and the effects are even less for contrawound elements.

The antennas should be located over ground screens in order to eliminate the effects of changing ground conductivity. These ground screens should be circular in order to retain the symmetry of the antennas. Also they should extend at least $\lambda/4$ beyond the largest horizontal extent of the antennas (the base radius) as this appears to be the most widely used convention for ground planes of any antenna [40]. This would result in a ground screen of approximately λ in diameter and at a wavelength of 24 meters the increased radiating efficiency achieved by extending it further is not believed to be worth the additional cost and construction time.

CHAPTER 8

SUMMARY AND CONCLUSIONS

Decametric telescopes require that measurements be corrected for absorption that has occurred in the earth's ionosphere. From a radio astronomical point of view, the most suitable method of determining ionospheric absorption employs an instrument referred to as a Relative Ionospheric Opacity METER or riometer.

There are two methods of riometry, standard riometry and dual-polarized riometry. It has been shown that the dual-polarized riometry method is capable of determining the quiet day curve in 1/3 to 1/4 of the time required by standard riometry, and in addition, greater accuracy can be achieved. Because of the method in which the quiet day curve is determined, the dual-polarized riometry technique, unlike its alternative, does not suffer from measurement errors due to uncertainty in the degree to which negligible absorption conditions occur in the ionosphere.

Nevertheless, problems peculiar to dual-polarized riometry do exist. One problem which is largely beyond the control of the designer is the variability in the height of absorption. As long as measurements are not taken during periods of rapid changes in electron density, i.e. sunrise and sunset, this should not result in significant measurement errors. Equipment errors can be minimized by eliminating the cross-polarization effects within the antenna system. It has been shown that as long as the axial ratio of both the left and right circularly polarized antennas is approximately 1.2 or less over the significant portion of the beam, cross-polarization effects would be on the order of 1%. Also, if the variation in the antenna's axial ratio with zenith

angle could be sufficiently determined, the effect could be completely
calibrated out. Due to an experimental program which required the design
and construction of a microwave antenna test range both of these antenna
requirements were achieved.

The axial ratio and power pattern measurements of antennas tested
on this microwave antenna test range were found to exhibit interference
variations due to stray reflections. However, it was shown that by taking
the mean of the measured values, excellent agreement with the expected
values of antennas with known radiating characteristics could be
achieved. Applying the same method of interpreting the measurement data
to antennas of unknown characteristics, the most suitable riometer
antenna could be determined. This antenna was found to be the cable-arm
wide cone angle conical spiral with parameters $2\theta = 70°$, $\alpha = 87°$, $H \sim \lambda/4$.

Whether the dual-polarized riometry method is capable of measure-
ments to within 1% accuracy, remains to be seen. There is little doubt,
however, that it is more accurate than standard riometry. Yet this is
not its only advantage. The method is capable of returning a substantial
amount of information on the heights of absorption, electron recombina-
tion rates and, if the large inherent bandwidth of the conical spirals
is exploited in multifrequency riometry experiments, the electron
density distribution with height. All of these are of scientific impor-
tance at 12.4 MHz and at the observing latitude of 60° N, geomagnetic.

The versatility of the instrument is therefore obvious, yet its
basic equipment is virtually identical to that of a standard riometer.
The prime differences of equipment occur in the antenna system; the
standard riometer receives radiation of linear polarization and the
dual-polarized riometer receives radiation of left and right circular

polarization. But it has been pointed out that the two conical spiral
elements of the dual-polarized antenna system need not be difficult to
construct. Nylon ropes,extending to ground·at the proper angle from
the top of a central pole,could generate the conical shape and cable,
placed on top of these ropes, could form the spiral arms.

Thus the dual-polarized riometer, with its carefully selected
antenna system, should be a versatile instrument capable of accurate
absorption measurements yet still basically simple. However, if for
whatever reason, the technique does not prove to be successful,
reversion to the standard riometry technique is not so much an equip-
ment modification as it is a data processing change.

REFERENCES

[1]   Appleton, E.V., "Wireless Studies of the Ionosphere,"
       J. IEE, vol. 71, pp. 642-650 (May 1932).

[2]   Hartree, D.R., "The Propagation of Electromagnetic Waves in a
       Reflecting Medium in a Magnetic Field," Proc. Cambridge Phil.
       Soc., vol. 27, p. 143 (1931).

[3]   Sen, H.K. and Wyller, A.A., "On the Generalization of the
       Appleton-Hartree Magnetoionic Formula," J. Geophys. Res.,
       vol. 65, pp. 3931-3950 (December 1960).

[4]   Hargreaves, J.K., "Auroral Absorption of H.F. Radio Waves in
       the Ionosphere:A Review of Results from the First Decade of
       Riometry," Proc. IEEE, vol. 57, pp. 1348-1372 (August 1969).

[5]   Appleton, E.V. and Barnett, M.A.F., "Local Reflection of
       Wireless Waves from the Upper Atmosphere," Nature, vol. 115,
       pp. 333-334 (1925).

[6]   Röttger, J. and Schwentek, H., "A Numerical Description of the
       Winter Anomaly in Ionospheric Absorption for a Sunspot Cycle,"
       J. Atm. Terr. Phys., vol. 36, pp. 363-366 (1974).

[7]   Breit, G. and Tuve, M.A., "A Test of the Existence of Conducting
       Layer," Phys. Rev., vol. 28, pp. 568-575 (1926).

[8]   Shain, C.A., "Galactic Radiation at 18.3 Mc/s," Aust. J. Sci.
       Res., vol. A3, pp. 258-267 (March 1951).

[9]   Little, C.G., and Leinbach, H., "Some Measurements of High
       Latitude Ionospheric Absorption Using Extraterrestrial Radio
       Waves," Proc. IRE, vol. 46, pp. 334-348 (January 1958).

[10]   Little, C.G. and Leinbach, H., "The Riometer – A Device for
       the Continuous Measurement of Ionospheric Absorption," Proc.
       IRE, vol. 47, pp. 315-320 (February 1959).

[11]   Lusignan, B., "Cosmic Noise Absorption Measurements," J. Atm.
       Terr. Phys., vol. 23, pp. 126-136 (December 1961).

[12]   Schwentek, H. and Gruschwitz, E.H., "Measurement of Absorption
       in the Ionosphere on 27.6 MHz at 52° N by Means of a Riometer
       and a Corner Reflector Directed at the Pole Star," J. Atm. Terr.
       Phys. vol. 32, pp. 1385-1402 (January 1970).

[13]   Heisler, R. and Hower, G.L., "Comparisons between Calculated
       Ionospheric Absorption and Riometer Measurements," J. Atm. Terr.
       Phys. vol. 32, pp. 1755-1764 (April 1970).

[14]   Mitra, A.P. and Shain, C.A., "The Measurement of Ionospheric Absorption Using Observations at 18.3 Mc/s," _J. Atm. Terr. Phys._, vol. 4, pp. 204-218 (September 1953).

[15]   Little, C.G., Lerfald, G.M. and Parthasarathy, R., "Extension of Cosmic Noise Absorption Measurements to Lower Frequencies Using Polarized Antennas," _Radio Science:J. Res. NBS_, vol. 68D, pp. 859-865 (August 1964).

[16]   Dyson, J.D., "The Coupling and Mutual Impedance Between Conical Log-Spiral Antennas in Simple Arrays," _IRE Int'l Conv. Record_, pt. 1, pp. 165-182 (1962).

[17]   Dyson, J.D., "The Unidirectional Equiangular Antenna," _IRE Trans. Ant. Prop._, vol. AP-7, pp. 329-334 (October 1959).

[18]   Dyson, J.D., "The Characteristics and Design of the Conical Log-Spiral Antenna," _IEEE Trans. Ant. Prop._, vol. AP-13, pp. 488-499 (July 1965).

[19]   Dietrich, F.J. and Long, R.K., "An Efficient Moderate - Size Vertical - Incidence Ionosonde Antenna for 2-20 MHz Polarization Studies," _IEEE Trans. Ant. Prop._, vol. AP-17, pp. 551-557 (September 1969).

[20]   Andrew, B.H., "The Spectrum of Low Radio Frequency Background Radiation," _Mon. Not. Roy. Astron. Soc._, vol. 132, pp. 79-86 (1966).

[21]   Lerfald, G.M., Hargreaves, J.K. and Watts, J.M., "D-Region Absorption at 10 and 15 Mc/s During the Total Eclipse of July 20, 1963," _Radio Science:J. Res. NBS_, vol. 69D, pp. 939-946 (July 1965).

[22]   Kraus, J.D., _Radio Astronomy_, McGraw-Hill, New York (1966).

[23]   Douglas, J.N., "Decametric Radiation from Jupiter," _IEEE Trans. Military Electronics_, vol. MIL-8, pp. 173-187 (July-October 1965).

[24]   Ratcliffe, J.A., _The Magneto-Ionic Theory_, Cambridge University Press, New York (1959).

[25]   Jordan, E.C. and Balmain, K.G., _Electromagnetic Waves and Radiating Systems_, Prentice-Hall Inc., Englewood Cliffs, N.J. (1968).

[26]   Beynon, W.J.G. and Brown, G.M., "The Ionosphere," _Annals IGY_, vol. 3, pt. 1, pp. 1-40 (1957).

[27]   Benson, R.F., "The Quasi-Longitudinal Approximation in the Generalized Theory of Radio Wave Absorption," _Radio Science:J. Res. NBS_, vol. 68D, pp. 219-223 (February 1964).

Parthasarathy, R., Lerfald, G.M. and Little, C.G., "Derivation of Electron Density Profiles in the Lower Ionosphere Using Radio Absorption Measurements at Multiple Frequencies," *J. Geophys. Res.*, vol. 68, pp. 3581-3588 (1963).

[29] Hultqvist, B., "On the Solution of the Integral Equation Relating Height Distribution to Radio-Wave Absorption," *Planet. Space Sci.*, vol. 16, pp. 529-537 (1968).

[30] Hultqvist, B., "Ionospheric Absorption of Cosmic Radio Noise," *Space Sci. Rev.*, vol. 5, pp. 771-817 (1966).

[31] Machin, K.E., Ryle, M. and Vonberg, D.D., "The Design of an Equipment for Measuring Small R.F. Noise Powers," *Proc. IEE*, vol. 99, pp. 127-134 (May 1952).

[32] Bird, I.G. and Humphreys, A.E., "An Unmanned Geophyscial Observatory for Antarctic Operation," *Proc. IREE*, vol. 33, pp. 7-22 (January 1972).

[33] Bird, I.G., Morton, B.R. and Williams, H.A., "The Riometer - A State - of - the - Art Design," *Proc. IREE*, vol. 35, pp. 133-139 (May 1974).

[34] Steiger, W.R. and Warwick, J.W., "Observations of Cosmic Radio Noise at 18 MHz in Hawaii," *J. Geophys. Res.*, vol. 66, pp. 57-66 (January 1961).

[35] *The Observer's Handbook 1975*, Roy. Astr. Soc. Canada, University of Toronto Press, Toronto (1975).

[36] Ecklund, W.L. and Hargreaves, J.K., "Some Measurements of Auroral Absorption Structure Over Distances of About 300 km and of Absorption Correlation Between Conjugate Regions," *J. Atm. Terr. Phys.*, vol. 30, pp. 265-280 (1968).

[37] Nicolet, M., "Constitution of the Atmosphere at Ionospheric Levels," *J. Geophys. Res.* vol. 64, pp. 2092-2101 (December 1959).

[38] Parthasarathy, R. and Lerfald, G., "Cosmic Noise Survey at 65°(N) Declination in the 5-50 Mc/s Band," *Mon. Not. Roy. Astron. Soc.*, vol. 129, pp. 395-409 (1965).

[39] Sinclair, G., "Theory of Models of Electromagnetic Systems," *Proc. IRE*, vol. 36, pp. 1364-1370 (November 1948).

[40] *The ARRL Antenna Book*, The American Radio Relay League, Inc., Newington, Connecticut (1974).

[41] David, P. and Voge, J., *Propagation of Waves*, Pergammon Press, Oxford (1969).

[42] Hodowanec, G., "High-Power Transistor Microwave Oscillators,"
      RCA Application Note AN-6084.

[43] Wollesen, D.L., "UHF Transmission-Line Oscillator Design
      Using the Smith Chart," Motorola Application Note AN-216.

[44] Klein, C.F., "Designing with Microstrip is Easy," Electronic
      Design 1, pp. 100-104 (January 4, 1970).

[45] Fisher, J., "Design Tests of the Fully Steerable Wideband
      Decametric Array at the Clark Lake Radio Observatory," Ph.D.
      Thesis, University Microfilms, Maryland (1972).

[46] Snell, W.W., "Low-Loss Microstrip Filters Developed by
      Frequency Scaling," Bell Syst. Tech. J., vol. 50, pp. 1919-1931
      (July-August 1971).

[47] Weirather, B., "Microstrip Can Reduce Multiplier Size,"
      Electronic Design 2, pp. 46-50 (January 21, 1971).

[48] Caulton, M., Hughes, J.J. and Sobol, H., "Measurements on
      the Properties of Microstrip Transmission Lines for Microwave
      Integrated Circuits," RCA Review, vol. 27, pp. 377-391
      (September 1966).

[49] Schneider, M.V., "Microstrip Lines for Microwave Integrated
      Circuits," Bell Syst. Tech. J., vol. 48, pp. 1421-1444
      (May-June 1969).

[50] Lied, H.F., Radio Communications with Emphasis on Polar Problems,
      Circa Publications, Inc., Pelham, New York (1967).

[51] Sarma, S.B.S.S. and Mitra, A.P., "Cosmic Radio Noise Absorption
      in the Ionosphere:A Review of Results for the First Two
      Decades of Riometry at Low Latitudes," Indian J. Radio Space
      Phys., vol. 1, pp. 84-92 (March 1972).

[52] Piggott, W.R., "The Reflection and Absorption of Radio Waves in
      the Ionosphere," Proc. IEE, vol. 100, pp. 61-72 (March 1953).

[53] Leinbach, H. and Basler, R.P., "Ionospheric Absorption of
      Cosmic Radio Noise at Magnetically Conjugate Auroral Zone
      Stations," J. Geophys. Res., vol. 68, pp. 3375-3380 (June 1963).

[54] Khodzha-Akmedov, CH.L., "Frequency Dependence of Ionospheric
      Absorption at High Latitudes," Geom. Aeron., vol. 6, pp. 58-62
      (September 1967).

[55] Chute, F.S., Englefield, C.G., Harding, P.J.R., James, C.R.,
      Routledge, D., "Site-Testing for a Proposed 12 MHz Radio
      Telescope in Alberta," Roy. Astron. Soc. Canada J., vol. 65,
      pp. 49-59 (1970).

[56]   Routledge, D., "Proposal for a Canadian Decametric Telescope," proposal prepared for submission to NRC Associate Committee on Astronomy, (December 10, 1973).

[57]   Hultqvist, B., "Ionospheric Absorption of Cosmic Radio Noise," Space Sci. Rev. vol. 5, pp. 771-817 (1966).

[58]   Conn, D.R. and Mitchell, R.H., "Design of Microstrip Transistor Oscillators," Int. J. Electron., vol. 35, pp. 385-395 (1973).

[59]   Kane, J.A., "Re-evaluation of Ionospheric Electron Densities and Collision Frequencies Derived from Rocket Measurements of Refractive Index and Attenuation," J. Atm. Terr. Phys., vol. 23, pp. 338-347 (1961).

[60]   Thrane, E., Electron Density Distribution in Ionosphere and Exosphere, John Wiley and Sons, New York (1964).

[61]   Kasha, M.A., The Ionosphere and Its Interaction with Satellites, Gordon and Breach, Science Publishers, New York (1969).

[62]   Reference Data for Radio Engineers, fifth edition, Howard W. Sams and Co., Inc., New York (1974).

[63]   Antenna Engineering Handbook, McGraw-Hill, New-York (1961).

[64]   Emerson, W.H., "Electromagnetic Wave Absorbers and Anechoic Chambers Through the Years," IEEE Trans. Ant. Prop., vol. Ap-21, pp. 484-490 (July 1973).

[65]   Dybdal, R.B. and Yowell, C.D., "VHF to EHF Performance of a 90 ft Quasi-Tapered Anechoic Chamber," IEEE Trans. Ant. Prop., vol. AP-21, pp. 579-581 (July 1973).

[66]   Appel-Hansen, J.,"Reflectivity Level of Radio Anechoic Chambers," IEEE Trans. Ant. Prop., vol. AP-21, pp. 490-497 (July 1973).

[67]   Johnson, R.C., Ecker, H.A. and Moore, R.A., "Compact Range Techniques and Measurements," IEEE Trans. Ant. Prop., vol. AP-17, pp. 568-576 (September 1969).

[68]   Cook, A.H., Physics of the Earth and Planets, Macmillan Press Ltd., London (1973).

APPENDIX A

A COMPUTER PROGRAM FOR USE IN THE FABRICATION OF SMALL

EQUIANGULAR SPIRAL ANTENNAS

The construction of an equiangular spiral antenna requires the accurate placement of its spiral arms on either a planar or conical structure. Fabrication patterns which can be formed into the appropriate planar or conical structure can be drawn quickly and accurately with the aid of a computer and digital plotter. The computer program which can accomplish this task is listed in Figure A.1. The program is written in FORTRAN and was run on the University of Alberta's IBM 360/67 computer. The digital plotter used was a Calcomp Model 925/1036.

The parameters of an equiangular spiral antenna (previously defined in sec. 5.1) required by the computer program are: the angle of wrap α; the cone angle θ_o ($\theta_o = 90$% for planar structures); the distance along the cone from the apex to the point of minimum radius ρ_{min}; and the distance along the cone from the apex to the base ρ_{max}. In addition, the angular increment in ϕ, with which it is desired to plot the arms, is required. All lengths are in inches and all angles in degrees. The maximum pattern that can be plotted depends on the size limitations imposed by the facilities used.

```
      REAL P(4,400),BETA(4,400),BETAX(4,400)
      INTEGER PHI(4,400),K(4,400),TO,AA,DA,A,K1(4)
      CALL PLOTS
      WRITE(6,99)
      WRITE(6,100)
      READ(5,103) PMIN,PMAX,TO,AA,DA,INC
      WRITE(6,101)PMIN,PMAX
      WRITE(6,102)TO,AA,DA,INC
      XX=0.0
      YY=2.0
      B=SIN(TO*3.14159/180.)/TAN(AA*3.14159/180.)
      C=SIN(TO*3.14159/180.)
      CT=C*360.
      IF(CT.GT.90.0)XX=16.0
      IF(CT.GT.180.0)YY=17.0
      IF(PMAX.GT.(32.-XX))WRITE(6,200)
      IF(PMAX.GT.(35.-YY))WRITE(6,201)
      T=(ALOG(PMAX/PMIN))/(6.28319*B)
      NGL=IFIX((T-IFIX(T))*360)
      M=IFIX(T)
      N=IFIX(T*360/INC)
      L1=360
      WRITE(6,104)B,N,M,NGL
      WRITE(6,107)L1
      A=0
      DO 10 I=1,4
      J1=1
      J=1
20    PHI(I,J)=INC*(J1-1)
      K(I,J)=PHI(I,J)/360
      P(I,J)=PMIN*EXP((PHI(I,J)*A)*3.14159/180.*B)
      BETA(I,J)=(PHI(I,J)/360.-IFIX(PHI(I,J)/361.))*6.28319*C
      BETAX(I,J)=(BETA(I,J)*180./3.14159)
      IF(PHI(I,J).EQ.0)GOTO30
      IF(PHI(I,J).NE.360*K(I,J))GOTO30
      PHI(I,J+1)=360*K(I,J)
      P(I,J+1)=P(I,J)
      K(I,J+1)=K(I,J)
      BETA(I,J+1)=0.0
      BETAX(I,J+1)=0.0
      J=J+1
30    CONTINUE
      J1=J1+1
      J=J+1
      IF(P(I,J-1).GE.PMAX)GOTO 15
      GOTO20
15    CONTINUE
      K1(I)=J-1
      GOTO(1,2,3,10),I
1     A=A+DA
      GOTO10
2     A=180
      GOTO10
3     A=180+DA
10    CONTINUE
      DO 40 I=1,4
40    WRITE(6,106)K1(I),P(I,K1(I)),BETAX(I,K1(I))
      WRITE(6,110)
      READ(5,108)IBLANK
99    FORMAT(' ','LENGTHS IN INCHES, ANGLES IN DEGREES')
100   FORMAT('INPUT PMIN,PMAX,THETA0,ALPHA,DELTA,INC'/'T')
101   FORMAT(' ','RHOMIN=',F9.4,' ',6X,'RHOMAX=',F9.4,' IN')
102   FORMAT('THETA0=',I4,6X,'ALPHA=',I4,6X,'DELTA=',I5,6X,'INC=',I5)
103   FORMAT(2F9.4,4I4)
104   FORMAT('B=',F9.6,6X,'TOT PTS=',I5,6X,'ANG DIST=',I3,'RY',I5,'DEG')
106   FORMAT(' ',I3,F9.4,F9.3)
107   FORMAT(' ',I4)
108   FORMAT(I4)
109   FORMAT(' ',4I4,2F9.4)
110   FORMAT(' ','?')
200   FORMAT(' ','DATA EXCEED X DIMENSIONS OF PHYSICAL PLOT PAPER')
201   FORMAT(' ','DATA EXCEEDS Y DIMENSIONS OF PHYSICAL PLOT PAPER')
      CALL ERASE
      CALL NEWPEN(1)
      CALL PLOT(XX,YY,-1)
      CALL PLOT(PMAX,0.0,2)
      CALL CIRCLE(PMAX,0.0,0.0,CT,PMAX,PMAX,0.0)
      CALL PLOT(0.0,0.0,2)
      CALL CIRCLE(PMIN,0.0,0.0,CT,PMIN,PMIN,0.0)
      CALL PLOT(0.0,0.0,3)
      CALL NEWPEN(2)
      NL=2
      IF(DA.EQ.0)NL=1
      DO 70 L=1,NL
      CALL POLAR(P(L,1),BETA(L,1),K1(L),4,0.0,-1.,1.)
70    CONTINUE
      CALL NEWPEN(3)
      ML=4
      IF(DA.EQ.0)ML=3
      DO 80 L=3,ML
      CALL POLAR(P(L,1),BETA(L,1),K1(L),4,0.0,-1.,1.)
80    CONTINUE
      CALL PLOT(0.0,0.0,999)
      STOP
      END
*END OF FILE
```

Fig. A.1 Computer program for the fabrication of spiral antennas.

THE DIPOLE ROTATION ASSEMBLY DRIVE MOTOR AND ITS POWER SUPPLY

The specifications of the 2-phase induction motor used to rotate the dipole are listed below:

manufacturer	Eastern Air Devices, Inc.
type	gear servo-generator
model	GSJIHLX7-15cc
frequency	400 Hz
no load speed	59 RPM
stalled torque	38 oz. in.
in phase null	.008 V RMS
quadrature null	.015 V RMS
phase shift	± 10°
total null	.019 V RMS
nominal operating voltage	30 V PTP @ 400 Hz

Because of its high power requirements, a push-pull amplifier was built to boost the power from the 400 Hz signal generator.

The schematic of the power amplifier and the equivalent circuit of the dipole induction motor are shown in Figure B.1.
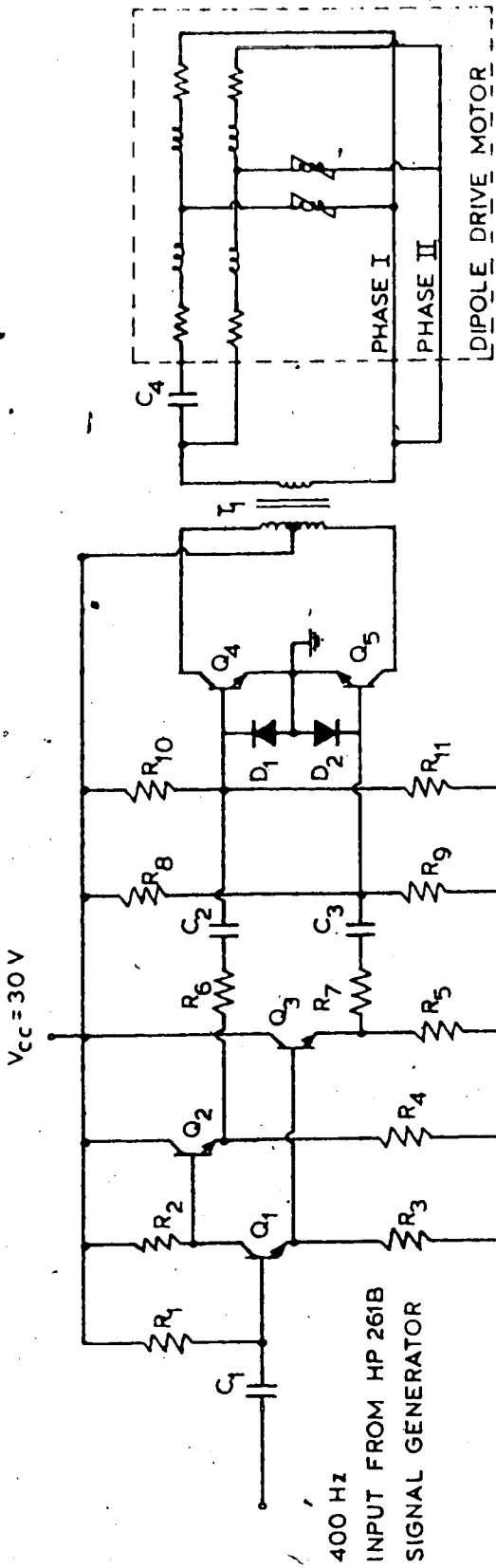
Fig. B.1 Schematic of the push-pull power amplifier required by the dipole induction motor and the equivalent circuit of that motor.

SPECIFICATIONS OF THE SCIENTIFIC-ATLANTA AZIMUTH POSITIONER

Maximum Vertical Load	3,000 pounds
Maximum Bending Moment	1,000 foot-pounds
Turntable Diameter	16 inches
Turntable Bore	3 inches
Turntable Bolt Circle	10 inches
Turntable Bolt Holes (tapped)	6, 3/8-16
Length	17-11/16 inches
Width	16-1/4 inches
Height	13 inches
Base Mounting	3-hole Isosceles Triangular Pattern 12" base x 8-1/2" height
Base Mounting Holes (clearance)	17/32 inch
Horsepower	1/15
Withstand Torque	290 foot-pounds
Deliver Torque	60 foot-pounds
Maximum Speed	2.2 rpm
Synchro Ratio	1:1 & 36:1
Position Accuracy	0.05 degree
Drivegear Backlash, less than	0.2 degree
Shipping Weight	150 pounds
Net Weight	110 pounds
Recommended Control Unit	PC 2-33

APPENDIX D

THE MICROSTRIP POWER OSCILLATOR AND BAND-PASS FILTER

Excellent papers exist in the literature on the design of both microstrip power oscillators [42], [43], [44] and microstrip filters [46], [47] and, hence, their designs will not be detailed here. Only the basic design equations, schematics and operating characteristics of the final designs will be presented.

D.1 General

The two most basic parameters required when designing with microstrip transmission line are its characteristic impedance z_o and guide wavelength λ_g. These parameters may be found from published curves [48] or calculated directly from the following equations:

$$z_o = \frac{377h}{\sqrt{\epsilon_R} \, W_{EFF}[1 + 1.735 \, \epsilon_R^{-0.0724}(W_{EFF}/h)^{-0.836}]} \quad \text{Ohms}$$

$$\lambda_g/\lambda_o = \begin{cases} \left[\dfrac{1}{1 + .63(\epsilon_R - 1)(W_{EFF}/h)^{0.1255}}\right]^{1/2} & W_{EFF}/h \geq .6 \\[3em] \left[\dfrac{1}{1 + .60(\epsilon_R - 1)(W_{EFF}/h)^{0.0297}}\right]^{1/2} & W_{EFF}/h \leq .6 \end{cases}$$

where

$$W_{EFF} = W + t/\pi[\ln(2h/t)+1]$$

ϵ_R = dielectric constant of the microstrip substrate

h = thickness of dielectric substrate

t = thickness of the conductor and ground plane

W = width of the conductor

λ_o = free space wavelength at operating frequency

CONDUCTOR

W

t

DIELECTRIC

h

ϵ_R

GROUND PLANE
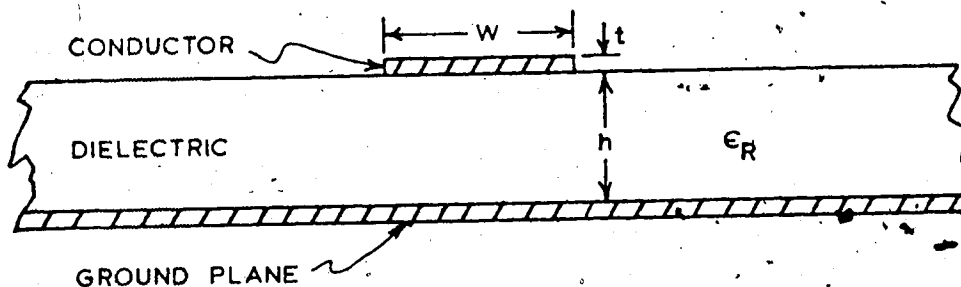
Fig. D.1 A cross section of microstrip transmission line.

The microstrip board used in both the oscillator and filter had the following parameters:

t = 2.8 mils

h = 25.6 mils

ϵ_R = 2.55

The width W will depend on the characteristic impedance required of the microstrip transmission line in any particular application.

D.2 The Power Oscillator

The power oscillator schematic shown in Figure D.2 is essentially

R_1= 1.2 KΩ

R_2= 300 Ω

R_3= 10 Ω
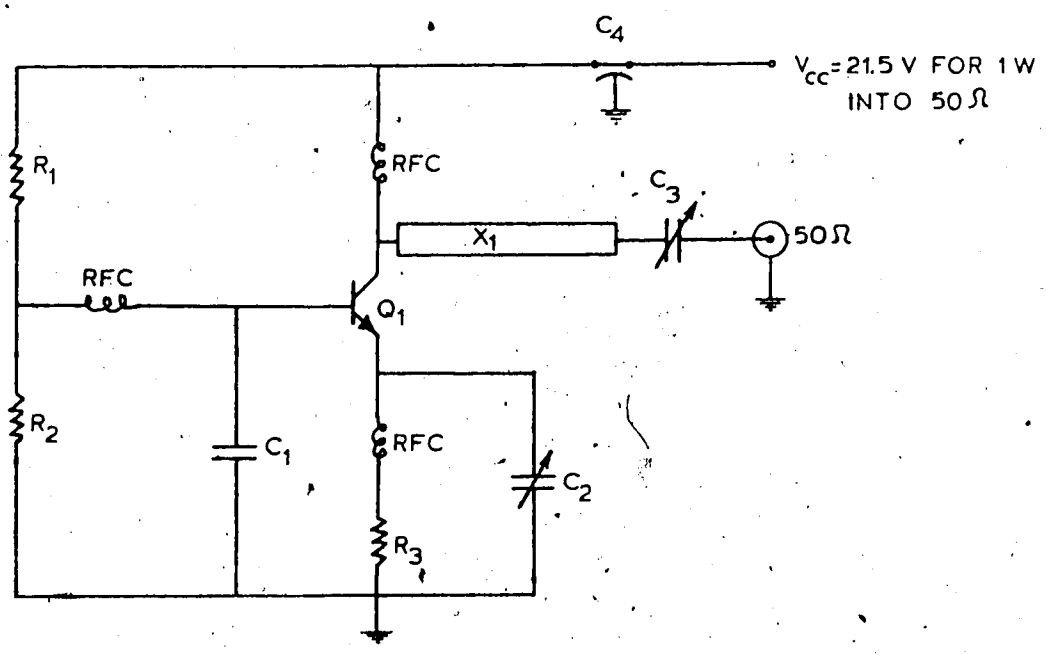
C_1= 500 pF (CHIP)

C_2= .35- 3.5 pF (JOHANSON 5802)

C_3= .8- 10 pF (JOHANSON 5202)

C_4= 500 pF (FEED THROUGH)

RFC= 5 TURNS #32 WIRE; D= 1/8", L= 1/4"

Q_1= MSC 80069

X_1= 1" x 3/32" CONDUCTOR ON 1/32" POLYETHYLENE BOARD

Fig. D.2 Schematic and component values of power oscillator.

that of a Microwave Semiconductor Corporation (MSC) test oscillator circuit.

By adjusting capacitor C_2 the frequency of the oscillator could be coarsely tuned to any frequency in the range 800 MHz to 1.2 GHz. The final output frequency did not only depend on capacitor C_2 but also on the matching capacitor C_3 and the D.C. power supply voltage V_{CC}.

The oscillator, which requires a heat sink, could produce up to 3 Watts of power depending on V_{CC} and resistor R_3 which was largely responsible for controlling its efficiency. For its purpose of feeding power to the transmitting antenna of the test range, the oscillator was tuned to a frequency of 959.0 MHz and adjusted for an output power of 1 Watt into 50 Ω.

D.3 The Band-Pass Filter

The important dimensions of the microstrip band-pass filter formed from two direct-coupled quarter-wave resonators are shown in Figure D.3. The resonators, which are formed from open- and short-circuited sections of microstrip transmission line, have an equivalent circuit as shown in Figure D.4.

If these open- and short-circuited sections comprising the resonators behaved as ideal capacitors and inductors, i.e. were not lossy, the filter would exhibit an infinitely small pass band, and the insertion loss at resonance would be zero. However, losses do occur and typically, as an attempt is made to make the bandwidth smaller, the insertion loss increases and vice-versa.

From the discussion of section D.1, the characteristic impedance of
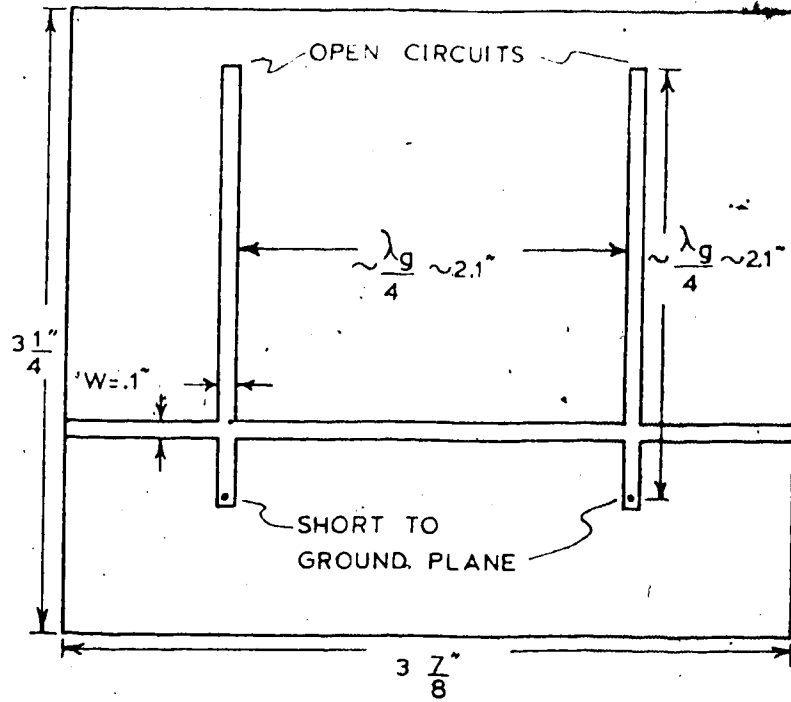
Fig. D.3 Schematic of the microstrip 2 resonator filter.
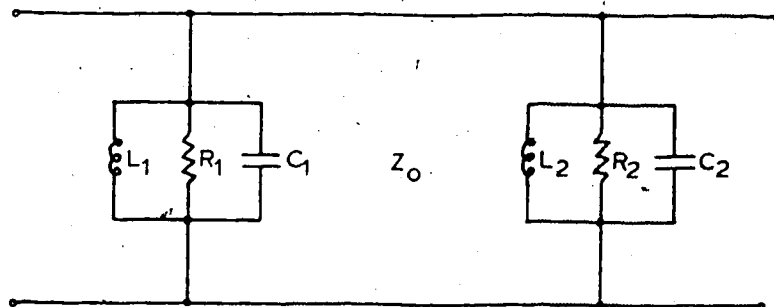
Fig. D.4 Equivalent circuit of filter shown in Figure D.3 .

the transmission line z_o is essentially set by the width of the conductors for a given dielectric board, and the filter's center frequency will be determined by the length of the resonators.

The filter response between .94 GHz and 1.00 GHz, illustrating the 3 dB bandwidth, is shown in Figure D.5.

The return loss of the filter when matched to 50Ω is shown in Figure D.6 between .92 GHz and 1.00 GHz. The figure shows that the reflected power is better than 25 dB below the input power at 959 MHz.
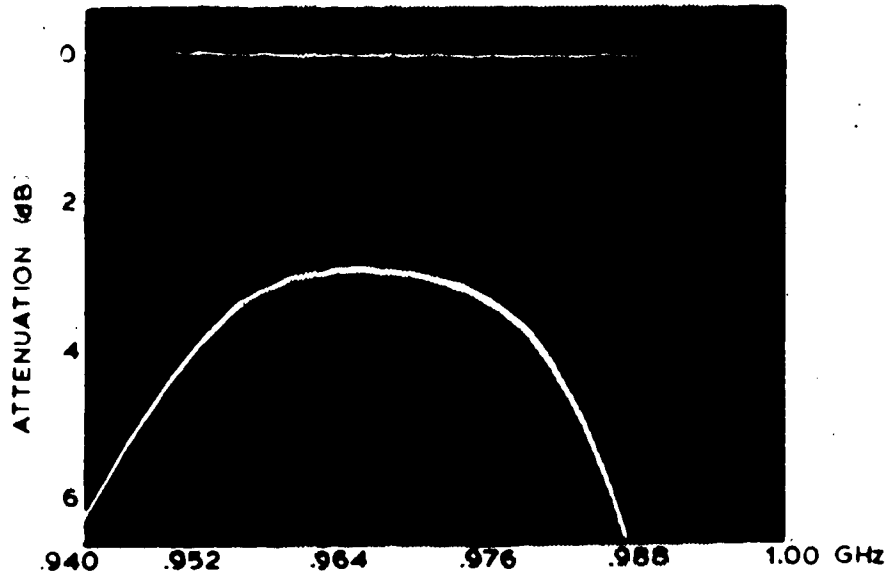
Fig. D.5. Filter response between .94 GHz and 1.00 GHz.
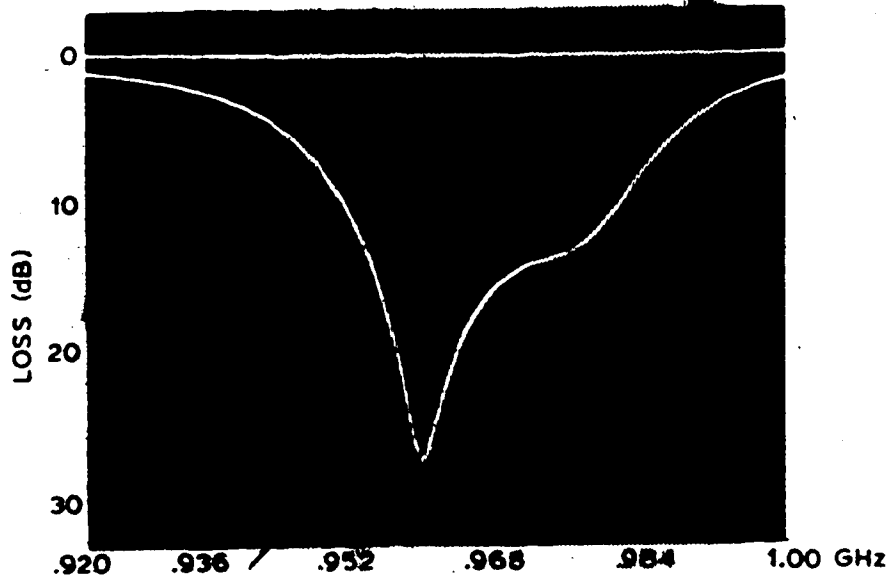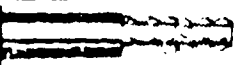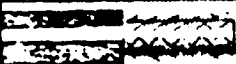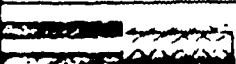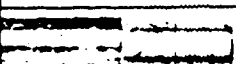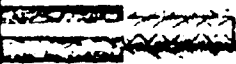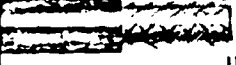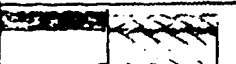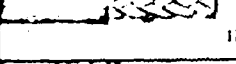
Fig. D.6 Return loss of filter working into 50 Ω between .92 GHz and 1.00 GHz. The marker is at 959 MHz.

CABLE SPECIFICATIONS

POLYETHYLENE DIELECTRIC

All Illustrations — Actual Size

RG CABLE TYPE	ALPHA PART NO	INNER CONDUCTOR MAT	STRAND	NOM O.D.	DIELECTRIC MAT	O.D.	SHIELDS Inner	Outer	O.D.	JACKET MAT	O.D.	20000 1.0170 ALUM WIRE	NOM VOLTS RMS	LBS PER M/FT	NOM IMPED Ohms	NOM CAP MMF/ FT.
6A/U	9006A CW	1		.0285	PE	.189	SC	C	.264	NCV	.336		2700	74	75	20
8/U	9008 C	7/.0285	.086		PE	.295	C	—	.340	V	.415		5000	105	52	29.5
8A/U	9008A C	7/.0285	.086		PE	.295	C	—	.340	NCV	.415		5000	99	52	29.5
9B/U	9009B SC	7/.0285	.086		PE	.285	SC	SC	.355	NCV	.430		5000	126	50	30
11/U	9011 TC	7/.0159	.048		PE	.295	C	—	.340	V	.415		5000	94	75	20.5
11A/U	9011A TC	7/.0159	.048		PE	.297	C	—	.340	NCV	.412		5000	89	75	20.5
12A/U	9012A TC	7/.0159	.048		PE	.292	C	—	.340	NCV	.412	.475	5000	113	75	20.5
14A/U	9014A C	1		.102	PE	.383	C	C	.463	NCV	.558		7000	291	52	29.5
17A/U	9017A C	1		.188	PE	.695	C	—	.760	NCV	.885		11000	462	52	29.5
19A/U	9319A C	1		.250	PE	.925	C	—	.990	NCV	1.135		14000	720	52	29.5

ALL TYPES LISTED CONFORM TO LATEST REVISION MIL-C-17.

—Bare Copper
PE—Solid Polyethylene
NP—Natural Polyethylene—Type III

TC—Tinned Copper
SSP—Semi Solid Polyethylene
V—Polyvinylchloride—Type I

SC—Silver Covered Copper
BP—Black Polyethylene—Type IIIA
NCV—Non Contaminating Polyvinylchloride—Type IIA

ALL DIMENSIONS ARE MAXIMUM EXCEPT WHERE INDICATED

*GRAY

ALPHA WIRE CORPORATION

65

Types

POLYETHYLENE DIELECTRIC
All Illustrations — Actual Size

RG CABLE TYPE	ALPHA PART NO	INNER CONDUCTOR			DIELECTRIC			SHIELDS		JACKET		NOMINAL (0.175 ALUM WIRE)	OPP VOLTS RMS	LBS. PER M/FT.	NOM IMPED OHMS	NOM CAP MMFD/FT
		MAT.	STRAND	O.D.	MAT	O.D.	Inner Outer	O.D.	MAT	O.D.						
228 U	90228	C	1 no 7/.0152	.047	PE	.291	TC	TC	.355	NCV	.430	1000	124	95	16
55 U	9055	C	1	.032	PE	.121	TC	TC	.176	RP	.206	1900	31	53.5	28.5
55B U	9055B	SC	1	.032	PE	.121	TC	TC	.176	BP	.206	1900	32	53.5	28.5
58 U	9058	C	1	.032	PE	.121	TC	—	.150	V	.200	1900	24	53.5	28.5
58A U	9058A	C	19/.0071	.0375	PE	.120	TC	—	.150	V	.199	1900	25	50	29.5
58C U	9055C	TC	19/.0071	.0375	PE	.120	TC	—	.150	NCV	.199	1900	25	50	29.5
59 U	9059	CW	1	.0253	PE	.150	C	—	.191	V	.250	2300	36	73	21
59B/U	9059B	CW	1	.023	PE	.150	C	—	.191	NCV	.246	2300	36	75	20.5
62 U	9062	CW	1	.025	SSP	.151	C	—	.191	V	.253	750	34	93	13.5
62A U	9062A	CW	1	.025	SSP	.151	C	—	.191	NCV	.249	750	34	93	13.5
63B U	9063B	CW	1	.0253	SSP	.295	C	—	.340	NCV	.415	1000	78	125	10
71B U	9071B	CW	1	.025	SSP	.151	C	TC	.208	BP	.250	750	42	93	13.5
174 U	9174	CW	7/.0063	.019	PE	.060	TC	—	.088	NCV	.105	1500	7	50	30
212/U	9212	SC	1	.056	PE	.185	SC	SC	.255	NCV	.335	3000	83	50	29.5
213 U	9213	C	7/.0296	.090	PE	.292	C	—	.340	NCV	.412	5000	100	50	30.5

ALL TYPES LISTED CONFORM TO LATEST REVISION MIL-C-17.

C—Bare Copper
TC—Tinned Copper
SC—Silver Covered Copper
CW—Copper Covered Steel

PE—Solid Polyethylene
SSP—Semi Solid Polyethylene
BP—Black Polyethylene—Type IIIA

RP—Reduced Polyethylene—Type IIIC
V—Polyvinylchloride—Type I
NCV—Non-Contaminating Polyvinylchloride—Type IIA

ALL DIMENSIONS ARE MAXIMUM EXCEPT WHERE INDICATED

ALPHA WIRE CORPORATION

186

Alpha RG Cable Types

POLYETHYLENE DIELECTRIC
All Illustrations — Actual Size

RG CABLE TYPE	ALPHA PART NO	INNER CONDUCTOR MAT	STRAND	NOM OD	DIELECTRIC MAT	OD	SHIELDS Inner	Outer	OD	JACKET MAT	OD	ARMOR (8178 ALUM WIRE)	OPR VOLTS RMS	LBS PER M/FT	NOM IMPED OHMS	NOM CAP MMF/FT
214/U	9214	SC	7/.0296	090	PE	292	SC	SC	360	NCV	.432		5000	129	50	30.5
215/U	9215	C	7/.0296	090	PE	292	C	—	340	NCV	.412	475	5000	122	50	30.5
217/U	9217	C	1	106	PE	380	C	C	.463	NCV	.555		7000	202	50	30
218.U	9218	C	1	195	PE	690	C	—	.760	NCV	.880		11000	457	50	30
219/U	9219	C	1	195	PE	690	C	—	.760	NCV	.880	.945	11000	507	50	30
223/U	9223	SC	1	036	PE	170	SC	SC	.176	NCV	.216		1900	36	50	30

ALL TYPES LISTED CONFORM TO LATEST REVISION MIL-C-17.

C—Bare Copper PE—Solid Polyethylene NP—Natural Polyethylene—Type III
TC—Tinned Copper SSP—Semi Solid Polyethylene V—Polyvinylchloride—Type I
SC—Silver Covered Copper BP—Black Polyethylene—Type IIIA NCV—Non-Contaminating Polyvinylchloride—Type IIA
CW—Copper Covered Steel

ALL DIMENSIONS ARE MAXIMUM EXCEPT WHERE INDICATED

TEFLON DIELECTRIC

ALPHA NO.	RG TYPE	COND.	NOM WALL THICK.	NOM JKT THICK.	JACKET TYPE	MAX OD	CAP NOM	IMPED OHMS	MAX OPER VOLTAGE
8178B	178B/U	7/.004	.012	.010	Extruded FEP	.075	27.9	50±2	1000
9179B	179B/U	7/.004	.021	.010	Extruded FEP	.105	20.4	75±3	1200
8180B	180B/U	7/.004	.045	.010	Extruded FEP	.145	15.3	93±2	850
9187A	187A/U	7/.004	.024	.012	Fused TFE Tape	.110	19.5	75±3	1200
8188A	188A/U	7/.0067	.020	.012	Fused TFE Tape	.110	27.5	50±2	1200
9195A	195A/U	7/.004	.045	.014	Fused TFE Tape	.155	14.5	95±3	1500
9196A	196A/U	7/.004	.011	.012	Fused TFE Tape	.080	28.5	50±2	1000

* Silver Coated Cadmium Bronze
** Operating Temperature 200°C.
Conductors Silver Plated Copperweld

ALPHA WIRE CORPORATION

67

Attenuation Ratings

POLYETHYLENE TYPES

RG CABLE TYPE	ATTENUATION (db/100 ft.) FREQUENCY IN MEGACYCLES							
	10 MC	50 MC	100 MC	200 MC	400 MC	600 MC	1000 MC	3000 MC
6A/U	.70	1.8	2.9	4.3	6.5	8.3	11.2	22
8/U	.56	1.35	2.1	3.1	5.0	6.5	8.0	17.5
8A/U	.56	1.35	2.1	3.1	5.0	6.5	8.8	17.5
9B/U	.45	1.26	2.3	3.4	5.2	6.5	9.0	17
11/U	.65	1.5	2.15	3.2	4.7	6.0	8.2	18
11A/U	.65	1.5	2.15	3.2	4.7	6.0	8.2	18
12A/U	.65	1.5	2.15	3.2	4.7	6.0	8.2	18
14A/U	.28	.85	1.5	2.3	3.5	4.4	6.0	11.7
17A/U	.23	.60	.95	1.5	2.4	3.2	4.5	9.5
19A/U	.14	.42	.69	1.1	1.8	2.45	3.5	7.7
22B/U	1.3	2.7	4.0	5.5	8.5	—	12.5	21.0
55/U	1.3	3.2	4.8	7.0	10.5	13.0	17	32
55D/U	1.3	3.2	4.8	7.0	10.5	13.0	17	32
58/U	1.4	3.5	5.3	8.3	11.5	17.8	20	40
58A/U	1.6	4.1	6.2	9.2	14.0	17.5	23.5	45
58C/U	1.6	4.1	6.2	9.2	14.0	17.5	23.5	45
59/U	1.1	2.7	4.0	5.7	8.5	10.8	14.0	26
59B/U	1.1	2.7	4.0	5.7	8.5	10.8	14.0	26
62/U	.62	1.9	2.7	3.9	5.8	7.0	9.0	17
62A/U	.82	1.9	2.7	3.9	5.8	7.0	9.0	17
63U/U	.60	1.4	2.0	2.9	4.1	5.1	6.5	11.3
71B/U	.82	1.9	2.7	3.9	5.8	7.0	9.0	17
174/U	—	—	—	—	20.0	—	—	16.7
212/U	.65	1.6	2.4	3.6	5.2	6.6	5.8	16.7
213/U	.56	1.35	2.1	3.1	5.0	6.5	8.8	17.5
214/U	.45	1.26	2.3	3.4	5.2	6.5	9.0	17
215/U	.56	1.35	2.1	3.1	5.0	6.5	8.8	16.7
217/U	.28	.85	1.5	2.3	3.5	4.4	6.0	11.7
218/U	.225	.60	.95	1.5	2.4	3.2	4.5	9.5
219/U	.225	.60	.95	1.5	2.4	3.2	4.5	9.5
223/U	1.3	3.2	4.8	7.0	10.5	13.0	17.0	32.

TEFLON TYPES

RG TYPE	MAX. ATTEN. DB/100 FT. @ 400 mc	RG TYPE	MAX. ATTEN. DB/100 FT. @ 400 mc	RG TYPE	MAX. ATTEN. DB/100 FT. @ 400 mc
178B/U	29.0	187A/U	21.0	196A/U	29.0
179B/U	21.0	188A/U	20.0		
180B/U	17.0	195A/U	17.0		

ALPHA WIRE CORPORATION